The influence of nitric oxide (NO) on histone acetylation in hypoxic *Arabidopsis thaliana* root tips

by

Madeline Rose Lee

A Thesis submitted to the Faculty of Graduate and Postdoctoral Studies of The University of Manitoba in partial fulfillment of the requirements of the degree of

MASTER OF SCIENCE

Department of Plant Science

University of Manitoba

Winnipeg

ACKNOWLEDGEMENTS

First I want to thank both of my advisors Dr. Claudio Stasolla and Dr. Jim Davie. Claudio you've been immensely helpful and welcoming. I did not have the best plant physiology knowledge coming into this program, but you were patient with me and kept me in the right direction. I'm also really happy with how inviting your lab was despite me only being around periodically. Jim your comprehensive knowledge of epigenetics has been instrumental for my entire project. Additionally, you've also always listened and respected my ideas when certain aspects of my project were not working which gave me confidence in my ability to problem solve. I also want to thank both of my committee members. Thank you Dr. Rob Hill for reviewing my literature review, I really appreciate that you took the time to give me good constructive feedback. Dr. Sylvie Renault I wanted to thank you for my insightful and beneficial experience taking your stress physiology course. Plant physiology was not my strongest topic, so I really appreciated the time you took teaching that course and meeting with me to discuss the topic. I also wanted to take some time to thank the lab members of both Claudio's and Jim's labs. Dr. Mohammed Mira and Shimaa both took time to teach me how to work with Arabidopsis and prepared a large amount of tissue for me to troubleshoot with. I know now how time consuming and tedious that was for them, and I appreciate it immensely. I want to thank Samadhi, Natalie, Hannah, Shruti, Gursimran, and Nick for their help with treatments and for making me feel at home in the plant science department. I also appreciate Dhanvi, the backbone of the Davie lab for the help with lab work, constant emotional support, and for putting up with my complaining over nothing. I want to thank the best undergraduate researcher Ishdeep for being nothing but supportive and wish you the best for your future studies. I wanted to thank Annan for keeping my spirits up, and for your help with admin issues. I appreciate Sadhana, Hedi, Kari, Marvellous and

Sheryl supporting me throughout my time in the Davie lab. Last but not least I want to thank my family and friends. I want to thank my mom Christine, my dad Joel, my brother Thomas, and my friends Molly and Caitlyn for the financial support, for keeping me sane, and for tolerating low contact during almost 7 years of university away from home.

TABLE OF CONTENTS

Page

ACKNOWLEDGEMENTS i

TABLE OF CONTENTS iii

LIST OF FIGURES vi

LIST OF TABLES vii

LIST OF ABBREVIATIONS viii

ABSTRACT xi

FOREWARD xii

1. LITERATURE REVIEW 1

1.1. Introduction 1

1.1.1. Climate change and flooding 1

1.1.2. Flooding and gas dynamics 2

1.2. Hypoxia 2

1.2.1. Hypoxia in roots 3

1.2.2. Root structure 3

1.2.3. The biochemical response to hypoxia 5

1.2.4. The physiological response to hypoxia 6

1.2.5. The morphological response to hypoxia 8

1.3. Nitric oxide 10

1.3.1. Nitric oxide and the hypoxic response 11

1.4. Phytoglobin 12

1.5. Plant epigenetics 14

1.5.1. Histone modifications 15

1.5.2. Histone variants and structures 16
1.5.3. DNA methylation 16
1.5.4. Nitric oxide and epigenetics....17
1.5.5. Histone acetylation and nitric oxide 17
1.5.6. Histone deacetylases and nitric oxide 18
1.5.7. Phytoglobin1 and histone acetylation 21
1.6. Hypothesis....21
1.7. Thesis objectives 22

2. MATERIALS AND METHODS....23

2.1. Plant material 23
2.2. Antibody quality control 24
2.2.1. Dot blots....24
2.2.2. Linear Curves....25
2.3. Western blotting 27
2.4. Data analyses 31

3. RESULTS....32

3.1. Antibody quality control 32
3.1.1. Dot blots....32
3.1.2. Linear curves....35
3.2. Western blot analysis 50
3.2.1. H3K9 and H3K14 acetylation response to hypoxia....50
3.2.2. *Phytoglobin1* deregulation affects H3K9 and H3K14 acetylation 55

4. DISCUSSION 68

4.1. Histone acetylation....68
4.1.1. Histone acetylation in response to hypoxia 68
4.1.2. Histone acetylation in response to *Phytoglobin1* down-regulation 69

4.1.3. Histone acetylation in response to nitric oxide in animal models 72
4.2. Histone deacetylase S-nitrosylation 73
4.3. Consequences of histone deacetylase S-nitrosylation.....75
4.4. Other epigenetic changes in response to hypoxia 79
4.4.1. DNA methylation in response to hypoxia 79
4.4.2. Histone methylation in response to hypoxia.....81
4.4.3. Nucleosome repositioning in response to hypoxia 82
4.5. Other epigenetic changes in response to nitric oxide.....82
4.5.1. DNA methylation in response to nitric oxide 82
4.5.2. Histone methylation in response to nitric oxide 83
4.5. The importance of antibody quality control.....85
4.6. Limitations 86
4.7. Future Work 88
4.8. Conclusion 88

5. REFERENCES.....90

SUPPLEMENTARY FIGURES 112

LIST OF FIGURES

Figure 1: Root developmental zones and the cell types within the root.. 4

Figure 2: Histone interaction with DNA within the nucleosome.....15

Figure 3: *Arabidopsis thaliana* H3.1 N-terminal sequence with acetyl groups bound to lysine 9, 14, and 27.....34

Figure 4: Oligopeptide dot blot assays determined the specificity of anti-H3K9ac and anti-H3K14ac antibodies.....35

Figure 5: Depiction of the trends in a typical linear curve where band intensity (RFU) is plotted against the amount of protein on the membrane (μg).....37

Figure 6: Immunoblot showing H3K9ac and H3K14ac band intensity when an increasing linear series of wild type normoxic cell lysate samples were loaded. 38

Figure 7: Immunoblot showing H3 band intensity when an increasing linear series of wild type normoxic cell lysate sample was loaded.....49

Figure 8: Immunoblots showing H3, H3K9ac and H3K14ac levels in root tips of Arabidopsis thaliana (Col-0) plants exposed to normoxia (N) or hypoxia (H) for 12 hours 51

Figure 9: Immunoblots showing H3, H3K9ac and H3K14ac levels in root tips of the 35S:PGB1 line, the Pgb1-RNAi line and the *pgb1-1* line exposed to normoxia (N) or hypoxia (H) for 12 hours.....58

Figure 10: Average (H/N) fold change values of both H3K9ac and H3K14ac of all biological and technical replicates at each of the four lines (wild type, 35S:PGB1, Pgb1-RNAi, and *pgb1-1*) .....

.....65

Figure 11: Proposed mechanism of hypoxia-induced increase in global H3K9 and H3K14 acetylation levels.....71

Supplemental Figure S1: Biological replicate 1 and biological replicate 2 (WT technical replicate 1-3, 35S:PGB1 technical replicates 1) of WT, 35S:PGB1, and Pgb-RNAi. 112

Supplemental Figure S2: Biological replicate 2 of the WT (tech. rep. 3-6), 35S:PGB1 (tech. rep. 2-4), and Pgb-RNAi lines (all tech. reps.).. 117

Supplemental Figure S3: Biological replicate 3 of the WT and Pgb1-RNAi lines, biological replicate 4 of the WT and 35S:PGB1 lines, and biological replicate 1 of the *pgb1-1* line.....121

Supplemental Figure S4: Biological replicate 5 of the WT and 35S:PGB1 lines, and biological replicate 2 of the *pgb1-1* line.. 128

LIST OF TABLES

Table 1: List of the peptides used to generate dot blots.. 24

Table 2: List of all the antibodies used.....27

Table 3: List of biological replicates, genotypes, and cell lysate protocols. 31

Table 4: Band intensity values and proportional protein conversions of all immunoblots detecting H3K9ac **(A)** and the corresponding immunoblots detecting the H3 loading control **(B)** 41

Table 5: Band intensity values and proportional protein conversions of all immunoblots detecting H3K14ac **(A)** and the corresponding immunoblots detecting the H3 loading control **(B)**. 45

Table 6: H3K9ac fold change levels in root tips of wild type Arabidopsis plants (Col-0) exposed to normoxia (N) or hypoxia (H).....52

Table 7: H3K14ac fold change levels in root tips of wild type Arabidopsis plants (Col-0) exposed to normoxia (N) or hypoxia (H).....54

Table 8: One-tailed t-test to assess whether (H/N) fold changes for each line (WT, 35S:PGB1, Pgb1-RNAi, and *pgb1-1*) at both histone PTMs (H3K9ac or H3K14ac) were statistically greater than 1.....55

Table 9: H3K9ac fold change levels in root tips of the 35S:PGB1 line exposed to normoxia (N) or hypoxia (H).....59

Table 10: H3K14ac fold change levels in root tips of the 35S:PGB1 line exposed to normoxia (N) or hypoxia (H). 60

Table 11: H3K9ac fold change levels in root tips of the Pgb1-RNAi line exposed to normoxia (N) or hypoxia (H).. 61

Table 12: H3K14ac fold change levels in root tips of the Pgb1-RNAi line exposed to normoxia (N) or hypoxia (H). 62

Table 13: H3K9ac fold change levels in root tips of the *pgb1-1* line exposed to normoxia (N) or hypoxia (H).. 63

Table 14: H3K14ac fold change levels in root tips of the *pgb1-1* line exposed to normoxia (N) or hypoxia (H).. 64

Table 15: Series of t-tests comparing H3K9 and H3K14 acetylation rates between the lines used (wild type, 35S:PGB1, Pgb1-RNAi, and *pgb1-1*), comparing the H3K9 and H3K14 acetylation rates within lines, and pooled acetylation (H3K9ac and H3K14ac) levels between the lines used. 67

LIST OF ABBREVIATIONS

ABA – Abscisic acid

ADH – Alcohol dehydrogenase

AGO1 – Argonaute1

AGO4 – Argonaute4

ATE – Arg-tRNA protein transferases

BR – Brassinosteroid

c-PTIO - 2-(4-Carboxyphenyl)-4,4,5,5-tetramethylimidazoline-1-oxyl-3-oxide

CBP – CREB-binding protein

COX – Cytochrome c oxidase

DNMT – DNA methyltransferases

DTT – Dithiothreitol

EDTA – Ethylenediaminetetraacetic acid

ERFVII – Group VII Ethylene Response Factor

GCN5 – General control nonderepressible 5

GNAT – GCN5-related N-acetyltransferase

GSNO – S-nitrosoglutathione

H3K14ac – Histone 3 lysine 14 acetylation

H3K27ac – Histone 3 lysine 27 acetylation

H3K9ac – Histone 3 lysine 9 acetylation

HD2 – HD-tuins 2

HDA19 – Histone deacetylase 19

HDA6 – Histone deacetylase 6

HDAC – Histone deacetylase

HRG – Hypoxia response genes

JmjC – Jumonji-C domain-containing

KAT – Lysine acetyltransferase

KDM – Lysine demethylase

miRNA – microRNA

MS – Murashige and Skoog

MYST - MO2-YBF2/SAS3-SAS2-TIP60

NO – Nitric oxide

NR – Nitrate reductase

PCO – Plant cysteine oxidase

PDC – Pyruvate decarboxylase

Pgb1 – Phytoglobin1

PLT – Plethora

PRC2 – Polycomb repressive complex 2

PRMT5 – Protein arginine methyltransferase 5

PRT6 – Proteolysis6

PTM – Post translational modification

QC – Quiescent center

RAM – Root apical meristem

RdDM – RNA-directed DNA methylation

ROS – Reactive oxygen species

RPD3/HDA1 – Reduced potassium dependency 3/histone deacetylase 1

SAM – S-adenosyl methionine

SCN – Stem cell niche

SDS-PAGE - Sodium dodecyl sulfate-polyacrylamide gel electrophoresis

SIR2-like – Silent information regulator 2

siRNA – small interfering RNA

SWI/SNF – Switch/Sucrose non-fermentable

TAF1 – TBP-associated factor

TBS – Tris-buffered saline

TBST – Tris-buffered saline with Tween-20

TSS – Transcription start site

VRN2 – Vernalization2

WOX5 – Wuschel-related homeobox 5

WT – wild type

ABSTRACT

Lee, Madeline Rose. M.Sc., The University of Manitoba, March 2026. **The influence of nitric oxide (NO) on histone acetylation in hypoxic *Arabidopsis thaliana* root tips**. Co-Supervisors: Dr. Claudio Stasolla and Dr. Jim Davie.

Climate change is increasing the frequency of flooding worldwide, which can damage crop plants by inhibiting gas exchange in below ground tissue. Low oxygen stress (hypoxia) in root tissue causes an increase in the levels of nitric oxide (NO) which interferes with epigenetic regulation through S-nitrosylation and inactivation of histone deacetylases such as HDA6. It is hypothesized that hypoxic stress could lead to an increase in both H3K9ac and H3K14ac because of elevated HDA6 S-nitrosylation by NO. To test this hypothesis the acetylation levels of lysine 9 and 14 of histone H3 (H3K9 and H3K14) were measured in root tips of WT plants and plants dysregulating the NO scavenger *PHYTOGLOBIN 1*. Low oxygen stress enhanced global acetylation levels H3K9 and H3K14. This effect was attenuated when *PGB1* was constitutively expressed and exacerbated when *PGB1* level was reduced. The Pgb1 modulation of H3K9ac and H3K14ac levels under hypoxia was consistent with NO being an epigenetic modifier in Arabidopsis root tips. The potential inhibition of HDA6 S-nitrosylation and mitigation of enhanced global levels of H3K9ac and H3K14ac by Pgb1 can protect the epigenome during hypoxic stress. Further understanding of the relationship between Pgb1 and the epigenome is important for elucidating how stress responses can be modified or accommodated to improve survival under waterlogging.

FORWARD

This thesis follows the paper style outlined by the Department of Plant Science and Faculty of Graduate Studies at the University of Manitoba. The manuscript follows the style recommended by the Journal of Plant Physiology. This thesis is presented as a single manuscript, containing an abstract, introduction, materials and methods, results, and discussion section. A literature review replaces the introduction of the manuscript, covering the broad background of research question. The discussion section also contains the conclusion, while supplemental figures and table are positioned after the body of the manuscript.

1. LITERATURE REVIEW

1.1. Introduction

1.1.1. Climate Change and Flooding

Warming of the oceans and atmosphere caused by the accumulation of greenhouse gases, as a result of climate change, has impacted global weather patterns (Ornes, 2018). One dangerous consequence of the changing climate is increased flooding, primarily driven by heavier, more frequent rainfall. Flooding events have increased in size by 20% and in frequency by 200% over the last 100 years (Swain *et al.*, 2020). Relative to undomesticated relatives, crop plants tend to be more susceptible to flooding because they are usually selected for high yield in low-stress environments (Mustroph, 2018). The effect of flooding on plant productivity and food security can be devastating. Between 2003 and 2013, 1.6 million tons of crops worldwide were damaged or destroyed by flooding, accounting for 57% of total crop loss from natural disasters (Rahman & Di, 2020). Flooding can result in complete plant submergence or waterlogging. Waterlogging occurs when the soil is saturated with water, but the photosynthetic tissue is above the water level. Both flooding and waterlogging have negative consequences for plant growth. In wheat, for example, 15-20% of global yield loss are caused by waterlogging (Nóia Júnior *et al.,* 2023). Excess moisture does not just impact large-scale farmers but also subsistence farmers who rely on their crop for year-round nutrition and are most vulnerable to weather unpredictability (Ngcamu, 2023). Waterlogging damages plant tissue, primarily by restricting its access to oxygen. However, it also restricts the movement of other gases, such as ethylene, CO_2, and nitric oxide (NO), which can be detrimental.

1.1.2. Flooding and gas dynamics

Oxygen is necessary for all aerobic organisms, including plants. Excess soil moisture limits oxygen exchange in submerged tissues, leading to a depletion of available oxygen. Normal oxygen conditions, defined as normoxia, are usually around 21% oxygen (Sasidharan *et al.,* 2017). However, under normoxic conditions, the oxygen level within plant tissues can vary significantly (van Dogen & Licausi, 2015). Tissues with significant cell proliferation, such as meristems, tend to have lower oxygen levels due to high rates of respiration (Greve *et al.,* 2003). The highly dividing region of the root maintains oxygen concentrations below 1% under normoxic conditions (Mira *et al.*, 2023a). Conversely, tissues that actively photosynthesize are less susceptible to low oxygen, as oxygen is produced as a byproduct (Loreti & Perata, 2020). When oxygen levels drop, cells initially become hypoxic and can eventually become anoxic. Hypoxia is characterized by below-normoxic oxygen concentrations (usually in the range of 1-5%, Sasidharan *et al.,* 2017). This range still allows some degree of biological functions. Anoxia describes a complete lack of oxygen, which is unlikely to occur in plants, because of the oxygen produced during photosynthesis (Mustroph & Albrecht, 2003). Hypoxic conditions are generally observed in roots when plants are waterlogged, but can also occur in photosynthetic tissues following partial or complete submergence. As a result, submergence is generally considered more detrimental than waterlogging (Visser *et al.,* 2003).

1.2. Hypoxia

Oxygen deprivation primarily affects the plant by inhibiting respiration, as oxygen is the terminal electron acceptor in aerobic respiration (Babcock, 1999). Hypoxic impairment of respiration leads to increased reliance on glycolysis and fermentation pathways (Mustroph & Albrecht, 2003). Oxygen availability is a central component of hypoxia, but gas exchange of

ethylene, CO_2, and nitric oxide (NO) can also be influenced by waterlogging. Unlike oxygen depletion, ethylene, CO_2, and NO tend to accumulate in waterlogged tissues (Liu *et al.,* 2022; Daniel & Hartman, 2024).

1.2.1. Hypoxia in roots

In instances of waterlogging or submergence, roots are often the first organs that experience an oxygen shortage (Sauter, 2013). Roots are composed of heterogeneous populations of cells and tissue types that, most likely, experience and respond to hypoxia differently. Understanding root cell and tissue heterogeneity is therefore central to comprehending the full breadth of root responses to hypoxia.

1.2.2. Root structure

Roots contain three developmental zones: the differentiation, elongation, and meristematic zones. The differentiation zone is where differentiation occurs and where root hairs begin to develop, the elongation zone is where cell elongation and expansion occur, and the meristematic zone is primarily where cells divide (Figure 1; Petricka *et al.*, 2012). Within the meristematic zone, the root apical meristem (RAM) maintains stem cell identity. The RAM contains the quiescent center (QC) surrounded by undifferentiated initials, which, through active proliferation, generate all the cell types of the root (Heyman *et al.,* 2014). The function of the QC is to confer an "undifferentiated state" to the adjacent initials; if the QC cells are damaged, the initials differentiate precociously (van den Berg *et al.*, 1997). Slow divisions of the QC cells are sometimes observed to replace nonfunctional initials (Strotmann & Stahl, 2021). The *Arabidopsis thaliana* (Arabidopsis) root contains about 20 initials: the lateral root cap initials, the columella initials, the cortex/endodermis initials, the pericycle initials, and the stele initials generating the vascular tissue (Figure 1; Jiang & Feldman, 2005).

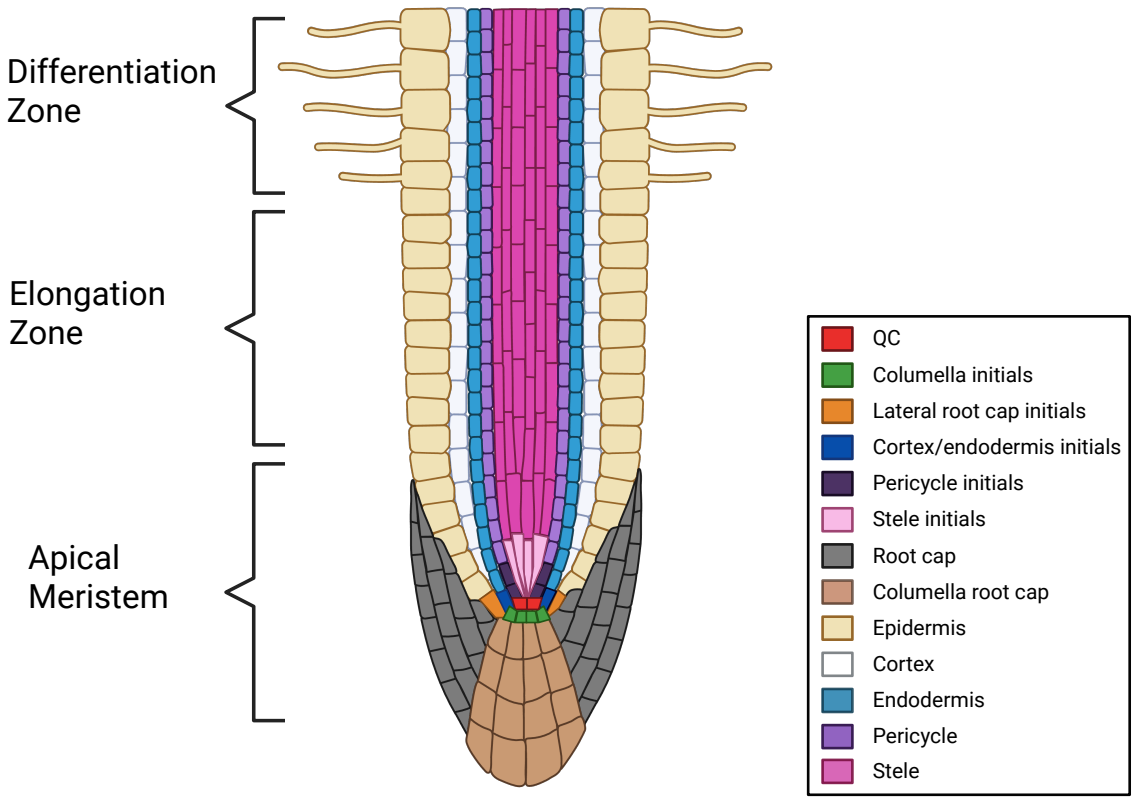

Figure 1: Root developmental zones and the cell types within the root. The apical meristem contains all the dividing cells and stem cells. The quiescent center (QC) is surrounded by actively dividing initials: columella initials, lateral root cap initials, cortex/endodermis initials, pericycle initials, and stele initials. The root cap below the meristem also contains the lateral root cap and the columella root cap. The elongation zone contains cells that are finished dividing but are still elongating to their final size. The differentiation zone contains cells actively differentiating. Both zones include epidermis, cortex, endodermis, pericycle, and stele. Created in https://BioRender.com.

The unique physiological environment that houses the QC and the initials is referred to as the stem cell niche (SCN) (Heyman *et al.,* 2014), whose function is regulated by plant growth regulators, including auxin and brassinosteroids (BRs) (Ackerman-Lavert *et al.*, 2021). Auxin is present as a gradient within the root tip, with high levels in the QC cells and lower levels in the actively dividing surrounding cells. Pharmacological and genetic studies have shown that the

auxin maximum in the QC is required for the state of quiescence, and perturbation of the auxin flow through dysregulation of the PIN-auxin transporters induces divisions of the QC cells with abnormalities in root growth (Friml *et al.*, 2003; Blilou *et al.*, 2005). The effect of auxin is counteracted by BRs and cytokinin, both of which enhance cell division by interfering with auxin levels through their influence on PIN protein dynamics (Hacham *et al.*, 2011; Zhang *et al.,* 2013).

1.2.3. The biochemical response to hypoxia

There are three main levels of hypoxia avoidance: biochemical, physiological, and morphological. Biochemical avoidance strategies usually employ changes in gene expression and/or protein dynamics to enable the plant to maintain baseline functioning under hypoxic conditions. Strategies to improve hypoxic stress tolerance may include a slowed metabolism to conserve energy, increased antioxidant production to mitigate oxidative stress, and upregulation of enzymes involved in fermentation to provide ATP in the absence of aerobic respiration (Zahra *et al.*, 2021). Physiological avoidance strategies include reduced stomatal conductance, decreased root permeability, and decreased photosynthetic rate (Parent *et al.*, 2008). Morphological avoidance strategies can include the formation of hypertrophied lenticels, aerenchyma, and adventitious roots (Leeggangers *et al.,* 2023). These mechanisms tend to reduce further oxygen loss and adjust the abundance of other gases, such as ethylene and CO_2.

As indicated above, flooding can affect plants primarily by restricting access to air and, consequently, to oxygen. Oxygen deprivation inhibits respiration, as oxygen is the terminal electron acceptor in aerobic respiration (Babcock, 1999). Hypoxic impairment of respiration leads to increased reliance on glycolysis and fermentation pathways (Mustroph & Albrecht, 2003). Alcoholic and lactic acid fermentation primarily replaces aerobic respiration through

increased expression of alcohol dehydrogenase (ADH), pyruvate decarboxylase (PDC), and lactate dehydrogenase (LDH; Perata & Alpi, 1993; Tadege *et al.,* 1999). Pyruvate, the product of glycolysis, under aerobic respiration would be oxidized and further processed in the mitochondria as a part of the TCA cycle. However, in ethanolic fermentation, pyruvate is instead decarboxylated into acetaldehyde by PDC in ethanolic fermentation (Jardine & McDowell, 2023). Some of the acetaldehyde is then reduced to ethanol to help regenerate NAD^+. In lactic acid fermentation pyruvate is converted to lactate using LDH. Ethanolic fermentation provides ATP and regenerated NAD^+ while lactic acid also provides ATP it also results in oxidation of NADH. Fermentation is less efficient than aerobic respiration and requires much more sugar to produce an adequate amount of usable energy. Yield is lowered from 36 ATP per glucose produced during aerobic respiration to 2-4 ATP produced during fermentation (Fukao & Bailey-Serres, 2004; Sauter, 2013). The decrease in ATP production disrupts essential cellular functions, including photosynthesis, nutrient intake and assimilation, hormone synthesis, and long-distance communication (shoot-to-root) (De Col *et al.*, 2017). It also leads to a rapid use of carbohydrate reserves. As carbohydrates begin to decline in root tissue, maintaining root growth becomes difficult (Sauter, 2013). If hypoxic conditions persist for long enough, the affected tissue will begin to die, and eventually, if the damage is severe, the plant itself will die (Loreti & Perata, 2020). Given the impairment of bioenergetic reactions in hypoxic environments, proliferating tissues with high energetic needs would be the first to be impacted.

1.2.4. The physiological response to hypoxia

Hypoxia caused by waterlogging can also affect physiological processes such as gas exchange and photosynthetic rate. Oxygen availability is a central component of hypoxia, but gas exchange of ethylene, CO_2, and NO can also be influenced by waterlogging (Daniel & Hartman,

2024). The diffusion of these gases is reduced in water-saturated soils, as with oxygen, often resulting in their accumulation within plant tissues, as they are produced in root tissue (Liu *et al.,* 2022; Daniel & Hartman, 2024). Ethylene is particularly important for the low oxygen response, as it slows down root extension to prevent growth in water-saturated soil (Liu *et al.,* 2022) and induces important morphological changes such as the formation of aerenchyma and adventitious roots (discussed in the next section; Leeggangers *et al.,* 2023).

Ethylene, a gaseous hormone, is normally released through the stomata and accumulates in water-saturated environments, leading to the activation of ETHYLENE-RESPONSE FACTORS (ERFs) that transduce ethylene responses (Xu *et al.*, 2008). The hypoxic response is known to be mediated by group VII ETHYLENE RESPONSE FACTOR (ERFVIIs), which are transcriptionally induced by ethylene (Gibbs *et al.,* 2015) and stabilized by low oxygen (Hartman *et al.*, 2019). ERFVIIs contribute to the hypoxic response by enhancing fermentation metabolism, enhancing the redox stress response, and by protecting against some of the negative effects that occur after normoxia is restored (Bailey-Serres *et al.*, 2012; Giuntoli & Perata, 2018). The conserved N-terminal domain on ERFVIIs contains methionine-cysteine residues (Licausi *et al.*, 2011). The methionine residue is cleaved by Methionine Aminopeptidases, which opens the cysteine residue for oxidative modification through Plant Cysteine Oxidases (PCOs) (Hu *et al.*, 2005; Weits *et al.*, 2014). The oxidized Cys is then arginylated by Arg-tRNA protein transferases (ATEs) and recognized by PROTEOLYSIS6 (PRT6), an N-end rule pathway E3 ligase. PRT6 targets the ERFVII for degradation through polyubiquitination (Gibbs *et al.*, 2011). In normoxic cells, there is ample oxygen to catalyze this reaction, and ERFVIIs are targeted for degradation; however, in hypoxic cells, as oxygen declines, ERFVIIs accumulate and orchestrate a transcriptional response (Gibbs *et al.*, 2011; Sasidharan & Mustroph, 2011). While ethylene is

the major regulator of ERFVIIs, other factors, such as cellular carbohydrates, energy status, plant hormones, cytosolic pH, calcium concentration, and ROS, fine tune their regulation (Daniel & Hartman, 2024). Although the production of ethylene is important for the hypoxic response, its over-accumulation can have negative effects on survival through the activation of programmed cell death within the root apical meristem (Mira *et al.*, 2016).

Like oxygen, CO_2 diffusion is also impaired in water-saturating environments. Voesenek & Bailey-Serres (2015) suggest that reduced CO_2 movement in submerged plants contributes to reduced photosynthesis, together with decreased stomatal conductance due to stomatal closure and the degradation of photosynthetic components. Waterlogging decreased the levels of chlorophyll a and b and carotenoids which was attributed to increased gene expression chlorophyll degradation enzymes (Anee *et al.*, 2019; Andrzejczak *et al.*, 2020). Waterlogging has also been shown to downregulate the enzyme Rubisco, the central enzyme of carbon fixation (Kuai *et al.*, 2014; Pan *et al.*, 2021).

1.2.5. The morphological response to hypoxia

Some morphological changes induced by hypoxia include stimulation of elongation of above ground organs, adventitious root formation, aerenchyma formation, and barrier formation in roots. Stimulation of elongation and development of adventitious roots, i.e., roots generated from non-root tissue, helps maintain above water atmospheric contact in tissues and organs (Parent *et al.,* 2008; Daniel & Hartman, 2024). Adventitious roots function to explore soil regions that are not saturated with water (Steffens & Rasmussen, 2015).

Aerenchyma are air pockets within plant tissues that allow for low resistance air movement of hypoxic tissues (Visser *et al.*, 2000**;** McDonald *et al.*, 2002**)**. Although aerenchyma can form through diverse mechanisms, the best characterized aerenchyma are called lysigenous

aerenchyma. The other types of aerenchyma form through cell enlargement or cell division, all of which create a gap between cells that can fill with air (Bailey-Serres & Voesenek, 2008). Lysigenous aerenchyma are formed through programmed cell death of the cortex tissue in the roots (Bailey-Serres & Voesenek, 2008). Programmed cell death in aerenchyma formation is thought to be induced by an increased ethylene, as ethylene biosynthesis is necessary for aerenchyma formation and was found to trigger aerenchyma formation (He *et al.*, 1996; Gunawardena *et al.*, 2001). Formation of lysigenous aerenchyma increases waterlogging stress tolerance by facilitating gas movement within the cortex. This results in increased movement of oxygen to the root tip and removal of gases than can accumulate in waterlogged tissue (CO_2, ethylene, NO; Evans, 2003)

Additionally, some species, generally wetland species, can form radial oxygen loss (ROL) barriers to limit oxygen diffusion in addition to aerenchyma formation (Daniel & Hartman, 2024). Radial oxygen loss barriers are mainly composed of suberin and are located in the outer cell layers including the epidermis (Ejiri *et al*., 2021). This barrier regulates water and nutrient movement into root tissues (Colmer, 2003). Development of aerenchyma primarily occur in adventitious roots that form following flooding (Colmer, 2003). The formation of structures such as aerenchyma and the ROL barrier to inhibit oxygen loss maintain sufficient oxygen at the root tip and support root elongation in hypoxic soil (Armstrong & Armstrong, 2005). Heterogeneity of root tissue impacts the area where adventitious roots, aerenchyma, and ROL barrier form. Adventitious roots are formed from non-root tissue, aerenchyma are formed within cortex tissue, and ROL barriers form around epidermal cells in root elongation and differentiation zones (Daniel & Hartman, 2024).

One of the earliest morphological events observed in hypoxic roots is the degradation of QC stem cells and growth inhibition, resulting from high ROS and ethylene accumulation (Mira *et al.*, 2016; 2023a). Degradation of the QC seen in hypoxic roots is largely controlled by a change in the auxin gradient necessary for root growth. Auxin is required for SCN specification. The QC needs a higher auxin concentration to maintain stem cell conformation (Yamoune *et al.*, 2021). Auxin controls QC development through its interaction with Wuschel-related homeobox 5 (WOX5) and Plethoras (PLTs; Blilou *et al.*, 2005). Both transcription factors confer a slow mitotic rate in QC cells; WOX5 specifically functions by suppressing cyclins 1 and 3 (Forzani *et al.*, 2014). In hypoxic roots, the auxin maxima dissipates because of PIN protein dysregulation (Mira et al., 2023b). In normoxic conditions, PIN proteins, primarily PIN1 and PIN4, direct auxin down the length of the root and cause it to accumulate in the RAM (Friml *et al.*, 2003; Vieten *et al.*, 2005). Without proper function of PIN proteins, auxin cannot accumulate and confer QC identity. This results in rapid cell division and cell degradation in the QC if the auxin maxima is not retained (Mira et al., 2023b).

1.3. Nitric oxide

Nitric oxide is a gaseous hormone that accumulates in waterlogging and submergence conditions. Its small size and lipophilic properties allow it to readily diffuse across the plasma membrane, making it an effective chemical messenger (Khan *et al.*, 2023). It is central to many important processes, including germination, root development, chlorophyll biosynthesis, vegetative growth, vascular differentiation, formation of symbiotic nodules, stomatal opening, iron homeostasis, senescence, and fruit ripening (Simontacchi *et al.*, 2015). Under various stress conditions, including hypoxia, physiological levels of NO can also help initiate and aid with stress responses (Rahim *et al.*, 2022; Khan *et al.*, 2023). The action of NO is often mediated by

other phytohormones, including auxin, abscisic acid, gibberellins, ethylene, and salicylic acid (Khan *et al.*, 2023).

NO can be produced through enzymatic and nonenzymatic reactions. The main route of enzymatic production is via cytosolic nitrate reductase (NRs), although other enzymes can also produce NO. Cytosolic nitrate reductase is induced under many stress conditions, such as hypoxia (Yamasaki *et al.*, 1999). Enzymes such as prohibitin 3 and cytochrome *c* oxidase (COX) are important in mitochondrial sensing of hypoxia, and COX contributes to NO production through nitrate reduction (Castello *et al.*, 2008; Kong *et al.*, 2018). Nitric oxide can also be produced nonenzymatically through the reduction of nitrate by antioxidants or reducing agents (Bethke *et al.*, 2004). It can also be produced as a byproduct of a reaction between nitrogen oxides and plant metabolites (Bethke *et al.*, 2004). The variety of pathways capable of producing NO contributes to the dynamic action of this signal molecule.

1.3.1. Nitric oxide and the hypoxic response

Under low oxygen stress, NO tends to accumulate to very high levels. This can disrupt the auxin maxima required for the maintenance of QC identity through its interaction with PIN proteins. Disruption of PIN-mediated auxin transport was shown by Mira *et al.* (2023a) to be caused by increased NO in hypoxic roots. Accumulation of NO increases root growth by decreasing the auxin maxima seen in the RAM (Sun *et al.*, 2018). Increasing NO inhibits the expression of several PIN proteins, disrupting auxin transport and the auxin gradient necessary for controlling the various cellular identities within the RAM (Guillotin & Binbaum, 2020). PIN1 has specifically been shown to interact with NO, leading to a reduction in PIN1 protein levels in a proteasome-independent manner (Fernandez-Marcos *et al.*, 2011). This disruption in the auxin gradient can be influenced by the protein Phytoglobin 1 (Pgb1) due to its ability to

scavenge NO (Mira et al., 2023b). Pgb1 reduces NO in hypoxic tissue, allowing the QC to remain functional (Mira et al., 2023b)

NO can also impact cellular dynamics by reacting with superoxide anions to form peroxynitrite. This molecule can induce post-translational protein modifications called S-nitrosylation, which mediates the majority of NO-mediated responses (Ageeva-Kieferle *et al.*, 2019; Khan *et al.*, 2023). S-nitrosylation specifically involves the addition of an NO group to a cysteine residue, but NO can also bind to protein metal centers and tyrosine residues (Ageeva-Kieferle *et al.,* 2019). The best example of NO action through protein S-nitrosylation is exemplified by its action on ERFVIIs. NO can act as an oxidizing agent alongside oxygen to modify ERFVIIs and target them for degradation through the N-degron pathway as described above (Gibbs *et al.*, 2014). When NO and/or oxygen increase, ERFVIIs become destabilized and are prone to degradation, thereby allowing downstream changes in transcription through targeted interactions (Gibbs *et al.,* 2015). Both nitric oxide and oxygen are required for ERFVIIs degradation through the N-degron pathway (Gibbs *et al.*, 2014). Increased NO, often induced by hypoxia, can dampen the hypoxic response by targeting the degradation of ERFVIIs.

1.4. Phytoglobin

To reduce the effect of NO under hypoxia, the cell can either downregulate NO production or upregulate phytoglobins (PGBs; Hebelstrup *et al.*, 2012; Chamizo-Ampudia *et al.*, 2017). Phytoglobins can be categorized into six types. These include nonsymbiotic hemoglobins (Phytogb0), class 1 nonsymbiotic hemoglobins (Phytogb1), class 2 nonsymbiotic hemoglobins (Phytogb2), class 3 nonsymbiotic hemoglobins (Phytobg3), symbiotic hemoglobins (SymPhytogb), and leghemoglobins (Lb) (Hill *et al.*, 2016). Phytogb1 or Pgb1 are the most well studied; they exhibit high oxygen affinity and are expressed under stress conditions such as

hypoxia (Dordas *et al.*, 2003; Gupta *et al.*, 2011). Phytogb2 or Pgb2 have a lower oxygen affinity than class 1 phytoglobins and are generally involved in development (Trevaskis *et al.*, 1997; Godee *et al.*, 2017). Phytogb3 or Pgb3 show sequence similarity to bacterial globins and are the least studied out of the three phytoglobins classes however class 3 phytoglobins have been implicated in NO-related pathways (Reeder & Hough, 2014; Mukhi *et al.*, 2016). Phytoglobin1, because of its well-known impact on NO dynamics during hypoxic stress is the focus of this study.

Pgb1 cycles through three forms as it scavenges NO (Das *et al.*, 1999). Once Pgb1 becomes oxygenated (Fe^{2+}), it can then rapidly react with NO to form nitrate (NO_3^-) to become metphytoglobin (Fe^{3+}). Metphytoglobin reductase then catalyzes the conversion of metphytoglobin back to the original form of phytoglobin, oxidizing NADH to NAD^+ in the process (Igamberdiev & Hill, 2004; Gupta *et al.*, 2011). Pgb1s are able to stabilize ERFVII proteins by scavenging and functionally removing NO (Dordas *et al.*, 2003; Perazzolli *et al.*, 2004). Pgbs are upregulated in hypoxic conditions by ERFVIIs, both of which are positive regulators of each other. In this way, ethylene can mediate NO levels independently of oxygen levels in hypoxic plants by upregulating Pgb1s (Hartman *et al.*, 2019).

Pgb1 can also confer a morphological advantage in hypoxic conditions through the protection of stem cell identity in the RAM. The RAM identity is maintained through the preservation of the auxin gradient and through efficient and rapid energy usage. Mira *et al.* (2023a) found that *PGB1* overexpression led to reduced degradation of the RAM through maintenance of the auxin maxima in the QC. The auxin maxima is maintained because Pgb1 mitigates NO-mediated PIN dysfunction (Mira et al., 2023b). Pgb1 can also mediate the biochemical effects of NO during hypoxia by reducing involvement of fermentation pathways on

energy production (Mira et al., 2023a). Mitochondrial machinery utilizes nitrite as an electron acceptor to both oxidize NADH/NADPH and generate ATP (Stoimenova *et al.*, 2007). This allows for greater energy production in hypoxic tissue and preserves the functionality of the tissue that is usually susceptible to it.

1.5. Plant epigenetics

Nitric oxide has been implicated to modulate epigenetic regulation in both plant and animal systems (Nott *et al.*, 2008; Mengel *et al.*, 2017; Ageeva-Kieferle *et al.*, 2021). Gaining an understanding of how NO can affect epigenetic regulation can provide insight into how the hypoxic response is initiated and how it can be modified by the action of Pgb1. Epigenetics is the regulation of gene expression through control over the three-dimensional organization of chromatin. The histone octamer is a protein complex that condenses and organizes nuclear DNA. It can be moved and modified to change DNA accessibility. Each histone octamer contains two copies each of H2A, H2B, H3, and H4 (Luger *et al.*, 1997). A stretch of DNA about 146 base pairs long wraps around each histone octamer. Histones are basic proteins caused by the higher amounts of lysine and arginine in their sequences. The most common histone modifications are acetylation and methylation, and these modifications are generally located on the N-terminal tails of histones, although globular domain modifications do exist (Strahl & Allis, 2000). Some common acetylation modifications on the N-terminal tail of H3 are depicted in Figure 2. These modifications are usually reversible and often exist in a dynamic relationship, interacting with one another through various chromatin-binding factors (Cheug *et al.*, 2000).

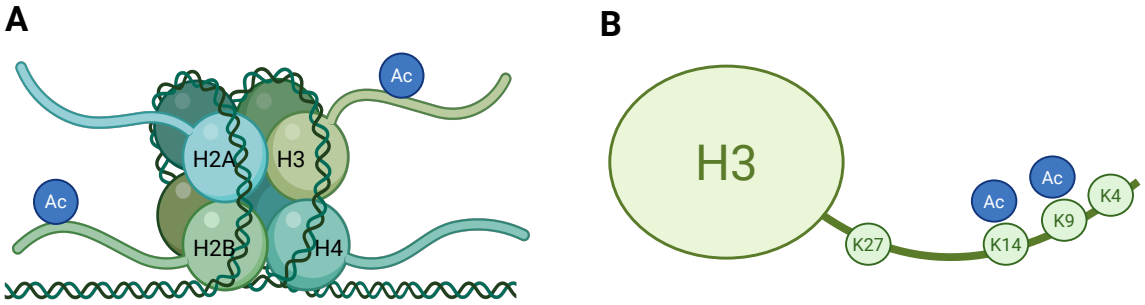

Figure 2: Histone interaction with DNA within the nucleosome. Nucleosome containing histones with acetylated N-terminal tails on the left (**A**). A closer view of histone H3 and its acetylated N-terminal tail is shown on the right (**B**). The acetylated lysines (K9 and K14) are common modifications associated with increased transcription. Created in https://BioRender.com.

1.5.1. Histone modifications

Histone acetylation is the addition of an acetyl group to amino acids such as lysine, serine, and threonine, although lysine acetylation is the most common. Acetylation marks tend to loosen histone association with DNA, allowing easier access for transcription factors (Pandey *et al.*, 2002). On the other hand, methylation tends to tighten histone-DNA association, reducing the potential for transcription of that region, although this is not always the case (Bannister *et al.*, 2002). Methylation on histone H3 lysine 4, for example, is a mark of transcriptionally active chromatin and associates with various acetylation marks (Beacon *et al.*, 2021). Histone methylation causes variable changes in chromatin conformation because methyl groups are small and uncharged. Additionally, multiple methyl groups can be added to the same amino acid because of the small size of methyl groups (Bannister & Kouzarides, 2011).

1.5.2. Histone variants and structures

Histone variants show some difference between plants and animals. Plant and animal histones are very similar in size and vary mostly in sequence (Borg *et al.*, 2021). Histones H3 and H4 are highly conserved between plants and animals, especially at the N-terminal end (Borg *et al.*, 2021). Histone H2B and histone H1 are the most divergent histones (Chaboute *et al.*, 1993). Histone H3 variants are highly conserved between plants and animals, while H2B variants are highly divergent (Borg *et al.*, 2021). Plants also lack the centromere-specific histone H3 variant CENH3; although histone H3.1 is enriched in pericentromeric regions, possibly filling the same role (Stroud *et al.*, 2012).

Histone structure also differs slightly between animals and plants; however, the function of the histones and their modifications are very similar. Many of the commonly studied histone marks confer similar chromatin conformations in plants, compared to those found in animals or yeast. For example, histone H3 lysine 4 methylation (mono-, di-, and tri-) will confer open chromatin, histone H3 lysine 27 and lysine 9 methylation will associate with closed/repressed chromatin (Feng & Jacobsen 2011). The various acetylation marks on the lysines within the N-terminal ends of histone 3 (K9, K14, K18, K23, K27, K36) and 4 (K5, K8, K12, K16, K20) have been reported to behave the same way as animal acetylation marks, associated with open chromatin (Berr *et al.*, 2011).

1.5.3. DNA methylation

DNA can also be methylated, which tends to confer tighter chromatin organization (Lewis & Bird, 1991). DNA methylation in plants is mainly initiated by the RNA-directed DNA methylation (RdDM) pathways and is enriched over transposable elements (Gallego-Bartolome, 2020). DNA methylation patterns differ from animal models in terms of the methylation patterns.

Methylation can be found in CG, CHG, and CHH patterning, where H is any base except guanine (Harris & Zemach, 2020). Distinct enzymes control these methylation patterns, confer distinct chromatin conformations, and associate with distinct transcriptional outcomes (Harris & Zemach, 2020). CG methylation in plants shows similar patterns when compared to animal CG methylation. DNA methylation is also more common in plants, as 14% of Arabidopsis cytosines are methylated, compared to 4% in humans (Capuano *et al.*, 2014).

1.5.4. Nitric oxide and epigenetics

As described above, NO is an important signaling molecule involved in many processes and has been found to influence a wide variety of genes involved in signal transduction, intracellular transport, cell death, metabolism, photosynthesis, transcription factors, ROS production, and ROS degradation (Polverari *et al.*, 2003; Panari *et al.*, 2004; Begara-Morales *et al.*, 2014). The broad nature of NO's effect on expression indicates that it influences multiple pathways (Ageeva-Kieferle *et al.*, 2019). NO can directly modify proteins important for certain physiological processes, such as photosynthesis (Ageeva-Kieferle *et al.*, 2021). It can also directly influence gene expression through S-nitrosylation of ERFVII transcription factors, as described above. However, there is still an opportunity for S-nitrosylation of other proteins that modulate transcription.

1.5.5. Histone acetylation and nitric oxide

Nitric oxide has been observed to affect histone acetylation dynamics. Upon application of the NO donor S-nitrosoglutathione (GSNO), global histone acetylation (including H3K9ac and H3K14ac) increased dramatically compared with treatment with both GSNO and the NO quencher carboxy-PTIO (Mengel *et al.*, 2017). The large-scale increase in histone acetylation was proposed to result from S-nitrosylation of histone deacetylases (HDACs). There are two

categories of enzymes that modify acetylation rates, HDACs and lysine acetyltransferases (KATs). Histone deacetylases remove acetyl groups while KATs add acetyl groups to histones. The increase of acetylation in response to NO can be caused by either a reduction of HDAC activity or the induction of KAT activity. Although either KATs or HDACs could be involved in this increase in acetylation, HDACs were chosen as the most likely candidate because work conducted in animal models shows HDAC inactivation in response to NO. HDAC (HDAC2) has been shown to reduce activity when S-nitrosylated at specific cysteine residues (Nott *et al*., 2008; Ageeva-Kieferle *et al.,* 2019).

1.5.6. Histone deacetylases and nitric oxide

Histone deacetylases are central regulators of chromatin structure and gene expression in developmental and stress responses. There are three families of HDACs in plants: RPD3/HDA1 (Reduced Potassium Dependency 3/histone deacetylase 1), HD2 (HD-tuins 2), and SIR2-like proteins (Silent Information Regulator 2; Kumar *et al.*, 2020). All three families contain a mix of nuclear and cytoplasmically located HDACs. Both SIR2-like proteins can localize to the nucleus, depending on the splicing variant (Jiang *et al.*, 2020). HD-tuins HD2A and HD2B can also localize to the nucleus (Han *et al.,* 2023). The RPD3-type family HDACs that are nuclear localized include HDA6, HDA9, HDA15, HDA18, and HDA19 (Fong *et al.*, 2006; Alinsung *et al.*, 2012; Kurita *et al.*, 2019).

The HDACs in the class I RPD3-type family (containing HDA6 and HDA19) are of particular interest because they are involved in diverse developmental and stress responses, and there is evidence that they can be modified by S-nitrosylation, like their human analogs (Ageeva-Kieferle *et al.*, 2019). Members of this HDAC family contain several cysteine residues that NO can modify. HDA6 and HDA19 show considerable homology with the sites on human HDAC2

that can be modified by NO (Cys262 and Cys274; Nott *et al.*, 2008; Ageeva-Kieferle *et al.,* 2019). Within the C-terminal region, there are 6 highly conserved cysteine residues, two of which (Cys262 and Cys274) are targets for NO in human HDAC2 (Ageeva-Kieferle *et al.*, 2019). When these sites are modified in human HDAC2, its catalytic activity is unchanged, but it stimulates its release from chromatin, leading to increased acetylation (Nott *et al.*, 2008).

The large-scale increase in histone acetylation seen after NO exposure is thought to be caused by S-nitrosylation of particular histone deacetylases (HDACs) in *Arabidopsis thaliana* (Ageeva-Kieferle *et al.*, 2019). This modification has the potential to alter the catalytic activity, DNA binding, or protein-protein interactions of HDACs, as NO does in human HDAC2 (Ageeva-Kieferle *et al.*, 2019). The effects of modifications on the activity of the enzyme will vary depending on which cysteine is modified, and comparing cysteine modification sites can help to explain why different HDACs may behave differently following S-nitrosylation. There are a few *Arabidopsis thaliana* HDACs similar in structure and sequence to human HDAC2. They include HDA19 and HDA6. The active site cystine in HDA19 (Cys 137) is in a similar position to the cystine at the active site at HDAC2 (Cys149). The cystines at each zinc finger domain (DNA-binding site) also remain fairly conserved in position when comparing HDA19 (Cys 256 and Cys 268) to human HDAC2 (Cys262 and Cys274; Ageeva-Kieferle *et al.,* 2019; Zheng *et al.*, 2023). Modifications at the active site may inhibit the removal of acetyl groups, while modifications at the zinc-finger domain may reduce the HDAC's binding efficiency to the chromatin.

There is direct evidence that both HDA6 and HDA19 are S-nitrosylated, and that this modification can alter their activity. When investigating how light intensity modifies histone acetylation, Ageeva-Kieferle *et al.* (2021) found that low light conditions can increase NO in

photosynthetic tissues and cause an increase in acetylation at H3K9ac and H3K14ac. HDA6 was identified as the cause of this acetylation increase because HDA6 activity decreased in response to low-light stress. Additionally, *hda6* mutants showed no change in acetylation in response to low-light stress (Ageeva-Kieferle *et al.*, 2021). Ageeva-Kieferle *et al.* (2021) showed that HDA6, when s-nitrosylated, decreases its activity, leading to global increases in acetylation.

HDA19, unlike HDA6, was found to increase activity when S-nitrosylated (Zheng *et al.*, 2023). Zheng *et al.* (2023) also found that the modified cysteines differed from what was predicted by comparing HDA19 to human HDAC2. Cys137 was identified as the most important target of NO in HDA19, rather than Cys262 or Cys274 (Ageeva-Kieferle *et al.*, 2019; Zheng *et al.*, 2023). S-nitrosylation of Cys137 was indicated to be important for activating HDA19 deacetylase activity, and when activated, HDA19 deacetylated H3K14ac marks on genes related to oxidative stress response (Zheng *et al.*, 2023). This is inconsistent with other results on human HDAC2, as S-nitrosylation decreases its activity (Nott *et al.*, 2008). This is also inconsistent with previous work in *Arabidopsis thaliana,* because as HDACs became S-nitrosylated acetylation levels increased (Mengel *et al.*, 2017).

HD2 is a plant-specific group of histone deacetylases. They were first discovered in maize and play a role in development and stress responses. Although there is no indication that this family of HDACs interacts with NO or participate in the hypoxic response, there is evidence that the HD2 family HDACs HD2A, HD2C, and HD2D can interact with HDA6 and HDA19 (Luo *et al.*, 2012). This indicates that they can coexist within the same complex, potentially influencing one another (Luo *et al.*, 2012).

HDACs can be inhibited by hypoxia through factors other than NO, such as changes in redox potential. Sirtuins, a group of histone deacetylases, are dependent on NAD^+ for

deacetylase activity (North & Verdin, 2004; Kumar *et al.*, 2020). NADH increases in hypoxia because the conversion of NAD^+ back to NADH requires oxygen (Yan *et al.*, 2020). With decreased access to NAD^+, the activity of Sirtuins during hypoxia is diminished. In Arabidopsis, Sirtuin 1 (SRT1) is a negative regulator of the stress response and glycolysis; when NAD^+ is depleted in hypoxic tissue, SRT1 loses its activity, stress response genes are activated, and glycolytic enzymes are activated (Liu *et al.*, 2017). Sirtuin 2 (SRT2) has primarily been reported as a negative regulator of pathogen response by downregulating salicylic acid biosynthesis (Wang *et al.*, 2010). Increased salicylic acid biosynthesis is seen in hypoxic plants through the action of the ERFVII transcription factor RAP2.12 and is thought to contribute to tissue regeneration (Bagautdinova *et al.*, 2022; Chirinos & Licausi, 2024).

1.5.7. Phytoglobin1 and histone acetylation

Although there is no direct evidence of how Pgb1 may affect acetylation rates, a relationship is possible. As mentioned above, Pgb1 can scavenge NO by converting NO to nitrate ($NO3^-$; Igamberdiev *et al.,* 2004). NO is responsible for an increase in histone acetylation, and the increase in histone acetylation is thought to be caused by S-nitrosylation and deactivation certain HDACs (HDA6 and/or HDA19; Mengel *et al.*, 2017; Ageeva-Kieferle *et al.*, 2019). Therefore, Pgb1, like cPTIO, should be able to reduce histone acetylation and maintain HDAC activity through its ability to scavenge NO.

1.6. Hypothesis

Hypoxia can elevate histone acetylation at H3K9 and H3K14 through the S-nitrosylation and inactivation of HDACs. The hypoxia-induced elevation in H3K9 and H3K14 acetylation can be mediated by Phytoglobin1 (Pgb1), through its ability to scavenge NO in *Arabidopsis thaliana* roots.

1.7. Thesis objectives

To test the hypothesis, antibody quality control was first performed to ensure accurate and reproducible immunoblot results. Subsequently, a WT (Col-0) Arabidopsis line was subjected to hypoxia and extracts from root tissue were immunoblotted for H3K9ac and H3K14ac to assess global acetylation levels in response to hypoxia. Finally, the effects of Pgb1 on H3K9 and H3K14 acetylation were determined using three transgenic lines, one that constitutively expressed *PGB1* (35S:PGB1), one with RNAi-mediated downregulation (Pgb-RNAi), and a Pgb1 T-DNA insertion knockout line (*pgb1-1).* These lines were subjected to hypoxia and the extracted cell lysates immunoblotted for both H3K9ac and H3K14ac.

2. MATERIALS AND METHODS

2.1 Plant material

All work was done with *Arabidopsis thaliana*. The experiment used a wild type (Col-0) line, a line overexpressing [35S:Pgb1] or down-regulating (Pgb1-RNAi) *PHYTOGLOBIN 1* (Hunt *et al.* 2002, Hebelstrup *et al.* 2007), as well as *pgb1* T-DNA insertion mutant line (*pgb1-1*, Hartman *et al.*, 2019). Every transgenic line used was a product of stable transformation completed through Agrobacterium based floral dip method. The Pgb1-RNAi line used the Hellsgate vector, while the 35S:PGB1 line and the *pgb1-1* line both used unnamed bacterial expression vectors (Hunt *et al.*, 2002; Alonso *et al.*, 2003; Hebelstrup et al., 2006). The 35S:Pgb1 line constitutively expresses *PGB1* with the cauliflower 35S promoter; the transcript expression level of *PGB1* was about 2 times higher relative to WT and this increase results in an elevation of the Pgb1 protein (Hartman *et al.*, 2019; Mira et al., 2023b). Compared to WT, Pgb1 protein levels were decreased by about half in the Pgb1-RNAi line (Mira et al., 2023b) and completely abolished in the *pgb1-1* line harboring a T-DNA insertion around 300 bp upstream from the *PGB1* start codon (Alonso *et al.*, 2003; Hartman *et al.*, 2019). While the Pgb1-RNAi line still contained 2-3% of the *PGB1* transcript levels observed in WT, the *pgb1-1* line completely lacks *PGB1* transcripts (Hebelstrup et al., 2006; Hartman *et al.*, 2019).

Seeds were sterilized with 70% ethanol and 0.05% (v/v) Triton X-100 and placed in a straight line on square Petri plates containing ½ Murashige and Skoog (MS) media. Plants were kept for 24 hours at 4°C, and then grown for 7-10 days under 18 hours light / 6 hours dark at 22°C. When plants reached 6-8 cm in length, they were subjected to either normoxic or hypoxic treatment. The Petri plates were transferred into a desiccator flushed with ambient air (normoxia) or 4% oxygen (hypoxia) for 12 hours (from 9 pm to 9 am). The desiccator was first flashed with

gas at 9 pm to fill it, and then again at 6 am to ensure a consistent oxygen percentage. Once the treatments were completed, the bottom 1 cm of the roots was collected and immediately frozen in liquid nitrogen. Samples were kept at –80°C until processed.

2.2 Antibody quality control

2.2.1 Dot blots

Dot blots were generated by pipetting 0.2 μg, 0.1 μg, 0.05 μg, and 0.02 μg of synthetic oligopeptides (listed in Table 1) onto a nitrocellulose membrane, which was then incubated at 65°C for 20 minutes in a micro hybridization incubator (Robbins Scientific model 2000). The blots were then incubated in 5% (w/v) skim milk in Tris-buffered saline (20 mM Tris base, 150 mM NaCl with Tween-20 (0.1% (v/v)); TBST) blocking solution for 30 minutes at room temperature. The blots were then processed as Western blots (described below). The primary antibodies tested (listed in Table 2) were either targeting H3K9ac or H3K14ac. For both antibodies, the same panel of N-terminal histone H3 oligopeptides was used: oligo-H3, oligo-H3K9ac, oligo-H3K14ac, and oligo-H3K27ac (Table 1). Oligo-H3 contains the first 19 amino acids in the H3 sequence; however, oligo-H3K9ac, oligo-H3K14ac, and oligo-H3K27ac peptide sequences were not disclosed.

Table 1: List of the peptides used to generate dot blots. All peptides were diluted from their original concentration of 1 μg/μl to 0.1 μg/μl. The oligo-H3 peptide was the only peptide that had a disclosed sequence.

Oligopeptide	Company	Catalog number	Lot number	Peptide Sequence
Oligo-H3	Abcam	ab7228	GR128273-1	ARTKQTARKSTGGKAPGGC
Oligo-H3K9ac	Abcam	ab16635	GR222358-1	Undisclosed
Oligo-H3K14ac	Abcam	ab112547	GR245563-1	Undisclosed
Oligo-H3K27ac	Abcam	ab24404	GR221083-1	Undisclosed

2.2.2 Linear Curves

The immunoblots used to generate the linear curves were made by pipetting an increasing series of wild type normoxia-treated cell lysate samples into an SDS-PAGE (sodium dodecyl sulfate polyacrylamide gel electrophoresis) gel. The SDS gels were electrophoresed and subsequently treated as Western blots and then imaged using the same methods listed below. Once imaged, the blot bands displaying protein signal were quantified using the technique described below. Band intensity was calculated using band volume and band area values (band intensity = band volume/ band area) provided by the Azure SpotPro software. Immunoblots with a range shorter than adequate (4 to 5 lanes between 5 µg and 25 µg) were run to generate preliminary linear curves. Once quantified, these immunoblots were used to approximate the linear detection range for each corresponding antibody. Preliminary linear curves contained a short linear portion and either a slight band under or oversaturation. A full linear curve was generated then by extending the linear range observed in the shorter linear curve in a subsequent immunoblot.

Immunoblots generated for the full linear curve contained an extended range of cell lysate protein loading values, both well above and below what each antibody was capable of detecting. This ensured that each immunoblot captured the undersaturated, linear, and oversaturated ranges. If the linear curve did not contain either under or oversaturation, the blot was repeated to ensure the full detection range of each antibody was captured. The H3K9ac and H3K14ac band intensities were plotted against the amount of cell lysate protein on the nitrocellulose membrane. The linear section of the standard curve was isolated and used to create a linear equation ($y = mx + b$; where y was band intensity and x was the amount of protein on the

membrane). Any band intensity values outside of the designated linear range of each antibody were removed from the data set.

Protein loading values used for Western blot analysis were determined using the linear equations described above. The linear portion of the standard curve was used to estimate the optimal protein loading that would maintain immunoblot linearity in subsequent analyses. An increase in H3K9 and H3K14 acetylation levels in response to hypoxia was hypothesized. This would most likely lead to excessive saturation in hypoxia-treated samples. The linear curves were created using wild type normoxia-treated samples. To mitigate oversaturation in hypoxia-treated samples, protein loading was set to values at the beginning of the linear detection range. This allowed for an increase in H3K9 and H3K14 acetylation levels to be measured while still maintaining linear detection within normoxia-treated samples.

Each antibody had a different linear detection range and, therefore, different protein loading values. To ensure proportionality when comparing protein levels in further analysis, immunoblot band intensities were normalized to the standard curve. Linear models were used to convert the immunoblot band intensities to proportional protein values. Band intensity values ascertained from immunoblot quantification (described below) were used as the y-value in the linear equations and proportional protein values were calculated by solving for the x-value.

A loading control immunostained with antibodies against H3 was used to ensure accurate and reproducible qualitative immunoblot data (Table 2). The use of H3 as the loading control allowed comparison of H3 levels with and H3K9 or H3K14 acetylation levels. A linear curve and a linear equation were created for this antibody utilizing the same technique described above. The linear equation was used to normalize immunoblot band intensity by converting these values to their

proportional protein values. This ensured that fold changes seen in both H3K9ac and H3K14ac immunoblots could be effectively normalized for loading.

Table 2: List of all the antibodies used. Histone H3 antibody lot #: 1031351-9 was used for wild type, 35S:PGB1, and Pgb-RNAi lines (Bio Rep 1-3) while lot#: 1084399-8 was used for wild type and 35S:PGB1 lines (Bio Rep 4-5) and the *pgb1-1* line (Bio Rep 1-2). H3K9ac antibody lot #: 1069519-4 was used for wild type, 35S:PGB1, and Pgb-RNAi lines (Bio Rep 1-3) while lot#: 1088902-6 was used for wild type and 35S:PGB1 lines (Bio Rep 4-5) and the *pgb1-1* line (Bio Rep 1-2). H3K14ac antibody from Invitrogen lot#: ZD4295643A was used for wild type, 35S:PGB1, and Pgb-RNAi lines (Bio Rep 1). H3K14ac antibody from Abcam lot #: 1029948-47 was used for wild type, 35S:PGB1, and Pgb-RNAi lines (Bio Rep 2-3), while lot#: 1029948-53 was used for wild type and 35S:PGB1 lines (Bio Rep 4-5) and the *pgb1-1* line (Bio Rep 1-2).

Antibody Target	Company	Catalog number	Lot Number	Dilution	Host	Clonality
Histone H3	Abcam	ab10799	1031351-9	1:1000	mouse	monoclonal
Histone H3	Abcam	ab10799	1084399-8	1:1000	mouse	monoclonal
H3K9ac	Abcam	ab32129	1069519-4	1:1000	rabbit	monoclonal
H3K9ac	Abcam	ab32129	1088902-6	1:1000	rabbit	monoclonal
H3K14ac	Invitrogen	MA5-32814	ZD4295643A	1:1000	rabbit	monoclonal
H3K14ac	Invitrogen	MA5-32814	AB4640083A	1:1000	rabbit	monoclonal
H3K14ac	Abcam	ab52946	1029948-47	1:1000	rabbit	monoclonal
H3K14ac	Abcam	ab52946	1029948-53	1:1000	rabbit	monoclonal
Anti-Mouse	Invitrogen	31430	YD375335	1:50000	goat	polyclonal
Anti-Rabbit	Invitrogen	32460	YK375337	1:1000	goat	polyclonal

2.3 Western blotting

For Western blotting, samples were processed using one of the two cell lysis protocols: *Protocol A* or *B*. A full list of both biological replicates and the corresponding cell lysate protocol is presented in Table 3. Only three biological replicates were completed for the Pgb-RNAi line as it was replaced by *pgb1-1* in subsequent treatments. The *pgb1-1* line only contained two biological replicates because the line was obtained at a later time.

Protocol A: The plant cell lysis buffer contained 50 mM Tris-HCl (pH 7.4), 150 mM NaCl, 1% (w/v) SDS, 1 mM EDTA, 1 mM DTT, and Pierce protease and phosphatase inhibitor tablets (cat#: A32961) added immediately before extraction. The tissue was ground in liquid nitrogen for no more than 1 minute and then added to the lysis buffer, approximately 500 µL of buffer per 1 g of tissue. The ratio of 500 µL per 1 g of tissue allowed for a final protein concentration of 2-4 µg/µL. The mixture was then briefly mixed and left on ice for 15 minutes. After the mixture was centrifuged at 15,000g for 10 minutes, the supernatant was collected.

Protocol B: RIPA buffer (used as cell lysis buffer) from Thermofischer (cat#: 89901, lot#: AB405091) and Pierce protease and phosphatase inhibitor tablets (cat#: A32961) were added before extraction began. The tissue was ground in liquid nitrogen for no more than 1 minute and then added to the lysis buffer, approximately 500 µL of buffer per 1 g of tissue. The ratio of 500 µL per 1 g of tissue allows for a final protein concentration of 2-4 µg/µL. The mixture was then sonicated for 10 seconds using the Sonic Dismembrator (Fischer Scientific model 100), followed by a 30-second rest period. This cycle of sonication followed by a rest period was repeated three times. The mixture was not centrifuged; it was found that centrifugation led to a loss of histones within the pellet. However, protocol B yielded protein concentrations similar to those of protocol A.

Cell lysates obtained using protocols A and B were processed as follows. Cell lysates were boiled for 5 mins after the addition of an equal volume of 2X SDS loading buffer (1.25 mM Tris-HCl (pH 6.8), 3% (w/v) SDS, 10% (v/v) glycerol, 20 mg/mL Bromophenol Blue 2%, 5% (v/v) β-mercaptoethanol) before electrophoresis on an SDS-PAGE gel. The SDS-PAGE gels had a 15% acrylamide resolving layer and a 4% acrylamide stacking layer. The gel was

electrophoresed at 200V for about 1h, until the bromophenol blue dye was electrophoresed from the gel.

Once the SDS-PAGE gel was electrophoresed, the gel was semi-dry transferred with the Trans-Blot Turbo Transfer System (Biorad cat# 1704150) to a nitrocellulose membrane. The blot was then stained with Ponceau S (0.5% Ponceau S (w/v) and 5% acetic acid (v/v)) and true color imaged using the Azure 400 imager (Azure Biosystems cat#: AZI400-01) to assess transfer quality. After staining the blots with Ponceau S, the blots were incubated in 5% (w/v) skim milk in Tris-buffered saline (20 mM Tris base, 150 mM NaCl) with Tween-20 (0.1% (v/v); TBST) blocking solution for 2 hours at room temperature. The blots were then washed once in TBST before being added to 3% (w/v) skim milk TBST blocking solution with primary antibody (anti-H3, -H3K9ac, or –H3K14ac; Table 2). The primary antibody was added to the 3% (w/v) skim milk TBST blocking solution at a 1:1000 dilution. The blot was sealed in plastic bags with the primary antibody and incubated at 4°C overnight. After removal from the primary antibody, the blot was washed 3 times in TBST for 5 minutes each. The blots were then placed in 3% (w/v) skim milk TBST with the secondary antibody (Table 2). The blots were incubated with the secondary antibody at room temperature for 1 hour. After secondary antibody incubation, the blots were again washed 3 times with TBST for 5 minutes and rinsed with Tris-Buffered Saline (20mM Tris base, 150mM NaCl; TBS) to remove residual Tween-20. The blots were then imaged by pipetting 300 µL-1 mL of ECL (Froggabio cat#: CCH345-B100ML) on top of the blot and imaged in the Azure 400 imager (cat#: AZI400-01), using 2-4-minute UV exposure.

The immunoblots were imaged by pipetting 300 µL-1 mL of ECL (Froggabio cat#: CCH345-B100ML) on top of the blot and imaged in the Azure 400 imager (cat#: AZI400-01), using 2-4-minute UV exposure. The blot images were then quantified using the Azure SpotPro

software on the Azure 400 imager. The TIFF file version of the image was uploaded to the software, where the lanes were selected, and the background was mitigated using Rolling Ball set to 6. The software then selected bands and provided both the band volume and area values. These values were then used to calculate band intensity (band intensity = band volume / band area).

The proportional protein values for both immunostained test proteins (H3K9 or H3K14 acetylation) and the immunostained loading control were calculated using the linear models described above. Normalization of the test protein levels was completed by dividing the test protein (H3K9ac or H3K14ac) proportional protein value by the corresponding immunostained loading control (H3) proportional protein value. The normalized ratio of each hypoxic sample was divided by the corresponding normalized normoxic ratio (H/N). The H/N ratio represents the change in H3K9 and H3K14 acetylation levels in response to hypoxia treatment.

Table 3: List of biological replicates, genotypes, and cell lysate protocols. 35S:PGB1 biological replicate 3 did not have enough root material to analyze. Pgb1-RNAi line only had 3 biological replicates because it was replaced with *pgb1-1* in later treatments; *pgb1-1* was acquired later. Cell lysate protocol A was only utilized for the first biological replicates (excluding *pgb1-1*). Cell lysate protocol B was used for all subsequent replicates.

Genotype	Biological Replicate #	Cell Lysate Protocol
wild type	1	A
wild type	2	B
wild type	3	B
wild type	4	B
wild type	5	B
35S:PGB1	1	A
35S:PGB1	2	B
35S:PGB1	4	B
35S:PGB1	5	B
Pgb1-RNAi	1	A
Pgb1-RNAi	2	B
Pgb1-RNAi	3	B
pgb1-1	1	B
pgb1-1	2	B

2.4 Data analyses

First, a one-tailed t-test was completed to assess whether H3K9ac and H3K14ac fold changes were significantly more than one. Normalized fold change values were further assessed for statistical significance using an unpaired t-test. The unpaired two-tailed t-test was used to compare both H3K9ac and H3K14ac levels between the transgenic lines (Col-0, 35S:PGB1, Pgb1-RNAi, and *pgb1-1*). Then H3K9 and H3K14 acetylation levels were compared with a two-tailed t-test within the same transgenic line. Finally, H3K9 and H4K14 acetylation levels were pooled together within each genotype, then genotypes were again assessed for significance with one-tailed t-tests and compared against each other with two-tailed t-tests.

3. RESULTS

3.1. Antibody quality control

To ensure that selected antibodies specifically detected H3K9 or H3K14 acetylation sites, antibody quality control measures were performed. Non-specific binding to other histones or other histone acetylation sites would negatively impact the ability of Western blot analysis to represent both H3K9 and H3K14 acetylation levels accurately.

3.1.1. Dot blots

Dot blots were performed to ensure antibody specificity to either H3K9ac or H3K14ac. All primary antibodies tested were monoclonal. Antibodies bind to an epitope 5-8 amino acids long. The amino acid sequence surrounding H3K9ac is similar to the sequence surrounding H3K27ac, both histone posttranslational modifications (PTMs) share an identical 4 amino acid sequence (Figure 3; Chaubet *et al.,* 1992). The sequence similarity surrounding H3K9ac and H3K27ac caused some antibodies that detect H3K9ac to also detect H3K27ac (Bock *et al.,* 2011). H3K14ac did not share a similar sequence with lysine residues on the H3 N-terminal tail. To ensure specific detection, the antibodies were tested using synthetic oligopeptides (described in the Materials and Methods). The oligopeptides had approximately a 19 amino acid sequence portion of histone H3 with no modifications (oligo-H3) or a single modification added (oligo-H3K9ac, oligo-H3K14ac, and oligo-H3K27ac) (shown in Table 1). The H3K9ac antibody only detected oligo-H3K9ac and did not detect oligo-H3, oligo-H3K14ac, or oligo-H3K27ac peptides (Figure 4A). Both H3K14ac antibodies only detected oligo-H3K14ac and did not detect oligo-H3, oligo-H3K9ac, or oligo-H3K27ac peptides (Figure 4B).

Bock *et al.* (2011) tested specificity of antibodies targeting histone PTMs; some antibodies showed cross-reactivity with other histone PTMs, and most were inhibited by additional PTMs proximal to the primary one. Additionally, Egelhofer *et al.* (2011) found that 25% of the antibodies raised against various histone modifications failed cross reactivity tests. Cross-reactivity to PTMs on other histones or other non-histone proteins can be almost entirely ruled out by Western blotting. In this case, because a cell lysate was used, the presence of more than one band on the immunoblot would indicate non-specific binding, potentially to both histone and non-histone proteins. However, if there was non-specific binding to proteins of a similar size to histone H3, differentiating the histone H3 band from the non-specific protein band would prove difficult. Subsequent dot blot assays would indicate cross-reactivity in similarly sequenced histone PTMs as explained above. However, the dot blot assays performed were not exhaustive, as only three histone PTMs were tested for cross-reactivity. To ensure cross-reactivity was completely absent, dot blot assays would need to be completed with a larger panel of acetylated lysine residues on H3.

Additionally, other histone PTMs adjacent to the test histone PTM may block antibody binding to the epitope. This process is called occlusion. Dot blots utilizing peptides with multiple PTMs adjacent to the test histone PTM would need to be used to ensure the antibody detects the test histone PTM regardless of adjacent histone PTMs.

Figure 3: *Arabidopsis thaliana* H3.1 N-terminal sequence with acetyl groups bound to lysine 9, 14, and 27. The amino acid sequences surrounding H3K9ac and H3K27ac, highlighted in yellow, contain an identical 4 amino acid sequence. Created in https://BioRender.com.

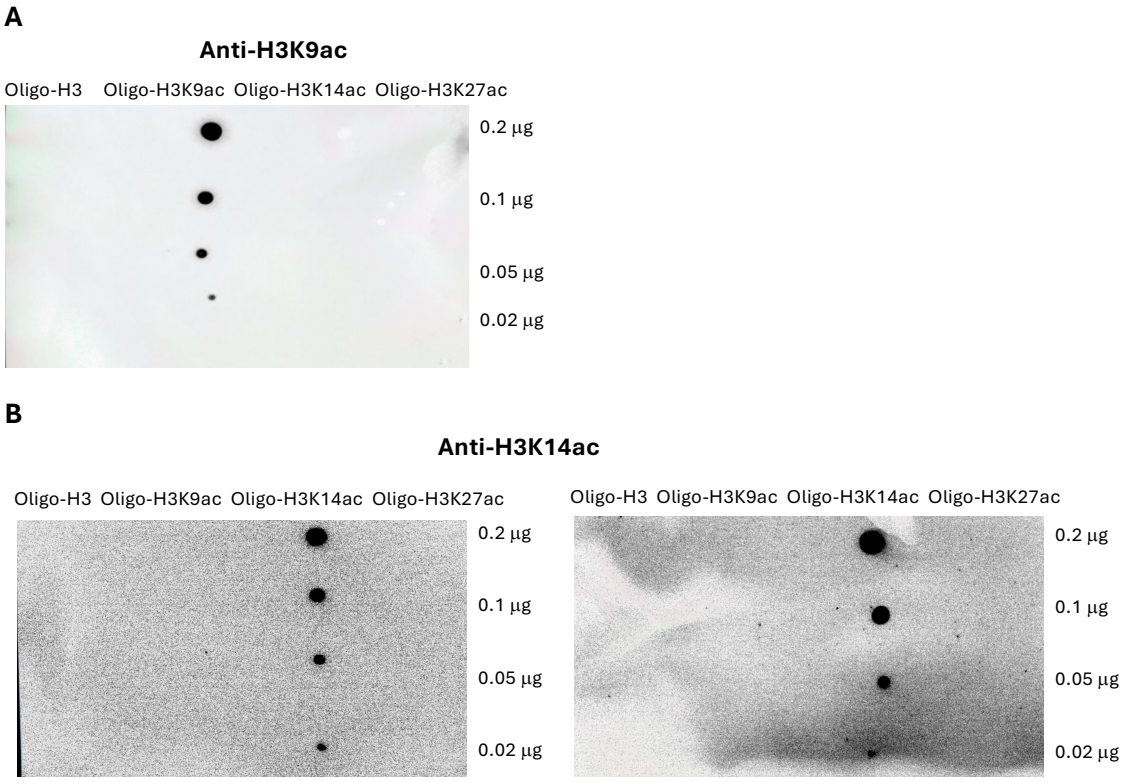

Figure 4: Oligopeptide dot blot assays determined the specificity of anti-H3K9ac and anti-H3K14ac antibodies. Oligopeptides used were listed in Table 1 **(A)** The dot blot assay used Abcam cat # ab32129 lot # 1069519-4 at a 1:2000 dilution as the primary antibody and Invitrogen cat # 32460 lot # YK375337 at a 1:2000 dilution as the secondary antibody. **(B)** The dot blot in the left panel used Invitrogen cat # MA5-32814 lot # AB4640083A at a 1:2000 dilution as the primary antibody and Invitrogen cat # 32460 lot # YK375337 at a 1:2000 dilution as the secondary antibody. The dot blot assay in the right panel used Abcam cat # AB52946 lot # 1029948-47 at a 1:2000 dilution as the primary antibody and Invitrogen cat # 32460 lot # YK375337 at a 1:2000 dilution as the secondary antibody. The amount of oligopeptide placed on the nitrocellulose membrane is indicated on the right.

3.1.2 Linear curves

Generally, Western blots can be used for both qualitative and quantitative analyses. Qualitative Western blot analyses demonstrate significant changes in protein or histone PTM levels that are visible to the naked eye. Identification and quantification of subtle changes in proteins or histone PTMs required additional steps to ensure that data collected from immunoblotting was robust and reproducible (Butler *et al.*, 2019). For quantitative analysis to be

possible, the immunoblot band intensities must reflect the amount of histone modification on the membrane. One essential step in ensuring reproducible quantitative immunoblotting is the creation and use of linear curves.

Linear curve plots were created to identify a proportional relationship between protein loading values and immunoblot signal detection. The curve plots generally consist of three parts: undersaturated, linear, and oversaturated. Undersaturation occurs when the band intensity signal falls below the detection limits of the chemistry or imaging systems. In contrast, oversaturation occurs when the band intensity signal exceeds the detection limits of the chemistry or imaging systems (Pillai-Kastoori *et al.*, 2020). The example of a linear curve in Figure 5 shows little increase between 2 μg and 4 μg, a linear increase between 4 μg and 8 μg and no further increase after 8 μg. The linear region between 4 μg and 8 μg represents the proportional relationship between protein on the membrane and band signal intensity. Band intensity is the ratio of band volume/band area, and when detection is linear, it represents the amount of protein or histone PTM on the membrane. In this experiment, immunoblots were performed to generate a proportional linear model representing the relationship between the amount of H3K9 or H3K14 acetylation on the membrane and band intensity (Figure 6A). Once the linear sections of each linear curve were identified (Figure 6B), the corresponding linear equation for anti-H3K9ac (Abcam cat# ab32129, lot#1088902-10) was $y = 4.17x - 14.33$ and the corresponding equation for anti-H3K14ac (Abcam cat# ab52946, lot#1029948-53), was $y = 2.39x - 11.99$.

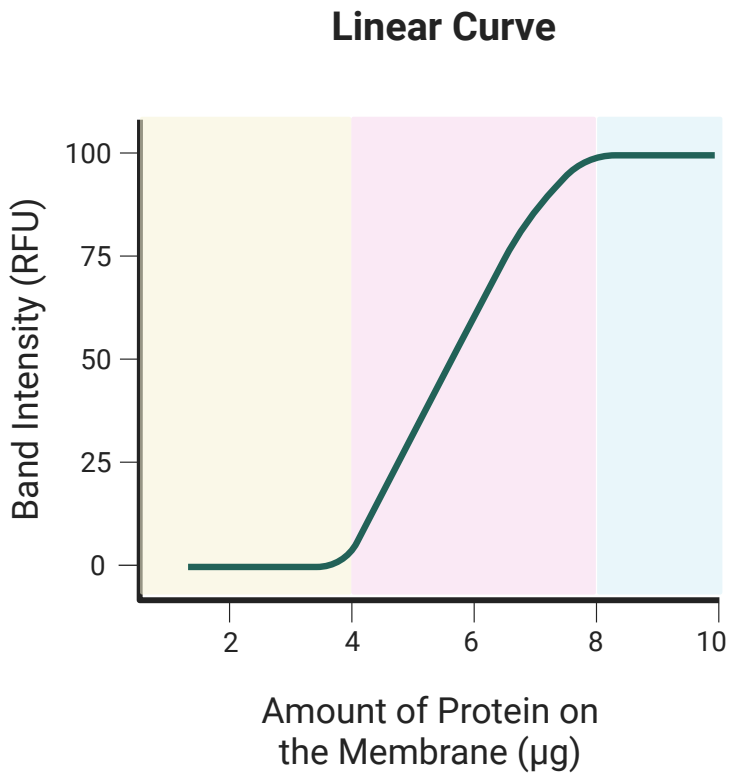

Figure 5: Depiction of the trends in a typical linear curve where band intensity (RFU) is plotted against the amount of protein on the membrane (µg). The yellow section represents undersaturation, the pink section shows the linear portion of the plot, and the blue section represents oversaturation. In this example, the linear range is between 4 µg and 8µg. Created in https://BioRender.com.

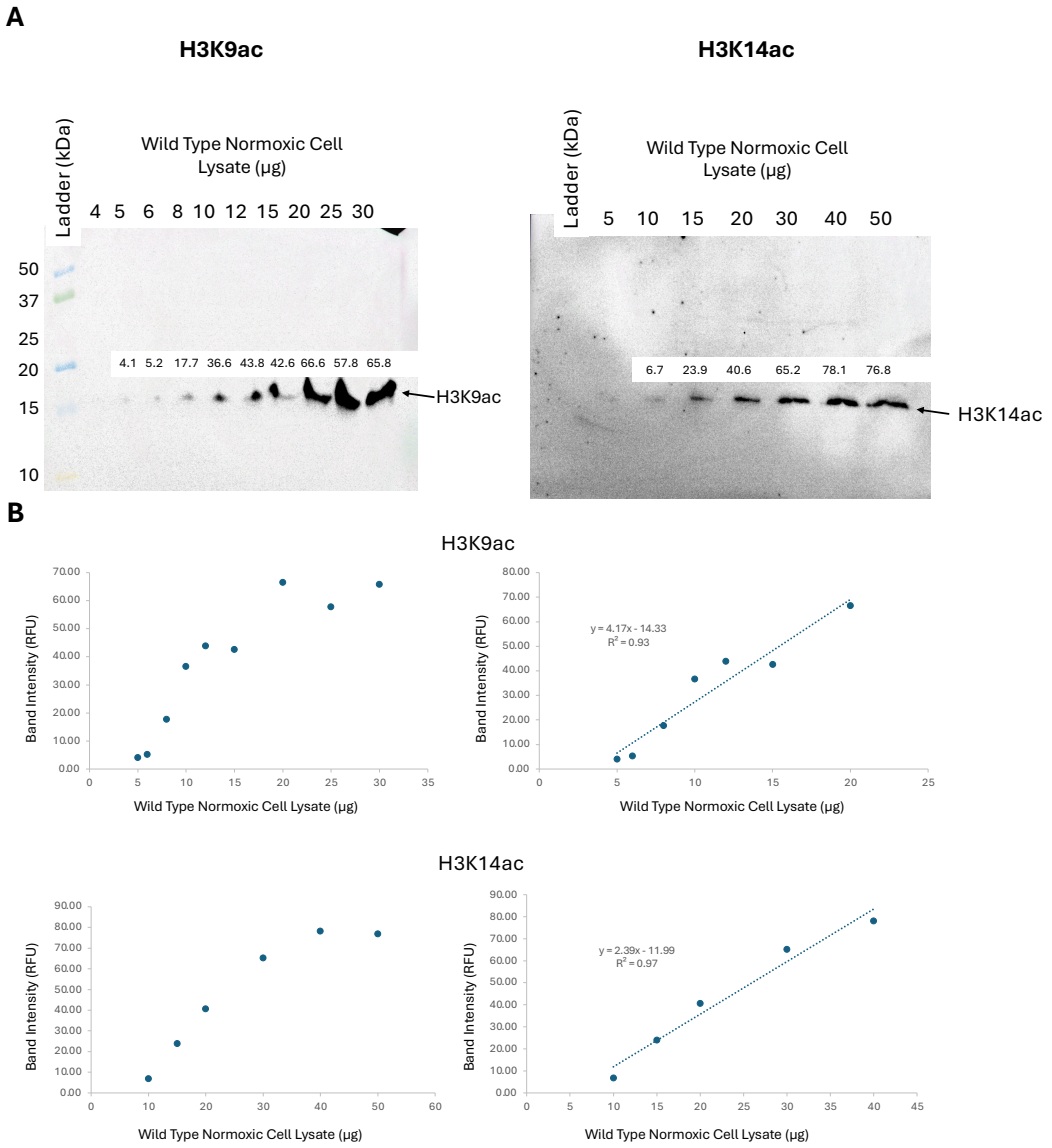

Figure 6: Immunoblot showing H3K9ac and H3K14ac band intensity when an increasing linear series of wild type normoxic cell lysate samples were loaded **(A).** The values above each band indicate the band intensity (band intensity = band volume / band area), which was provided by the Azure SpotPro quantification software. The wild type normoxic cell lysate loading range was between 4 µg and 30 µg for the H3K9ac immunostained blot and between 5 µg and 50 µg for the H3K14ac immunostained blot. The primary antibody for the immunoblot in the left panel was rabbit anti-H3K9ac, Abcam cat # AB32129 lot # 1088902-6 at a 1:1000 dilution. The secondary antibody was Invitrogen goat anti-rabbit cat # 32460 lot # YK375337 at a 1:1000 dilution. The primary antibody for the blot on the left was rabbit anti-H3K14ac, Abcam cat # AB52946 lot # 1029948-53 at a 1:1000 dilution. The secondary antibody was Invitrogen goat anti-rabbit cat # 32460 lot # YK375337 at a 1:1000 dilution. Froggabio Pico Ultra Western substrate was used to image this blot (cat# CCH345). **(B)** Band intensity values were plotted against the amount of

wild type cell lysate loaded on the immunoblot, with the H3K9ac linear curve above and the H3K14ac linear curve below. The graphs on the left show the full range of the linear curve, while the graphs on the right show the isolated linear range used to create the linear equation. The linear range for the H3K9ac antibody was between 5 µg and 20 µg, and the linear range for the H3K14ac antibody was between 10 µg and 40 µg. The linear equation for the H3K9ac antibody was y = 4.17x - 14.33, and the linear equation for the H3K14ac antibody was y = 2.39x - 11.99.

This proportional linear model provided a numeric cutoff for under and oversaturation in further Western blot analysis (described more in the next section). Proportional protein values calculated using the linear equations were classified as either outside or within the linear range. The linear range of the antibody detecting H3K9ac was between 5 µg and 20 µg of sample lysate (Figure 6B). Similarly, the linear range of the antibody detecting H3K14ac was between 10 µg and 40 µg (Figure 6B). Any proportional protein values calculated in subsequent immunoblots found to be outside the corresponding linear ranges above were removed from further analysis.

Linear curves were used to determine an acceptable loading range of cell lysate for each antibody. The protein value chosen for immunoblot loading was on the lower end of the linear range because an increase in H3K9 and H3K14 acetylation was hypothesized to occur during hypoxia. For the antibody targeting H3K9ac (Abcam cat# ab32129, lot#1088902-10), the linear range was between 5 µg and 20 µg of sample lysate, so a loading amount of 10 µg was chosen. For the antibody targeting H3K14ac (Abcam cat# ab52946, lot#1029948-53), the linear range was between 10 µg and 40 µg and a loading amount of 25 µg was chosen.

To ensure equivalent fold change ratios in Western blot analyses, both H3K9ac and H3K14ac immunostained signals were normalized using the linear equations described above. The band intensity values ascertained from H3K9ac or H3K14ac immunostaining were set as the y-value in the corresponding linear equation above. Proportional protein values were then calculated by

solving for the x-value (Table 4 and 5). Table 4 displays the band intensity and proportional protein values of all immunoblots detecting H3K9ac while Table 5 displays the band intensity and proportional protein values of all immunoblots detecting H3K14ac. Both Table 4 and 5 also contain the corresponding H3 loading control immunoblot band intensities and proportional protein values (described below). Normalization against each linear curve was essential because all histone PTMs and the loading control require different protein loading ranges to maintain linearity. Comparison of target protein (H3K9 and H3K14 acetylation) band intensities and loading control band intensities without normalization caused fold change inflation, which can either increase or decrease outlying fold-change values. This generated more variability within the dataset emphasizing the necessity of fold change normalization.

Table 4: Band intensity values and proportional protein conversions of all immunoblots detecting H3K9ac **(A, B, C)** and the corresponding immunoblots detecting the H3 loading control **(D, E, F)**. Band intensity values were converted to proportional protein values by utilizing the H3K9ac linear equation y = 4.17x - 14.33 and the H3 linear equation y = 13.01x – 2.41. The band intensity values were represented by the y-value, and the proportional protein value was found by solving for the x-value (i.e. x = (y + 14.33)/ 4.17).

A

		Biological Replicate 1		Biological Replicate 2					Biological Replicate 3		
		Technical Replicate 1	Technical Replicate 2	Technical Replicate 1	Technical Replicate 2	Technical Replicate 3	Technical Replicate 4	Technical Replicate 5	Technical Replicate 1	Technical Replicate 2	Technical Replicate 3
Wild Type Normoxic	H3K9ac band intensity	61.0	87.0	11.0	45.2	68.4	21.9	27.9	53.0	17.4	52.7
	H3K9ac proportional protein value (µg)	18.1	24.3	6.1	14.3	19.8	8.7	10.1	16.2	7.6	16.1
Wild Type Hypoxic	H3K9ac band intensity	75.4	135.5	7.6	46.8	59.7	35.5	25.6	70.7	21.0	52.6
	H3K9ac proportional protein value (µg)	21.5	35.9	5.3	14.7	17.8	12.0	9.6	20.4	8.5	16.1

		Biological Replicate 1			Biological Replicate 2				Biological Replicate 3		
		Technical Replicate 1	Technical Replicate 2	Technical Replicate 3	Technical Replicate 1	Technical Replicate 2	Technical Replicate 3	Technical Replicate 4	Technical Replicate 1	Technical Replicate 2	Technical Replicate 3
35S:PGB1 Normoxic	H3K9ac band intensity	42.9	38.7	26.6	79.4	98.4	26.2	47.2	21.9	66.7	60.7
	H3K9ac proportional protein value (µg)	13.7	12.7	9.8	22.5	27.0	9.7	14.8	8.7	19.4	18.0
35S:PGB1 Hypoxic	H3K9ac band intensity	38.6	27.3	32.3	53.1	93.2	27.2	45.2	57.7	57.4	79.2
	H3K9ac proportional protein value (µg)	12.7	10.0	11.2	16.2	25.8	10.0	14.3	17.3	17.2	22.4

		Biological Replicate 1				Biological Replicate 2			Biological Replicate 3		
		Technical Replicate 1	Technical Replicate 2	Technical Replicate 3	Technical Replicate 4	Technical Replicate 1	Technical Replicate 2	Technical Replicate 3	Technical Replicate 1	Technical Replicate 2	Technical Replicate 3
Pgb1-RNAi Normoxic	H3K9ac band intensity	58.6	38.5	43.3	15.8	28.0	23.1	4.6	60.8	31.8	62.1
	H3K9ac proportional protein value (µg)	17.5	12.7	13.8	7.2	10.2	9.0	4.5	18.0	11.1	18.3
Pgb1-RNAi Hypoxic	H3K9ac band intensity	81.6	49.6	50.2	48.9	26.6	37.7	17.0	74.9	32.9	69.5
	H3K9ac proportional protein value (µg)	23.0	15.3	15.5	15.2	9.8	12.5	7.5	21.4	11.3	20.1

		Biological Replicate 1						Biological Replicate 2			
		Technical Replicate 1	Technical Replicate 2	Technical Replicate 3	Technical Replicate 4	Technical Replicate 5	Technical Replicate 6	Technical Replicate 1	Technical Replicate 2	Technical Replicate 3	Technical Replicate 4
pgb1-1 Normoxic	H3K9ac band intensity	36.9	90.8	51.5	60.8	61.1	55.2	3.85	9.5	15.8	35.8
	H3K9ac proportional protein value (µg)	12.3	25.2	15.8	18.0	18.1	16.7	4.4	5.7	7.2	12.0
pgb1-1 Hypoxic	H3K9ac band intensity	31.4	76.3	88.8	37.0	16.0	52.6	53.3	30.9	24.6	67.7
	H3K9ac proportional protein value (µg)	11.0	21.7	24.7	12.3	7.3	16.1	16.2	10.8	9.3	19.7

B

		Biological Replicate 3				Biological Replicate 4					
		Technical Replicate 4	Technical Replicate 5	Technical Replicate 6	Technical Replicate 7	Technical Replicate 1	Technical Replicate 2	Technical Replicate 3	Technical Replicate 4	Technical Replicate 5	Technical Replicate 6
Wild Type Normoxic	H3K9ac band intensity	52.3	41.2	26.6	59.0	27.6	74.9	37.5	52.2	54.5	49.1
	H3K9ac proportional protein value (µg)	16.0	13.3	9.8	17.6	10.1	21.4	12.4	16.0	16.5	15.2
Wild Type Hypoxic	H3K9ac band intensity	57.7	66.9	50.2	74.1	18.4	69.8	96.9	82.5	68.4	48.9
	H3K9ac proportional protein value (µg)	17.3	19.5	15.5	21.2	7.9	20.2	26.7	23.2	19.8	15.2

		Biological Replicate 3			Biological Replicate 5			
		Technical Replicate 4	Technical Replicate 5	Technical Replicate 6	Technical Replicate 1	Technical Replicate 2	Technical Replicate 3	Technical Replicate 4
35S:PGB1 Normoxic	H3K9ac band intensity	64.6	51.8	51.9	49.1	52.1	51.7	68.1
	H3K9ac proportional protein value (µg)	18.9	15.9	15.9	15.2	15.9	15.8	19.8
35S:PGB1 Hypoxic	H3K9ac band intensity	60.8	77.6	58.4	31.6	49.7	45.3	71.8
	H3K9ac proportional protein value (µg)	18.0	22.1	17.4	11.0	15.4	14.3	20.7

		Biological Replicate 3			
		Technical Replicate 4	Technical Replicate 5	Technical Replicate 6	Technical Replicate 7
Pgb1-RNAi Normoxic	H3K9ac band intensity	43.4	45.5	19.3	50.7
	H3K9ac proportional protein value (µg)	13.8	14.4	8.1	15.6
Pgb1-RNAi Hypoxic	H3K9ac band intensity	59.5	62.2	53.1	47.1
	H3K9ac proportional protein value (µg)	17.7	18.4	16.2	14.7

C

		Biological Replicate 5			
		Technical Replicate 1	Technical Replicate 2	Technical Replicate 3	Technical Replicate 4
Wild Type Normoxic	H3K9ac band intensity	51.8	35.5	28.3	59.9
	H3K9ac proportional protein value (µg)	15.9	12.0	10.2	17.8
Wild Type Hypoxic	H3K9ac band intensity	31.6	32.9	54.2	69.3
	H3K9ac proportional protein value (µg)	11.0	11.3	16.4	20.1

D

		Biological Replicate 1		Biological Replicate 2					Biological Replicate 3		
		Technical Replicate 1	Technical Replicate 2	Technical Replicate 1	Technical Replicate 2	Technical Replicate 3	Technical Replicate 4	Technical Replicate 5	Technical Replicate 1	Technical Replicate 2	Technical Replicate 3
Wild Type Normoxic	H3 band intensity	43.8	85.2	32.3	41.4	75.1	36.4	45.8	47.2	19.5	40.4
	H3 proportional protein value (µg)	3.5	6.7	2.7	3.4	6.0	3.0	3.7	3.8	1.7	3.3
Wild Type Hypoxic	H3 band intensity	41.8	64.0	33.7	55.7	28.1	42.4	43.2	63.5	12.6	20.2
	H3 proportional protein value (µg)	3.4	5.1	2.8	4.5	2.3	3.4	3.5	5.1	1.2	1.7

		Biological Replicate 1			Biological Replicate 2				Biological Replicate 4		
		Technical Replicate 1	Technical Replicate 2	Technical Replicate 3	Technical Replicate 1	Technical Replicate 2	Technical Replicate 3	Technical Replicate 4	Technical Replicate 1	Technical Replicate 2	Technical Replicate 3
35S:PGB1 Normoxic	H3 band intensity	82.7	63.6	58.9	48.1	72.6	40.4	44.6	12.4	11.4	60.5
	H3 proportional protein value (µg)	6.5	5.1	4.7	3.9	5.8	3.3	3.6	1.1	1.1	4.8
35S:PGB1 Hypoxic	H3 band intensity	83.1	82.1	57.7	48.9	84.4	39.4	45.9	22.7	65.1	66.9
	H3 proportional protein value (µg)	6.6	6.5	4.6	3.9	6.7	3.2	3.7	1.9	5.2	5.3

		Biological Replicate 1				Biological Replicate 2			Biological Replicate 3		
		Technical Replicate 1	Technical Replicate 2	Technical Replicate 3	Technical Replicate 4	Technical Replicate 1	Technical Replicate 2	Technical Replicate 3	Technical Replicate 1	Technical Replicate 2	Technical Replicate 3
Pgb1-RNAi Normoxic	H3 band intensity	102.8	58.9	88.1	28.5	38.9	87.4	39.5	56.8	7.4	17.9
	H3 proportional protein value (µg)	8.1	4.7	7.0	2.4	3.2	6.9	3.2	4.6	0.8	1.6
Pgb1-RNAi Hypoxic	H3 band intensity	111.1	29.7	93.0	45.1	17.4	60.5	44.6	60.2	8.1	23.9
	H3 proportional protein value (µg)	8.7	2.5	7.3	3.7	1.5	4.8	3.6	4.8	0.8	2.0

		Biological Replicate 1						Biological Replicate 2			
		Technical Replicate 1	Technical Replicate 2	Technical Replicate 3	Technical Replicate 4	Technical Replicate 5	Technical Replicate 6	Technical Replicate 1	Technical Replicate 2	Technical Replicate 3	Technical Replicate 4
pgb1-1 Normoxic	H3 band intensity	25.7	74.5	72.6	77.3	40.0	36.0	23.8	26.4	26.0	60.1
	H3 proportional protein value (µg)	2.2	5.9	5.8	6.1	3.3	3.0	2.0	2.2	2.2	4.8
pgb1-1 Hypoxic	H3 band intensity	19.4	23.6	92.1	37.0	8.1	4.2	39.7	31.5	15.8	47.3
	H3 proportional protein value (µg)	1.7	2.0	7.3	3.0	0.8	0.5	3.2	2.6	1.4	3.8

E

		Biological Replicate 3				Biological Replicate 4					
		Technical Replicate 4	Technical Replicate 5	Technical Replicate 6	Technical Replicate 7	Technical Replicate 1	Technical Replicate 2	Technical Replicate 3	Technical Replicate 4	Technical Replicate 5	Technical Replicate 6
Wild Type Normoxic	H3 band intensity	38.8	29.1	33.2	23.1	22.2	64.7	70.7	45.7	33.1	20.2
	H3 proportional protein value (µg)	3.2	2.4	2.7	2.0	1.9	5.2	5.6	3.7	2.7	1.7
Wild Type Hypoxic	H3 band intensity	26.9	40.1	43.0	21.7	34.4	34.8	74.6	59.1	50.8	35.9
	H3 proportional protein value (µg)	2.3	3.3	3.5	1.9	2.8	2.9	5.9	4.7	4.1	2.9

		Biological Replicate 3			Biological Replicate 5			
		Technical Replicate 4	Technical Replicate 5	Technical Replicate 6	Technical Replicate 1	Technical Replicate 2	Technical Replicate 3	Technical Replicate 4
35S:PGB1 Normoxic	H3 band intensity	78.6	23.5	20.2	36.1	25.7	40.2	48.5
	H3 proportional protein value (µg)	6.2	2.0	1.7	3.0	2.2	3.3	3.9
35S:PGB1 Hypoxic	H3 band intensity	61.0	18.9	36.0	36.0	31.9	36.8	66.4
	H3 proportional protein value (µg)	4.9	1.6	3.0	2.9	2.6	3.0	5.3

		Biological Replicate 3			
		Technical Replicate 4	Technical Replicate 5	Technical Replicate 6	Technical Replicate 7
Pgb1-RNAi Normoxic	H3 band intensity	57.4	25.3	17.7	5.4
	H3 proportional protein value (µg)	4.6	2.1	1.5	0.6
Pgb1-RNAi Hypoxic	H3 band intensity	69.4	39.6	20.9	7.8
	H3 proportional protein value (µg)	5.5	3.2	1.8	0.8

F

		Biological Replicate 5			
		Technical Replicate 1	Technical Replicate 2	Technical Replicate 3	Technical Replicate 4
Wild Type Normoxic	H3 band intensity	46.3	26.2	32.7	47.0
	H3 proportional protein value (µg)	3.7	2.2	2.7	3.8
Wild Type Hypoxic	H3 band intensity	23.8	27.4	22.8	52.3
	H3 proportional protein value (µg)	2.0	2.3	1.9	4.2

Table 5: Band intensity values and proportional protein conversions of all immunoblots detecting H3K14ac **(A, B)** and the corresponding immunoblots detecting the H3 loading control **(C, D)**. Band intensity values were converted to proportional protein values by utilizing the H3K14ac linear equation y = 2.39x - 11.99 and the H3 linear equation y = 13.01x - 2.41. The band intensity values were represented by the y-value, and the proportional protein value was found by solving for the x-value (i.e. x = (y + 11.99)/ 2.39).

A

		Biological Replicate 1		Biological Replicate 2					
		Technical Replicate 1	Technical Replicate 2	Technical Replicate 1	Technical Replicate 2	Technical Replicate 3	Technical Replicate 4	Technical Replicate 5	Technical Replicate 6
Wild Type Normoxic	H3K14ac band intensity	13.4	28.6	34.3	37.1	18.1	67.2	24.1	36.5
	H3K14ac proportional protein value (µg)	10.6	17.0	19.4	20.6	12.6	33.2	15.1	20.3
Wild Type Hypoxic	H3K14ac band intensity	30.5	52.1	52.8	45.9	12.4	55.2	11.1	64
	H3K14ac proportional protein value (µg)	17.8	26.9	27.2	24.3	10.2	28.2	9.7	31.8

		Biological Replicate 1			Biological Replicate 2			
		Technical Replicate 1	Technical Replicate 2	Technical Replicate 3	Technical Replicate 1	Technical Replicate 2	Technical Replicate 3	Technical Replicate 4
35S:PGB1 Normoxic	H3K14ac band intensity	65.4	49.7	35.9	49.3	92.6	49.2	36.2
	H3K14ac proportional protein value (µg)	32.4	25.9	20.1	25.7	43.8	25.6	20.2
35S:PGB1 Hypoxic	H3K14ac band intensity	65.8	85.1	43.3	54.2	79.4	30.8	45.9
	H3K14ac proportional protein value (µg)	32.6	40.7	23.2	27.7	38.3	17.9	24.3

		Biological Replicate 1				Biological Replicate 2		
		Technical Replicate 1	Technical Replicate 2	Technical Replicate 3	Technical Replicate 4	Technical Replicate 1	Technical Replicate 2	Technical Replicate 3
Pgb1-RNAi Normoxic	H3K14ac band intensity	11.3	75.0	35.0	19.4	22.4	62.1	59.0
	H3K14ac proportional protein value (µg)	9.8	36.5	19.7	13.2	14.4	31.1	29.8
Pgb1-RNAi Hypoxic	H3K14ac band intensity	18.3	99.1	45.4	33.0	33.5	87.3	70.4
	H3K14ac proportional protein value (µg)	12.7	46.6	24.0	18.9	19.1	41.6	34.5

		Biological Replicate 1				Biological Replicate 2		
		Technical Replicate 1	Technical Replicate 2	Technical Replicate 3	Technical Replicate 4	Technical Replicate 1	Technical Replicate 2	Technical Replicate 3
pgb1-1 Normoxic	H3K14ac band intensity	34.3	81.2	10.3	7.4	5.3	6.5	8.8
	H3K14ac proportional protein value (µg)	19.4	39.1	9.3	8.1	7.2	7.7	8.7
pgb1-1 Hypoxic	H3K14ac band intensity	21.9	62.8	20.5	4.4	3.5	72.2	15.5
	H3K14ac proportional protein value (µg)	14.2	31.3	13.6	6.9	6.5	35.3	11.5

B

		Biological Replicate 3				Biological Replicate 5		
		Technical Replicate 1	Technical Replicate 2	Technical Replicate 3	Technical Replicate 4	Technical Replicate 1	Technical Replicate 2	Technical Replicate 3
Wild Type Normoxic	H3K14ac band intensity	6.9	61.2	31	2.2	3.0	48.4	18.7
	H3K14ac proportional protein value (µg)	7.9	30.7	18.0	5.9	6.3	25.3	12.9
Wild Type Hypoxic	H3K14ac band intensity	7.4	14.6	17.7	31.3	5.4	57.5	28
	H3K14ac proportional protein value (µg)	8.1	11.1	12.4	18.1	7.3	29.1	16.8

		Biological Replicate 4			Biological Replicate 5			
		Technical Replicate 1	Technical Replicate 2	Technical Replicate 3	Technical Replicate 1	Technical Replicate 2	Technical Replicate 3	Technical Replicate 4
35S:PGB1 Normoxic	H3K14ac band intensity	83.6	29.8	2.0	9.9	60.9	61.3	49.8
	H3K14ac proportional protein value (µg)	40.1	17.5	5.9	9.2	30.5	30.7	25.9
35S:PGB1 Hypoxic	H3K14ac band intensity	82.7	19.7	3.6	11.4	86.6	64	60.7
	H3K14ac proportional protein value (µg)	39.7	13.3	6.5	9.8	41.3	31.8	30.5

		Biological Replicate 3		
		Technical Replicate 1	Technical Replicate 2	Technical Replicate 3
Pgb1-RNAi Normoxic	H3K14ac band intensity	32.1	37.8	10.8
	H3K14ac proportional protein value (µg)	18.5	20.9	9.6
Pgb1-RNAi Hypoxic	H3K14ac band intensity	16.1	51.7	6.9
	H3K14ac proportional protein value (µg)	11.8	26.7	7.9

C

		Biological Replicate 1		Biological Replicate 2					
		Technical Replicate 1	Technical Replicate 2	Technical Replicate 1	Technical Replicate 2	Technical Replicate 3	Technical Replicate 4	Technical Replicate 5	Technical Replicate 6
Wild Type Normoxic	H3 band intensity	43.8	85.2	20.2	41.4	32.3	75.1	36.4	45.8
	H3 proportional protein value (µg)	3.5	6.7	1.7	3.4	2.7	6.0	3.0	3.7
Wild Type Hypoxic	H3 band intensity	41.8	64.0	31.9	55.7	33.7	28.1	42.4	43.2
	H3 proportional protein value (µg)	3.4	5.1	2.6	4.5	2.8	2.3	3.4	3.5

		Biological Replicate 1			Biological Replicate 2			
		Technical Replicate 1	Technical Replicate 2	Technical Replicate 3	Technical Replicate 1	Technical Replicate 2	Technical Replicate 3	Technical Replicate 4
35S:PGB1 Normoxic	H3 band intensity	82.7	63.6	63.6	48.1	72.6	40.4	44.6
	H3 proportional protein value (µg)	6.5	5.1	5.1	3.9	5.8	3.3	3.6
35S:PGB1 Hypoxic	H3 band intensity	83.1	82.1	82.1	48.9	84.4	39.4	45.9
	H3 proportional protein value (µg)	6.6	6.5	6.5	3.9	6.7	3.2	3.7

		Biological Replicate 1				Biological Replicate 2		
		Technical Replicate 1	Technical Replicate 2	Technical Replicate 3	Technical Replicate 4	Technical Replicate 1	Technical Replicate 2	Technical Replicate 3
Pgb1-RNAi Normoxic	H3 band intensity	88.1	83.7	58.9	28.5	38.9	87.4	39.5
	H3 proportional protein value (µg)	7.0	6.6	4.7	2.4	3.2	6.9	3.2
Pgb1-RNAi Hypoxic	H3 band intensity	93.0	64.4	29.7	45.1	17.4	60.5	44.6
	H3 proportional protein value (µg)	7.3	5.1	2.5	3.7	1.5	4.8	3.6

		Biological Replicate 1				Biological Replicate 2		
		Technical Replicate 1	Technical Replicate 2	Technical Replicate 3	Technical Replicate 4	Technical Replicate 1	Technical Replicate 2	Technical Replicate 3
pgb1-1 Normoxic	H3 band intensity	74.5	72.6	40.0	36.0	23.8	26.4	26.0
	H3 proportional protein value (µg)	5.9	5.8	3.3	3.0	2.0	2.2	2.2
pgb1-1 Hypoxic	H3 band intensity	23.6	92.1	8.1	4.2	39.7	31.5	15.8
	H3 proportional protein value (µg)	2.0	7.3	0.8	0.5	3.2	2.6	1.4

D

		Biological Replicate 3				Biological Replicate 5		
		Technical Replicate 1	Technical Replicate 2	Technical Replicate 3	Technical Replicate 4	Technical Replicate 1	Technical Replicate 2	Technical Replicate 3
Wild Type Normoxic	H3 band intensity	40.4	38.8	29.1	23.1	46.3	26.2	32.7
	H3 proportional protein value (µg)	3.3	3.2	2.4	2.0	3.7	2.2	2.7
Wild Type Hypoxic	H3 band intensity	20.2	26.9	40.1	21.7	23.8	27.4	22.8
	H3 proportional protein value (µg)	1.7	2.3	3.3	1.9	2.0	2.3	1.9

		Biological Replicate 4			Biological Replicate 5			
		Technical Replicate 1	Technical Replicate 2	Technical Replicate 3	Technical Replicate 1	Technical Replicate 2	Technical Replicate 3	Technical Replicate 4
35S:PGB1 Normoxic	H3 band intensity	60.5	23.5	20.2	36.1	25.7	40.2	48.5
	H3 proportional protein value (µg)	4.8	2.0	1.7	3.0	2.2	3.3	3.9
35S:PGB1 Hypoxic	H3 band intensity	66.9	18.9	36.0	36.0	31.9	36.8	66.4
	H3 proportional protein value (µg)	5.3	1.6	3.0	2.9	2.6	3.0	5.3

		Biological Replicate 3		
		Technical Replicate 1	Technical Replicate 2	Technical Replicate 3
Pgb1-RNAi Normoxic	H3 band intensity	87.3	57.4	25.3
	H3 proportional protein value (µg)	6.9	4.6	2.1
Pgb1-RNAi Hypoxic	H3 band intensity	82.6	69.4	39.6
	H3 proportional protein value (µg)	6.5	5.5	3.2

A loading control was the last measure used to ensure accurate and reproducible data. Without the inclusion of a loading control, neither qualitative nor quantitative arguments are possible (Pillai-Kastoori *et al.*, 2020). The loading control functioned as a reference to compare changes in H3K9ac and H3K14ac levels between normoxic and hypoxic samples. This was an appealing option because it allowed for a correlation to be made between the amount of H3 in the sample and both H3K9ac and H3K14ac. However, this option was not perfect because both the target protein and the loading control had to be detected on separate blots, which introduced variation.

A linear curve was also created for the anti-histone H3 loading control (Figure 7). The corresponding linear equation for the loading control anti-H3 (Abcam cat # ab10799,

lot#1084399-8) was y = 13.01x - 2.41 and the linear range was between 1 µg and 6 µg of sample lysate. For this experiment, 3 µg was the protein loading amount used (Figure 7). The band intensity values ascertained from each H3 loading control immunoblot were used as the y-value in the equation above to calculate proportional protein values and solved for the x-value (Tables 1 and 2). Each H3 band intensity value to proportional protein value conversion is paired to specific H3K9ac and H3K14ac blots indicated in Tables 1 and 2.

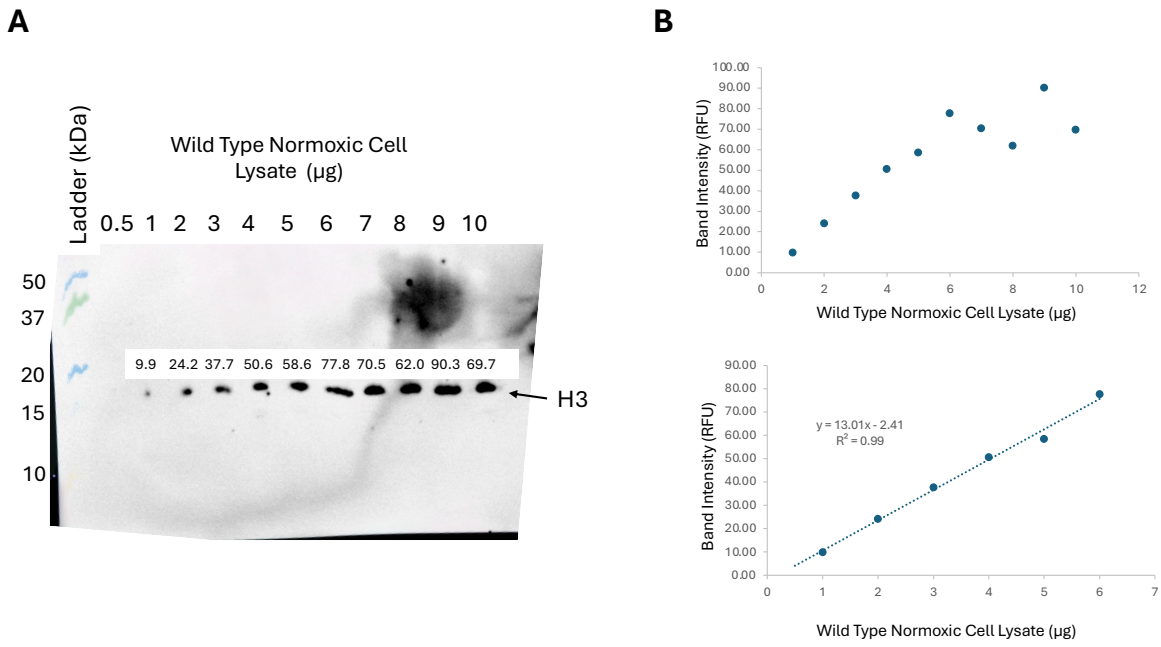

Figure 7: Immunoblot showing H3 band intensity when an increasing linear series of wild type normoxic cell lysate sample was loaded **(A).** The values above each band indicate the band intensity (band intensity = band volume / band area) which was provided by the Azure SpotPro quantification software. The wild type normoxic cell lysate loading range was between 0.5 µg and 10 µg for the blot detecting H3. The primary antibody was mouse anti-H3, Abcam cat # AB10799 lot #1084399-8 at a 1:1000 dilution. The secondary antibody was Invitrogen goat anti-mouse cat # 31430 lot # YD375335 at a 1:50000 dilution. Froggabio Pico Ultra Western substrate was used to image this blot (cat# CCH345). **(B)** Band intensity values plotted against amount of wild type cell lysate with the H3 linear curve. The graph on the top contains all intensity values from the linear curve. The graph on the bottom contains the isolated linear range which was used to create the linear equation. The linear range for the H3 antibody was between 1 µg and 6 µg. The linear equation for the H3 antibody was y = 13.01x – 2.41.

3.2. Western blot analysis

3.2.1. H3K9 and H3K14 acetylation response to hypoxia

Nitric oxide, known to accumulate during hypoxia (Hebelstrup *et al.,* 2012), increases histone acetylation at H3K9 and H3K14 through deactivation of specific HDACs in the class I RPD3-type family (Mengel *et al.,* 2017; Ageeva-Kieferle *et al.*, 2019). HDA6 showed decreased activity upon S-nitrosylation, leading to increased H3K9 and H3K14 acetylation (Ageeva-Kieferle *et al.,* 2021). In contrast, deactivation of HDA19 through S-nitrosylation caused no major change in H3K9 or H3K14 acetylation (Zheng *et al.,* 2023). To gain an understanding of how hypoxia impacted H3K9 and H3K14 acetylation levels, immunoblotting using anti-H3K9ac and H3K14ac antibodies was performed on cell lysates from root tips of *Arabidopsis thaliana* (Col-0).

Sample immunoblots are shown in Figure 8, comparing the converted proportional protein values under normoxia or hypoxia for H3 (used as the loading control to normalize the hypoxia (H)/normoxia (N) fold changes), H3K9ac, and H3K14ac. Normalized (H/N) fold changes of the five (H3K9ac) or four (H3K14ac) biological replicates, each comprising several technical replicates, utilized in this study are listed in Table 6 (H3K9ac) and Table 7 (H3K14ac). Some technical replicates (in bold) were not utilized for the analyses, as the calculated proportional protein values from the corresponding immunoblot band intensities were outside the linear range of detection (technical replicate 2 of biological replicate 1 for H3K9ac, and technical replicate 1 of biological replicates 3 and 5 for H3K14ac). As shown in Table 6, the (H/N) fold change values for H3K9ac were 1.22, 1.24, 1.36, 1.13 and 1.37 for biological replicates 1, 2, 3, 4, and 5. For H3K14ac, the (H/N) fold change values were 1.90, 1.17, 1.41, and 1.48 for biological replicates 1, 2, 3, and 5 (Table 7). The antibody used to detect H3K14ac required double the amount of

protein sample as the antibody used to detect H3K9ac. To ensure effective detection and quantification, biological replicate 4 was immunostained only with antibodies against H3K9ac. The averaged (H/N) fold change for H3K9ac was 1.27, while the average fold change value for H3K14ac was 1.39 (Table 8). One-sided t-tests were performed to understand whether each (H/N) fold change was greater than 1, as 1 represents no change in global H3K9 or H3K14 acetylation levels due to hypoxia. The p-value of all wild type replicates immunostained for H3K9ac was 0.01, and the p-value for all wild type replicates immunostained for H3K14ac was 0.06 (Table 8).

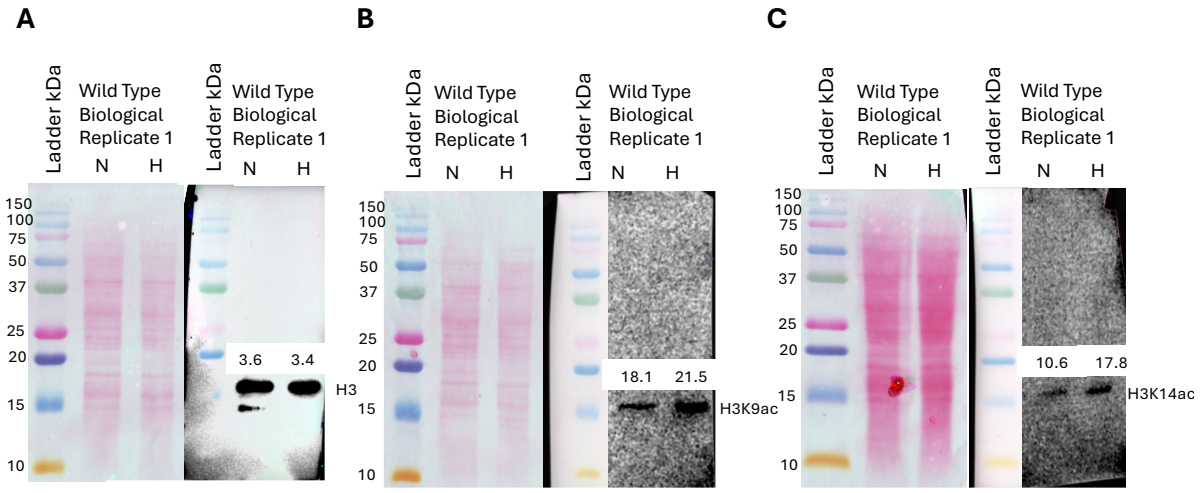

Figure 8: Immunoblots showing H3, H3K9ac and H3K14ac levels in root tips of *Arabidopsis thaliana* (Col-0) plants exposed to normoxia (N) or hypoxia (H) for 12 hours. The sample used was wild type technical replicate 1 of biological replicate 1. The Ponceau S-stained blot of WT normoxic and hypoxic cell lysates (left panels), and the accompanying blot immunostained with antibodies against the H3 loading control **(A)**, H3K9ac **(B)**, and H3K14ac **(C)** are shown (right panels). Abcam mouse anti-H3 (cat# 10799) primary antibody and Invitrogen goat anti-mouse (cat# 31430) were used for the H3 blot. Abcam rabbit anti-H3K9ac (cat# ab32129) primary antibody and Invitrogen goat anti-rabbit secondary (cat# 32460) were used for the H3K9ac blot. **(**Invitrogen rabbit anti-H3K14ac (cat# MA5-32814) primary antibody and an Invitrogen goat anti-rabbit (cat# 32460) secondary antibody were used for the H3K14ac blot. Froggabio Pico ECL (cat# CCH345-B100ML) was used for the H3 blot, while Revvity ECL (cat# NEL105001EA) was used for the H3K9ac and H3K14ac blots. The values above each band represent the proportional protein value (µg) calculated by converting band intensities through the linear model generated for each antibody in the last chapter.

Table 6: H3K9ac fold change levels in root tips of wild type Arabidopsis plants (Col-0) exposed to normoxia (N) or hypoxia (H). The proportional protein values (μg) were calculated using the linear curve equations described in the previous chapter. The H3K9ac proportional protein value was normalized for loading using the corresponding H3 proportional protein value (H3K9ac proportional protein value / H3 proportional protein value). The (H/N) fold changes were calculated by generating a ratio of normalized hypoxia-treated sample to normalized normoxic-treated sample. Standard deviation is indicated with SD and standard error mean is indicated with SEM. The n-value represents the number of technical replicates per biological replicate. Bolded values indicate protein levels that are outside of the preestablished linear ranges for both the test antigen and the loading control as defined in the previous section. If deemed outside of the linear range, the fold changes were removed from further analysis. Experiments were conducted on several technical replicates per biological replicate.

H3K9ac	H3K9ac Proportional Protein Value (µg)	H3 Proportional Protein Value (µg)	Ratio H3K9ac / H3 loading control	Ratio H/N	Average	n	SD	SEM
Biological Replicate 1								
WT N tech rep 1	18.1	3.5	5.2		1.22	1	-	-
WT H tech rep 1	**21.5**	3.4	6.3	1.22				
WT N tech rep 2	**24.3**	**6.7**	3.6					
WT H tech rep 2	**35.9**	5.1	7.0	**1.94**				
Biological Replicate 2								
WT N tech rep 1	6.1	2.7	2.3		1.24	5	0.64	0.29
WT H tech rep 1	5.3	2.8	1.9	0.84				
WT N tech rep 2	14.3	3.4	4.2					
WT H tech rep 2	14.7	4.5	3.3	0.78				
WT N tech rep 3	19.8	6.0	3.3					
WT H tech rep 3	17.8	2.3	7.7	2.35				
WT N tech rep 4	8.7	3.0	2.9					
WT H tech rep 4	12.0	3.4	3.5	1.22				
WT N tech rep 5	10.1	3.7	2.7					
WT H tech rep 5	9.6	3.5	2.7	1.00				
Biological Replicate 3								
WT N tech rep 1	16.2	3.8	4.3		1.36	7	0.34	0.13
WT H tech rep 1	**20.4**	5.1	4.0	0.94				
WT N tech rep 2	7.6	1.7	4.5					
WT H tech rep 2	8.5	1.2	7.1	1.58				
WT N tech rep 3	16.1	3.3	4.9					
WT H tech rep 3	16.1	1.7	9.5	1.94				
WT N tech rep 4	16.0	3.2	5.0					
WT H tech rep 4	17.3	2.3	7.5	1.50				
WT N tech rep 5	13.3	2.4	5.5					
WT H tech rep 5	19.5	3.3	5.9	1.07				
WT N tech rep 6	9.8	2.7	3.6					
WT H tech rep 6	15.5	3.5	4.4	1.22				
WT N tech rep 7	17.6	2.0	8.8					
WT H tech rep 7	**21.2**	1.9	11.2	1.27				
Biological Replicate 4								
WT N tech rep 1	10.1	1.9	5.3		1.13	6	0.63	0.26
WT H tech rep 1	7.9	2.8	2.8	0.53				
WT N tech rep 2	**21.4**	5.2	4.1					
WT H tech rep 2	20.2	2.9	7.0	1.69				
WT N tech rep 3	12.4	5.6	2.2					
WT H tech rep 3	**26.7**	5.9	4.5	2.04				
WT N tech rep 4	16.0	3.7	4.3					
WT H tech rep 4	**23.2**	4.7	4.9	1.14				
WT N tech rep 5	16.5	2.7	6.1					
WT H tech rep 5	19.8	4.1	4.8	0.79				
WT N tech rep 6	15.2	1.7	8.9					
WT H tech rep 6	15.2	2.9	5.2	0.59				
Biological Replicate 5								
WT N tech rep 1	15.9	3.7	4.3		1.37	4	0.63	0.31
WT H tech rep 1	11.0	2.0	5.5	1.28				
WT N tech rep 2	12.0	2.2	5.5					
WT H tech rep 2	11.3	2.3	4.9	0.90				
WT N tech rep 3	10.2	2.7	3.8					
WT H tech rep 3	16.4	1.9	8.6	2.28				
WT N tech rep 4	17.8	3.8	4.7					
WT H tech rep 4	20.1	4.2	4.8	1.02				

Table 7: H3K14ac fold change levels in root tips of wild type Arabidopsis plants (Col-0) exposed to normoxia (N) or hypoxia (H). The proportional protein values (µg) were calculated using the linear curve equations described in the previous chapter. The H3K14ac proportional protein value was normalized for loading using the corresponding H3 proportional protein value (H3K14ac proportional protein value / H3 proportional protein value). The (H/N) fold changes were calculated by generating a ratio of normalized hypoxia-treated sample to normalized normoxic-treated sample. Standard deviation is indicated with SD and standard error mean is indicated with SEM. The n-value represents the number of technical replicates per biological replicate. Bolded values indicate protein levels that are outside of the preestablished linear ranges for both the test antigen and the loading control as defined in the previous section. If deemed outside of the linear range, the fold changes were removed from further analysis. Experiments were conducted on several technical replicates per biological replicate.

H3K14ac	H3K14ac Proportional Protein Value (µg)	H3 Proportional Protein Value (µg)	Ratio H3K14ac / H3 loading control	Ratio H/N	Average	n	SD	SEM
Biological Replicate 1								
WT N tech rep 1	10.6	3.5	3.0		1.90	2	0.25	0.18
WT H tech rep 1	17.8	3.4	5.2	1.73				
WT N tech rep 2	17.0	**6.7**	2.5					
WT H tech rep 2	26.9	5.1	5.3	2.08				
Biological Replicate 2								
WT N tech rep 1	19.4	1.7	11.4		1.17	6	0.73	0.30
WT H tech rep 1	27.2	2.6	10.5	0.92				
WT N tech rep 2	20.6	3.4	6.1					
WT H tech rep 2	24.3	4.5	5.4	0.89				
WT N tech rep 3	12.6	2.7	4.7					
WT H tech rep 3	10.2	2.8	3.6	0.78				
WT N tech rep 4	33.2	6.0	5.5					
WT H tech rep 4	28.2	2.3	12.3	2.22				
WT N tech rep 5	15.1	3.0	5.0					
WT H tech rep 5	9.7	3.4	2.9	0.57				
WT N tech rep 6	20.3	3.7	5.5					
WT H tech rep 6	31.8	3.5	9.1	1.66				
Biological Replicate 3								
WT N tech rep 1	**7.9**	3.3	2.4		1.41	3	1.57	0.91
WT H tech rep 1	**8.1**	1.7	4.8	**1.99**				
WT N tech rep 2	30.7	3.2	9.6					
WT H tech rep 2	11.1	2.3	4.8	0.50				
WT N tech rep 3	18.0	2.4	7.5					
WT H tech rep 3	12.4	3.3	3.8	0.50				
WT N tech rep 4	**5.9**	2.0	3.0					
WT H tech rep 4	18.1	1.9	9.5	3.23				
Biological Replicate 5								
WT N tech rep 1	**6.3**	3.7	1.7		1.48	2	0.53	0.38
WT H tech rep 1	**7.3**	2.0	3.7	**2.14**				
WT N tech rep 2	25.3	2.2	11.5					
WT H tech rep 2	29.1	2.3	12.7	1.10				
WT N tech rep 3	12.9	2.7	4.8					
WT H tech rep 3	16.8	1.9	8.8	1.85				

Table 8: One-tailed t-test to assess whether (H/N) fold changes for each line (WT, 35S:PGB1, Pgb1-RNAi, and *pgb1-1*) at H3K9ac (**A**) or H3K14ac (**B**) were statistically greater than 1. All biological and technical replicates were combined for each given line and histone PTM listed below. The n-value represents the number of replicates included in each group and SD represents standard deviation.

A

H3K9ac	n	Average	SD	p-value
WT	23	1.27	0.51	0.01
35S:PGB1	15	0.92	0.35	0.19
Pgb1-RNAi	10	1.47	0.51	0.01
pgb1-1	8	2.21	1.41	0.02

B

H3K14ac	n	Average	SD	p-value
WT	13	1.39	0.82	0.06
35S:PGB1	10	1.01	0.16	0.41
Pgb1-RNAi	7	1.7	0.69	0.02
pgb1-1	5	2.92	2.00	0.05

3.2.2. *Phytoglobin1* deregulation affects H3K9 and H3K14 acetylation

To assess the effects of the NO scavenger Phytoglobin 1 (Pgb1) on H3K9 and H3K14 acetylation levels, three previously characterized lines were used: the 35S:PGB1 line, the Pgb1-RNAi line, and the *pgb1-1* line. The 35S:Pgb1 line constitutively expresses *PGB1*; the expression level of *PGB1* was about 2 times higher relative to WT and this increase results in an elevation of the Pgb1 protein (Hartman *et al.*, 2019; Mira et al., 2023b). Compared to WT, Pgb1 protein levels were decreased by about half in the Pgb1-RNAi line (Mira et al., 2023b) and completely abolished in the *pgb1-1* line harboring a T-DNA insertion around 300 bp upstream from the *PGB1* start codon (Hartman *et al.*, 2019). A sample of immunoblotting detecting H3, H3K9ac, and H3K14ac in the three lines is shown in Figure 9.

In the 35S:PGB1 line, the (H/N) fold change values for H3K9ac were 0.89, 0.90, 1.01, and 0.82 for biological replicates 1, 2, 4, and 5, respectively (Table 9) while those for H3K14ac were 1.07, 0.99, 0.92, and 1.05 (Table 10). In H3K9ac, 2 technical replicates were omitted due to oversaturation, one each from biological replicates 1 and 2. In H3K14ac, 4 technical replicates were omitted due to the out-of-range proportional protein values, one from each biological replicate. Biological replicate 3 was treated but not used for analysis because too little sample tissue was collected. The averaged (H/N) fold change across all replicates was 0.92 for H3K9ac and 1.01 for H3K14ac (Table 8). One-sided t-tests analyzed whether each data set was more than one provided a p-value of 0.19 for H3K9ac and a p-value of 0.41 for H3K14ac (Table 8).

Two of the three biological replicates used for the Pgb1-RNAi line exhibited larger (H/N) fold change values for H3K9ac than wild type, i.e., 1.82 and 1.83, whereas the third replicate showed a value of 1.11 (Table 11). The averaged H3K9ac (H/N) fold change in response to hypoxia was 1.47 (Table 8). In the same line, the H3K14ac (H/N) fold change were 1.28, 1.90, and 2.35 for three biological replicates, with the average of all replicates as 1.70 (Table 12, Table 8). Three biological replicates were used for the Pgb1-RNAi line because the *pgb1-1* line was used in subsequent treatments after it was acquired. One-sided t-tests to assess whether the (H/N) fold change in response to hypoxia was greater than one gave p-values of 0.01 for H3K9ac and 0.02 for H3K14ac (Table 8).

Relative to the 35S:PGB1 and Pgb1-RNAi lines, hypoxia increased both H3K9ac and H3K14ac in the *pgb1-1* line. The (H/N) fold change values for the *pgb1-1* line were 2.43 and 1.99 for H3K9ac (Table 13) 2.89 and 2.97 for H3K14ac (Table 14). The averaged fold changes across both biological replicates were 2.21 for H3K9ac and 2.92 for H3K14ac. The p-values of the one-sided t-tests determining whether (H/N) fold change values were more than 1 were 0.02

for H3K9ac and 0.05 for H3K14ac (Table 8). Unfortunately, only two biological replicates were used for this experiment, because the line was obtained later. A graph summarizing the averaged (H/N) fold changes across biological and technical replicates of all *Arabidopsis thaliana* lines utilized in this study shows the highest values in the *pgb1-1* line (Figure 10).

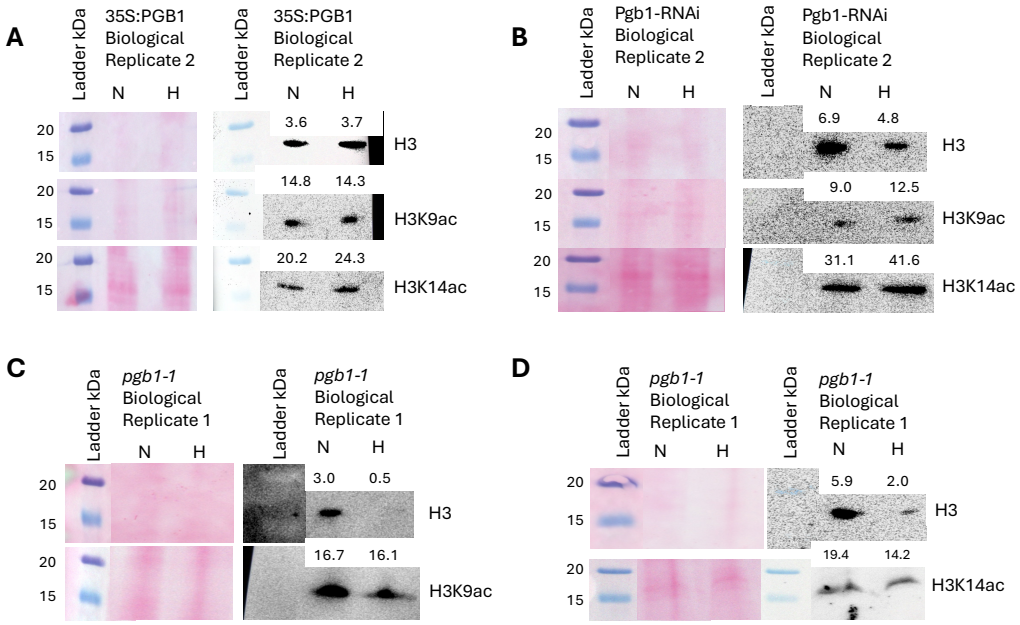

Figure 9: Immunoblots showing H3, H3K9ac and H3K14ac levels in root tips of the 35S:PGB1 line, the Pgb1-RNAi line and the *pgb1-1* line exposed to normoxia (N) or hypoxia (H) for 12 hours. The sample used for the 35S:PGB1 line was technical replicate 4 of biological replicate 2, the sample used for the Pgb1-RNAi line was technical replicate 2 of biological replicate 2, and the sample used for the *pgb1-1* line was technical replicate 6 for H3K9ac and technical replicate 1 for H3K14ac of biological replicate 1. The Ponceau S-stained blot of 35S:PGB1 **(A),** Pgb1-RNAi **(B),** and *pgb1-1* line **(C,D)** normoxic and hypoxic cell lysates (left panels), and the accompanying blot immunostained with antibodies against the H3 loading control, H3K9ac, and H3K14ac are shown (right panels). Abcam mouse anti-H3 (cat# 10799) primary antibody and Invitrogen goat anti-mouse (cat# 31430) were used for the H3 blot. Abcam rabbit anti-H3K9ac (cat# ab32129) primary antibody and Invitrogen goat anti-rabbit secondary (cat# 32460) were used for the H3K9ac blot. **(**Invitrogen rabbit anti-H3K14ac (cat# MA5-32814) primary antibody and an Invitrogen goat anti-rabbit (cat# 32460) secondary antibody were used for the H3K14ac blot. Froggabio Pico ECL (cat# CCH345-B100ML) was used for all immunoblots. The values above each band represent the proportional protein value (µg) calculated by converting band intensities through the linear model generated for each antibody in the last chapter.

Table 9: H3K9ac fold change levels in root tips of the 35S:PGB1 line exposed to normoxia (N) or hypoxia (H). The proportional protein values (µg) were calculated using the linear curve equations described in the previous chapter. The H3K9ac proportional protein value was normalized for loading using the corresponding H3 proportional protein value (H3K9ac proportional protein value / H3 proportional protein value). The (H/N) fold changes were calculated by generating a ratio of normalized hypoxia-treated sample to normalized normoxic-treated sample. Standard deviation is indicated with SD and standard error mean is indicated with SEM. The n-value represents the number of technical replicates per biological replicate. Bolded values indicate protein levels that are outside the preestablished linear ranges for the test antigen and the loading control, as defined in the previous section. If deemed outside of the linear range, the (H/N) fold changes were removed from further analysis. Experiments were conducted on several technical replicates of per biological replicate.

H3K9ac	H3K9ac Proportional Protein Value (µg)	H3 Proportional Protein Value (µg)	Ratio H3K9ac / H3 loading control	Ratio H/N	Average	n	SD	SEM
Biological Replicate 1								
35S:PGB1 N tech rep 1	13.7	**6.5**	2.1					
35S:PGB1 H tech rep 1	12.7	**6.6**	1.9	**0.92**				
35S:PGB1 N tech rep 2	12.7	5.1	2.5		0.89	2	0.39	0.27
35S:PGB1 H tech rep 2	10.0	**6.5**	1.5	0.61				
35S:PGB1 N tech rep 3	9.8	4.7	2.1					
35S:PGB1 H tech rep 3	11.2	4.6	2.4	1.16				
Biological Replicate 2								
35S:PGB1 N tech rep 1	**22.5**	3.9	5.8					
35S:PGB1 H tech rep 1	16.2	3.9	4.1	0.71				
35S:PGB1 N tech rep 2	**27.0**	5.8	4.7					
35S:PGB1 H tech rep 2	**25.8**	**6.7**	3.9	**0.83**	0.90	3	0.17	0.10
35S:PGB1 N tech rep 3	9.7	3.3	3.0					
35S:PGB1 H tech rep 3	10.0	3.2	3.1	1.05				
35S:PGB1 N tech rep 4	14.8	3.6	4.1					
35S:PGB1 H tech rep 4	14.3	3.7	3.8	0.94				
Biological Replicate 4								
35S:PGB1 N tech rep 1	8.7	1.1	7.6					
35S:PGB1 H tech rep 1	17.3	1.9	9.0	1.17				
35S:PGB1 N tech rep 2	19.4	1.1	18.3					
35S:PGB1 H tech rep 2	17.2	5.2	3.3	0.18				
35S:PGB1 N tech rep 3	18.0	4.8	3.7					
35S:PGB1 H tech rep 3	**22.4**	5.3	4.2	1.13	1.01	6	0.52	0.21
35S:PGB1 N tech rep 4	18.9	**6.2**	3.0					
35S:PGB1 H tech rep 4	18.0	4.9	3.7	1.22				
35S:PGB1 N tech rep 5	15.9	2.0	8.0					
35S:PGB1 H tech rep 5	**22.1**	1.6	13.4	1.69				
35S:PGB1 N tech rep 6	15.9	1.7	9.1					
35S:PGB1 H tech rep 6	17.4	3.0	5.9	0.65				
Biological Replicate 5								
35S:PGB1 N tech rep 1	15.2	3.0	5.1					
35S:PGB1 H tech rep 1	11.0	2.9	3.8	0.74				
35S:PGB1 N tech rep 2	15.9	2.2	7.4					
35S:PGB1 H tech rep 2	15.4	2.6	5.8	0.79	0.82	4	0.11	0.05
35S:PGB1 N tech rep 3	15.8	3.3	4.8					
35S:PGB1 H tech rep 3	14.3	3.0	4.8	0.98				
35S:PGB1 N tech rep 4	19.8	3.9	5.1					
35S:PGB1 H tech rep 4	**20.7**	5.3	3.9	0.77				

Table 10: H3K14ac fold change levels in root tips of the 35S:PGB1 line exposed to normoxia (N) or hypoxia (H). The proportional protein values (µg) were calculated using the linear curve equations described in the previous chapter. The H3K14ac proportional protein value was normalized for loading using the corresponding H3 proportional protein value (H3K14ac proportional protein value / H3 proportional protein value). The (H/N) fold changes were calculated by generating a ratio of the normalized hypoxia-treated sample to the normalized normoxic-treated sample. Standard deviation is indicated with SD and standard error mean is indicated with SEM. The n-value represents the number of technical replicates per biological replicate. Bolded values indicate protein levels that are outside the preestablished linear ranges for the test antigen and the loading control, as defined in the previous section. If deemed outside of the linear range, the (H/N) fold changes were removed from further analysis. Experiments were conducted on several technical replicates per biological replicate.

H3K14ac	H3K14ac Proportional Protein Value (µg)	H3 Proportional Protein Value (µg)	Ratio H3K14ac / H3 loading control	Ratio H/N	Average	n	SD	SEM
Biological Replicate 1								
35S:PGB1 N tech rep 1	32.4	**6.5**	5.0					
35S:PGB1 H tech rep 1	32.6	**6.6**	4.9	**0.99**				
35S:PGB1 N tech rep 2	25.9	5.1	5.1		1.07	2	0.23	0.16
35S:PGB1 H tech rep 2	**40.7**	**6.5**	6.3	1.23				
35S:PGB1 N tech rep 3	20.1	5.1	3.9					
35S:PGB1 H tech rep 3	23.2	**6.5**	3.6	0.91				
Biological Replicate 2								
35S:PGB1 N tech rep 1	25.7	3.9	6.6					
35S:PGB1 H tech rep 1	27.7	3.9	7.1	1.08				
35S:PGB1 N tech rep 2	**43.8**	5.8	7.6		0.99	3	0.24	0.14
35S:PGB1 H tech rep 2	38.3	**6.7**	5.7	**0.76**				
35S:PGB1 N tech rep 3	25.6	3.3	7.8					
35S:PGB1 H tech rep 3	17.9	3.2	5.6	0.72				
35S:PGB1 N tech rep 4	20.2	3.6	5.6					
35S:PGB1 H tech rep 4	24.3	3.7	6.6	1.17				
Biological Replicate 4								
35S:PGB1 N tech rep 1	40.1	4.8	8.4					
35S:PGB1 H tech rep 1	39.7	5.3	7.5	0.90				
35S:PGB1 N tech rep 2	17.5	2.0	8.8		0.92	2	0.04	0.03
35S:PGB1 H tech rep 2	13.3	1.6	8.3	0.95				
35S:PGB1 N tech rep 3	**5.9**	1.7	3.5					
35S:PGB1 H tech rep 3	**6.5**	3.0	2.2	**0.62**				
Biological Replicate 5								
35S:PGB1 N tech rep 1	**9.2**	3.0	3.1					
35S:PGB1 H tech rep 1	**9.8**	2.9	3.4	**1.10**				
35S:PGB1 N tech rep 2	30.5	2.2	13.9		1.05	3	0.16	0.09
35S:PGB1 H tech rep 2	41.3	2.6	15.9	1.15				
35S:PGB1 N tech rep 3	30.7	3.3	9.3					
35S:PGB1 H tech rep 3	31.8	3.0	10.6	1.14				
35S:PGB1 N tech rep 4	25.9	3.9	6.6					
35S:PGB1 H tech rep 4	30.5	5.3	5.8	0.87				

Table 11: H3K9ac fold change levels in root tips of the Pgb1-RNAi line exposed to normoxia (N) or hypoxia (H). The proportional protein values (µg) were calculated using the linear curve equations described in the previous chapter. The H3K9ac proportional protein value was normalized for loading using the corresponding H3 proportional protein value (H3K9ac proportional protein value / H3 proportional protein value). The (H/N) fold changes were calculated by generating a ratio of normalized hypoxia-treated sample to normalized normoxic-treated sample. Standard deviation is indicated with SD and standard error mean is indicated with SEM. The n-value represents the number of technical replicates per biological replicate. Bolded values indicate protein levels that are outside of the preestablished linear ranges for the test antigen and the loading control, as defined in the previous section. If deemed outside of the linear range, the (H/N) fold changes were removed from further analysis. Experiments were conducted on several technical replicates of per biological replicate.

H3K9ac	H3K9ac Proportional Protein Value (µg)	H3 Proportional Protein Value (µg)	Ratio H3K9ac / H3 loading control	Ratio H/N	Average	n	SD	SEM
Biological Replicate 1								
Pgb1-RNAi N tech rep 1	17.5	**8.1**	2.2					
Pgb1-RNAi H tech rep 1	**23.0**	**8.7**	2.6	**1.22**				
Pgb1-RNAi N tech rep 2	12.7	4.7	2.7					
Pgb1-RNAi H tech rep 2	15.3	2.5	6.1	2.28	1.82	2	0.64	0.45
Pgb1-RNAi N tech rep 3	13.8	**7.0**	2.0					
Pgb1-RNAi H tech rep 3	15.5	**7.3**	2.1	**1.07**				
Pgb1-RNAi N tech rep 4	7.2	2.4	3.0					
Pgb1-RNAi H tech rep 4	15.2	3.7	4.2	1.37				
Biological Replicate 2								
Pgb1-RNAi N tech rep 1	10.2	3.2	3.2					
Pgb1-RNAi H tech rep 1	9.8	1.5	6.5	2.02				
Pgb1-RNAi N tech rep 2	9.0	**6.9**	1.3		1.83	3	0.30	0.18
Pgb1-RNAi H tech rep 2	12.5	4.8	2.6	1.98				
Pgb1-RNAi N tech rep 3	**4.5**	3.2	1.4					
Pgb1-RNAi H tech rep 3	7.5	3.6	2.1	1.48				
Biological Replicate 3								
Pgb1-RNAi N tech rep 1	18.0	4.6	4.0					
Pgb1-RNAi H tech rep 1	**21.4**	4.8	4.4	1.12				
Pgb1-RNAi N tech rep 2	11.1	**0.8**	14.8					
Pgb1-RNAi H tech rep 2	11.3	**0.8**	14.0	**0.95**				
Pgb1-RNAi N tech rep 3	18.3	1.6	11.8					
Pgb1-RNAi H tech rep 3	**20.1**	2.0	10.0	0.85				
Pgb1-RNAi N tech rep 4	13.8	4.6	3.0		1.11	5	0.32	0.14
Pgb1-RNAi H tech rep 4	17.7	5.5	3.2	1.07				
Pgb1-RNAi N tech rep 5	14.4	2.1	6.7					
Pgb1-RNAi H tech rep 5	18.4	3.2	5.7	0.84				
Pgb1-RNAi N tech rep 6	8.1	1.5	5.4					
Pgb1-RNAi H tech rep 6	16.2	1.8	9.0	1.68				
Pgb1-RNAi N tech rep 7	15.6	**0.6**	26.0					
Pgb1-RNAi H tech rep 7	14.7	**0.8**	18.9	**0.73**				

Table 12: H3K14ac fold change levels in root tips of the Pgb1-RNAi line exposed to normoxia (N) or hypoxia (H). The proportional protein values (µg) were calculated using the linear curve equations described in the previous chapter. The H3K14ac proportional protein value was normalized for loading using the corresponding H3 proportional protein value (H3K14ac proportional protein value / H3 proportional protein value). The (H/N) fold changes were calculated by generating a ratio of normalized hypoxia-treated sample to normalized normoxic-treated sample. Standard deviation is indicated with SD and standard error mean is indicated with SEM. The n-value represents the number of technical replicates per biological replicate. Bolded values indicate protein levels that are outside of the preestablished linear ranges for the test antigen and the loading control, as defined in the previous section. If deemed outside of the linear range, the (H/N) fold changes were removed from further analysis. Experiments were conducted on several technical replicates of per biological replicate.

H3K14ac	H3K14ac Proportional Protein Value (µg)	H3 Proportional Protein Value (µg)	Ratio H3K14ac / H3 Loading control	Ratio H/N	Average	n	SD	SEM
Biological Replicate 1								
Pgb1-RNAi N tech rep 1	9.8	**7.0**	1.4		1.28	3	0.36	0.21
Pgb1-RNAi H tech rep 1	12.7	**7.3**	1.7	**1.24**				
Pgb1-RNAi N tech rep 2	36.5	**6.6**	5.5					
Pgb1-RNAi H tech rep 2	**46.6**	5.1	9.1	1.65				
Pgb1-RNAi N tech rep 3	19.7	4.7	4.2					
Pgb1-RNAi H tech rep 3	24.0	4.6	5.2	1.25				
Pgb1-RNAi N tech rep 4	13.2	2.4	5.5					
Pgb1-RNAi H tech rep 4	18.9	3.7	5.2	0.93				
Biological Replicate 2								
Pgb1-RNAi N tech rep 1	14.4	3.2	4.5		1.90	3	0.87	0.50
Pgb1-RNAi H tech rep 1	19.1	1.5	12.5	2.77				
Pgb1-RNAi N tech rep 2	31.1	**6.9**	4.5					
Pgb1-RNAi H tech rep 2	41.6	4.8	8.6	1.91				
Pgb1-RNAi N tech rep 3	29.8	3.2	9.2					
Pgb1-RNAi H tech rep 3	34.5	3.6	9.6	1.04				
Biological Replicate 3								
Pgb1-RNAi N tech rep 1	18.5	**6.9**	2.7		2.35	1	-	-
Pgb1-RNAi H tech rep 1	11.8	**6.5**	1.8	**0.67**				
Pgb1-RNAi N tech rep 2	20.9	4.6	4.5					
Pgb1-RNAi H tech rep 2	26.7	2.5	10.7	2.35				
Pgb1-RNAi N tech rep 3	**9.6**	2.1	4.5					
Pgb1-RNAi H tech rep 3	**7.9**	3.2	2.5	**0.55**				

Table 13: H3K9ac fold change levels in root tips of the *pgb1-1* line exposed to normoxia (N) or hypoxia (H). The proportional protein values (µg) were calculated using the linear curve equations described in the previous chapter. The H3K9ac proportional protein value was normalized for loading using the corresponding H3 proportional protein value (H3K9ac proportional protein value / H3 proportional protein value). The (H/N) fold changes were calculated by generating a ratio of normalized hypoxia-treated sample to normalized normoxic-treated sample. Standard deviation is indicated with SD and standard error mean is indicated with SEM. The n-value represents the number of technical replicates per biological replicate. Bolded values indicate protein levels that are outside of the preestablished linear ranges for the test antigen and the loading control, as defined in the previous section. If deemed outside of the linear range, the (H/N) fold changes were removed from further analysis. Experiments were conducted on several technical replicates per biological replicate.

H3K9ac	H3K9ac Proportional Protein Value (µg)	H3 Proportional Protein Value (µg)	Ratio H3K9ac / H3 loading control	Ratio H/N	Average	n	SD	SEM
Biological Replicate 1								
pgb1-1 N tech rep 1	12.3	2.2	5.7		2.43	4	2.10	1.05
pgb1-1 H tech rep 1	11.0	1.7	6.5	1.15				
pgb1-1 N tech rep 2	**25.2**	5.9	4.3					
pgb1-1 H tech rep 2	**21.7**	2.0	10.9	**2.55**				
pgb1-1 N tech rep 3	15.8	5.8	2.7					
pgb1-1 H tech rep 3	**24.7**	**7.3**	3.4	**1.25**				
pgb1-1 N tech rep 4	18.0	**6.1**	2.9					
pgb1-1 H tech rep 4	12.3	3.0	4.1	1.38				
pgb1-1 N tech rep 5	18.1	3.3	5.5					
pgb1-1 H tech rep 5	7.3	**0.8**	9.0	1.62				
pgb1-1 N tech rep 6	16.7	3.0	5.7					
pgb1-1 H tech rep 6	16.1	**0.5**	31.5	5.57				
Biological Replicate 2								
pgb1-1 N tech rep 1	**4.4**	2.0	2.2		1.99	4	0.29	0.15
pgb1-1 H tech rep 1	16.2	3.2	5.0	2.30				
pgb1-1 N tech rep 2	5.7	2.2	2.6					
pgb1-1 H tech rep 2	10.8	2.6	4.1	1.59				
pgb1-1 N tech rep 3	7.2	2.2	3.3					
pgb1-1 H tech rep 3	9.3	1.4	6.7	2.03				
pgb1-1 N tech rep 4	12.0	4.8	2.5					
pgb1-1 H tech rep 4	19.7	3.8	5.2	2.06				

Table 14: H3K14ac fold change levels in root tips of the *pgb1-1* line exposed to normoxia (N) or hypoxia (H). The proportional protein values (µg) were calculated using the linear curve equations described in the previous chapter. The H3K14ac proportional protein value was normalized for loading using the corresponding H3 proportional protein value (H3K14ac proportional protein value / H3 proportional protein value). The (H/N) fold changes were calculated by generating a ratio of normalized hypoxia-treated sample to normalized normoxic-treated sample. Standard deviation is indicated with SD and standard error mean is indicated with SEM. The n-value represents the number of technical replicates per biological replicate. Bolded values indicate protein levels that are outside of the preestablished linear ranges for the test antigen and the loading control, as defined in the previous section. If deemed outside of the linear range, the (H/N) fold changes were removed from further analysis. Experiments were conducted on several technical replicates of per biological replicate.

H3K14ac	H3K14ac Proportional Protein Value (µg)	H3 Proportional Protein Value (µg)	Ratio H3K14ac / H3 loading control	Ratio H/N	Average	n	SD	SEM
Biological Replicate 1								
pgb1-1 N tech rep 1	19.4	5.9	3.3					
pgb1-1 H tech rep 1	14.2	2.0	7.1	2.16				
pgb1-1 N tech rep 2	39.1	5.8	6.8					
pgb1-1 H tech rep 2	31.3	**7.3**	4.3	0.64	2.89	3	2.69	1.55
pgb1-1 N tech rep 3	**9.3**	3.3	2.9					
pgb1-1 H tech rep 3	13.6	**0.8**	16.8	5.87				
pgb1-1 N tech rep 4	**8.1**	3.0	2.8					
pgb1-1 H tech rep 4	**6.9**	**0.5**	13.5	**4.89**				
Biological Replicate 2								
pgb1-1 N tech rep 1	**7.2**	2.0	3.6					
pgb1-1 H tech rep 1	**6.5**	3.2	2.0	**0.56**				
pgb1-1 N tech rep 2	**7.7**	2.2	3.5					
pgb1-1 H tech rep 2	35.3	2.6	13.5	3.86	2.97	2	1.26	0.89
pgb1-1 N tech rep 3	**8.7**	2.2	4.0					
pgb1-1 H tech rep 3	11.5	1.4	8.2	2.08				

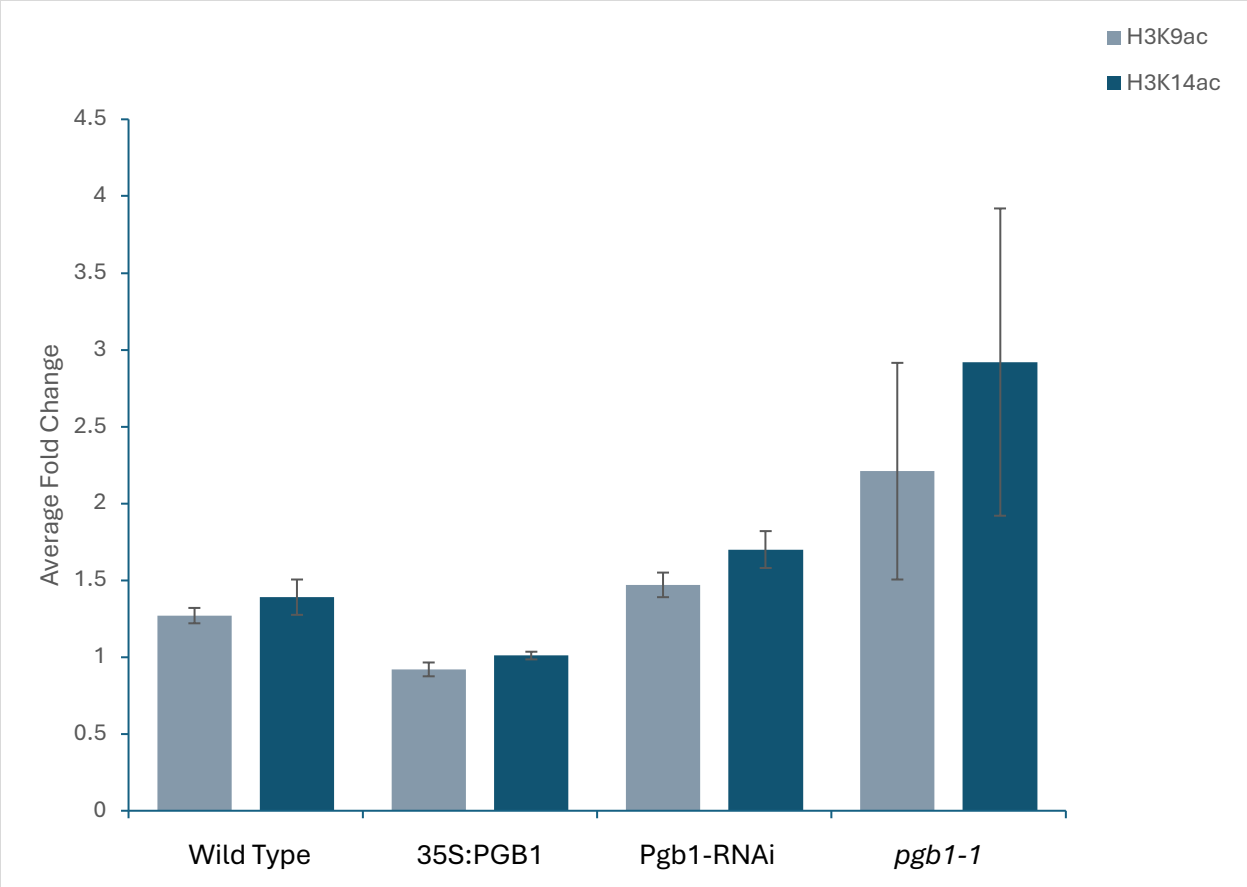

Figure 10: Average (H/N) fold change values of both H3K9ac and H3K14ac of all biological and technical replicates at each of the four lines (wild type, 35S:PGB1, Pgb1-RNAi, and *pgb1-1*). The error bars represent the standard error mean of the wild type, 35S:PGB1, and Pgb1-RNAi data sets. The error bars for the pgb1-1 line represent standard deviation of the data set. The sample sizes for each group are: n = 23 for wild type H3K9ac, n = 14 for wild type H3K14ac, n = 16 for 35S:PGB1 H3K9ac, n = 10 for 35S:PGB1, n = 10 for Pgb1-RNAi H3K9ac, n = 7 for Pgb1-RNAi, n = 8 for *pgb1-1* H3K9ac, and n = 5 for *pgb1-1* H3K14ac.

Independent two-tailed t-tests were conducted to assess statistical significance ($p<0.05$) among the values obtained. The first analysis compared H3K9 and H3K14 acetylation levels among the four lines to assess the effect of the genotype (Table 15A and 15B). For H3K9ac (H/N) fold changes, statistically significant differences were observed between WT vs. 35S:PGB1, as well as between 35S:PGB1vs. Pgb1-RNAi, and 35S:PGB1 vs. *pgb1-1.* No statistically significant differences between genotypes were observed in H3K14ac (H/N) fold

changes; this was likely due to smaller sample size in H3K14ac immunoblots compared to H3K9ac immunoblots.

The second analysis tested whether the (H/N) fold changes in H3K9ac and H3K14ac levels were statistically different within each line (Table 15C). Hypoxia induced no statistically significant change in H3K9 or H3K14 acetylation levels within each of the four lines.

In the third analysis, the H3K9 and H3K14 acetylation level data sets were pooled together within each line. The pooled acetylation (H/N) fold change values were then assessed using a one-tailed t-test and a two-tailed t-test. The one-tailed t-test with pooled acetylation (H/N) fold change values was found to be significantly greater than one for the WT, Pgb-RNAi, and *pgb1-1* lines (Table 15D). The two-tailed t-test found statistically significant differences between all lines, except for WT vs. Pgb1-RNAi and Pgb1-RNAi vs *pgb1-1* (Table 15E).

Table 15: Series of t-tests comparing H3K9 and H3K14 acetylation rates between the lines used (wild type, 35S:PGB1, Pgb1-RNAi, and *pgb1-1*), comparing the H3K9 and H3K14 acetylation rates within lines, and pooled acetylation (H3K9ac and H3K14ac) levels between the lines used. **(A)** Two-tailed t-tests comparing H3K9ac and **(B)** H3K14ac (H/N) fold changes between lines. **(C)** H3K9 and H3K14 acetylation levels were compared within the same lines. **(D)** This set also contains one-tailed t-tests assessing whether pooled acetylation average (H/N) fold changes are more than one, and **(E)** two-tailed t-tests comparing average (H/N) fold changes of pooled acetylation between lines. The n-value represents the number of replicates included in each group, and SD represents standard deviation. Each table contains the resulting p-values from the t-test listed above.

A

H3K9ac two-tailed t-test				
	Col-0	35S:PGB1	Pgb1-RNAi	*pgb1-1*
WT	-	0.02	0.31	0.1
35S:PGB1		-	0.01	0.04
Pgb1-RNAi			-	0.19
pgb1-1				-

B

H3K14ac two-tailed t-test				
	Col-0	35S:PGB1	Pgb1-RNAi	*pgb1-1*
WT	-	0.13	0.38	0.16
35S:PGB1		-	0.04	0.1
Pgb1-RNAi			-	0.25
pgb1-1				-

C

H3K9ac v H3K14ac	p-value
WT	0.65
35S:PGB1	0.38
Pgb1-RNAi	0.47
pgb1-1	0.51

D

Pooled acetylation one-tailed t-test				
	n	Average	SD	p-value
WT	36	1.28	0.63	0.003
35S:PGB1	26	0.96	0.28	0.23
Pgb1-RNAi	17	1.49	0.56	0.001
pgb1-1	13	2.49	1.62	0.003

E

Pooled acetylation two-tailed t-test				
	Col-0	35S:PGB1	Pgb1-RNAi	*pgb1-1*
WT	-	0.005	0.16	0.02
35S:PGB1		-	0.001	0.005
Pgb1-RNAi			-	0.07
pgb1-1				-

4. DISCUSSION

4.1. Histone acetylation

Histone acetylation (such as H3K9ac and H3K14ac) tends to confer open transcriptionally active chromatin. This has the potential to affect regulation of gene transcription and the hypoxic response. To understand how histone acetylation dynamics were affected by hypoxia in *Arabidopsis thaliana*, H3K9ac and H3K14ac levels were analyzed in the root tips of a WT line.

4.1.1. Histone acetylation in response to hypoxia

Hypoxia was found in this study to enhance global acetylation levels of H3K9 and H3K14 in WT Arabidopsis (Col-0) root tips. Hypoxia-induced enhancement of H3K9 and H3K14 acetylation levels was hypothesized in this study to be driven by increased NO levels because NO levels are elevated in hypoxic conditions, and NO has been implicated as an epigenetic modifier.

Previous work has been completed analyzing H3K9ac and H3K14ac levels in response to hypoxia. Lee and Bailey-Serres (2019) performed ChIP-Seq experiments on 2- and 9-hour anoxic treated whole seedlings. They found that H3K9ac significantly increased over hypoxic responsive genes in both 2- and 9-hour treatment but there was no significant change in in global H3K9ac levels over gene bodies (Lee & Bailey-Serres, 2019). There was also no change in global H3K14ac levels over gene bodies or over hypoxic responsive genes (Lee & Bailey-Serres, 2019). Lee and Bailey-Serres did not do any antibody quality control or ChIP-seq internal controls. The lack of antibody quality control measures leaves the possibility for cross reactivity in the H3K9ac antibody especially, as H3K9ac and H3K27ac have similar flanking amino acid

sequences (Chaubet *et al*., 1992). Internal ChIP controls, such as a spike-in control, serve to normalize ChIP-seq data to effectively account for read coverage (Bonhoure *et al.,* 2014). This allows for the normally qualitative ChIP-seq to reflect quantitative values. The difference between what was found by Lee and Bailey-Serres (2019) and this thesis was likely due to the lack of an internal control.

4.1.2. Histone acetylation in response to *Phytoglobin1* down-regulation

Nitric oxide levels are increased in root tip tissue under low-oxygen conditions (Dordas *et al.*, 2003; Mira *et al*., 2023b). NO is primarily produced via nitrite reduction pathways, as oxidative pathways are hindered under hypoxia (Gupta *et al.*, 2022). Nitrite reduction under hypoxia primarily occurs in the mitochondria through the action of members of the electron transport chain: complex III (bc1), complex IV (cytochrome c oxidase), and the alternative oxidase (AOX) (Gupta *et al.*, 2020).

Evidence is available that NO enhances H3K9 and H3K14 acetylation and that S-nitrosylation modifies the activity of multiple HDACs (Mengel *et al.*, 2016; Ageeva-Kieferle *et al.*, 2021; Zheng *et al.*, 2023). Pgb1 was used to investigate the connection between NO and the epigenome because Pgb1 can confer hypoxia tolerance when overexpressed and reduced hypoxia tolerance when suppressed. The connection between Pgb1 and enhanced hypoxia and/or waterlogging tolerance has been demonstrated in *Arabidopsis thaliana* (Hunt *et al.*, 2002; Mira *et al.*, 2023b), *Brassica napus* (El-Khateeb *et al.*, 2023), maize (*Zea mays*; Mira *et al.,* 2016; Mira *et al.*, 2023a), soybean (*Glycine max*; Mira *et al.,* 2021), and barley (*Hordeum vulgare L.*; Cochrane *et al.,* 2017). To understand how altered Pgb1 may affect H3K9 and H3K14 acetylation levels, H3K9ac and H3K14ac were assessed in transgenic lines with modified *PGB1* expression (35S:PGB1, Pgb-RNAi, and *pgb1-1* lines). Lines with enhanced PGB1 expression

(35S:PGB1) were hypothesized in this study to have reduced NO levels, maintained HDAC activity, and therefore maintained normoxic H3K9 and H3K14 acetylation levels. In contrast, the lines with reduced *Pgb1* expression (PGB-RNAi and *pgb1-1*) were hypothesized in this study to have elevated NO levels, reduced HDAC activity, and enhanced H3K9 and H3K14 acetylation.

In the 35SPGB1 line, hypoxia did not change the level of H3K9ac and H3K14ac in root tip tissue. An elevation in Pgb1 protein levels most likely mitigated the enhancement of H3K9 and H3K14 acetylation levels caused by low oxygen. In contrast, the *pgb1-1* line exacerbated the hypoxia-induced enhancement of H3K9ac and H3K14ac levels observed in WT. Under hypoxia, H3K9ac and H3K14ac levels doubled in the *pgb1-1* line compared to the WT line. The absence of Pgb1 caused a significant elevation in both H3K9 and H3K14 acetylation levels. This indicates that Pgb1, by acting on NO, is involved in mediates of epigenetic regulation during hypoxia. The proposed mechanism of hypoxia-induced increases in H3K9ac and H3K14ac levels shown in indicated in Figure 11.

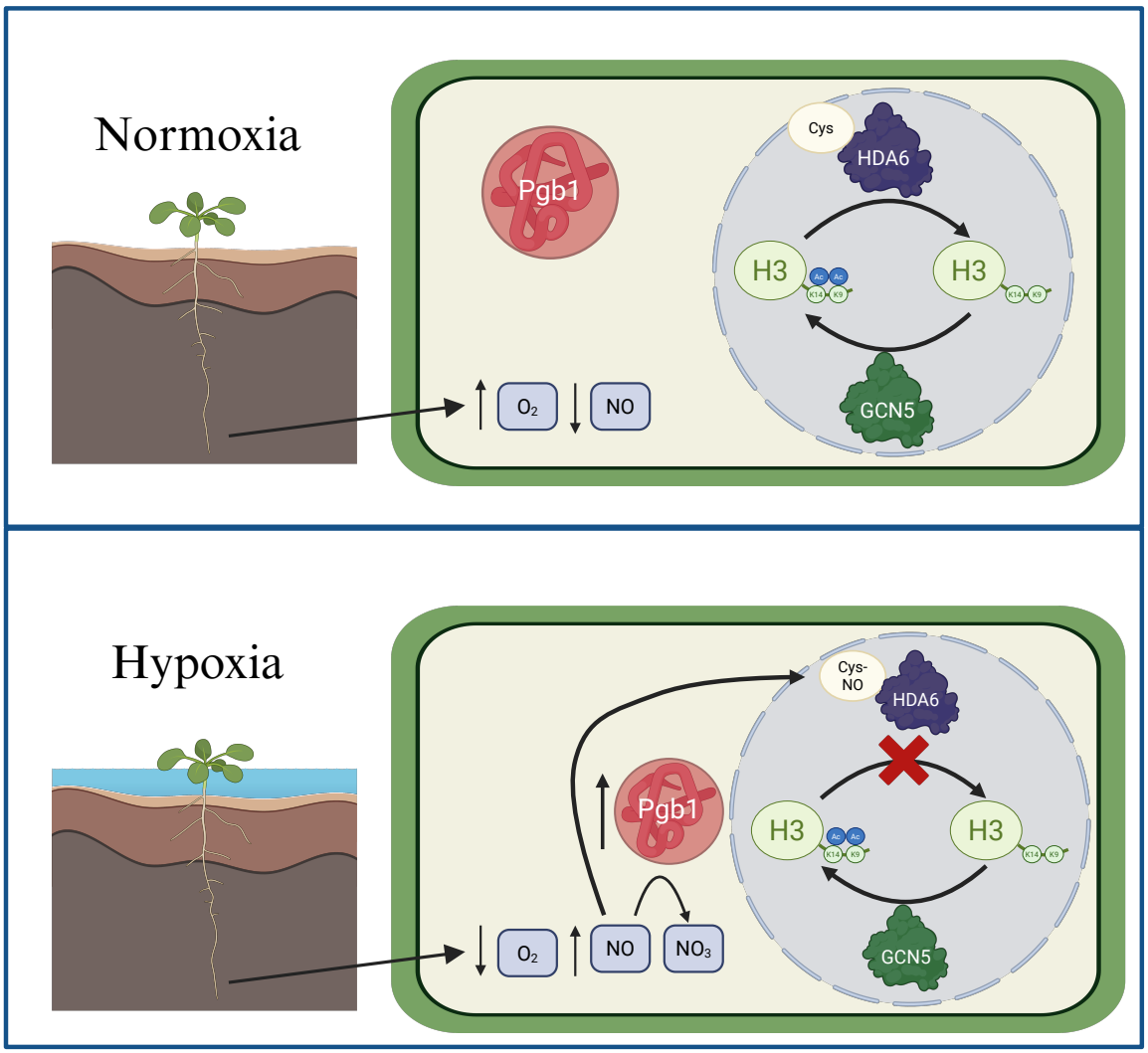

Figure 11: Proposed mechanism of hypoxia-induced increase in global H3K9 and H3K14 acetylation levels. Under normoxic conditions, oxygen is at normal physiological levels, Pgb1 is present but at low levels, and NO levels are not high enough to S-nitrosylate HDA6. HDA6 and lysine acetyltransferases such as GCN5, are both active and work antagonistically to maintain acetylation at H3K9 and H3K14. Increased NO levels under hypoxic conditions cause S-nitrosylation of HDA6, thereby decreasing HDAC activity. When HDA6 activity decreases, levels at H3K9 and H3K14 acetylation increase because GCN5 activity has not changed. As Phytoglobin1 increases in expression under hypoxic conditions, it can scavenge NO converting it to nitrate. Therefore, Phytoglobin1 can restore both the HDA6 activity and H3K9 and H3K14 acetylation to those levels observed under normoxia. Created in https://BioRender.com.

In the Pgb1-RNAi line, the levels of both H3K9ac and H3K14ac increased slightly more than what was observed in WT. However, the increase in H3K9 and H3K14 acetylation levels was not significantly different ($p < 0.05$) from the WT values. The absence of a marked increase in H3K9ac and H3K14ac in the Pgb1-RNAi line may be caused by potentially higher Pgb1 protein levels than the levels present in the *pgb1-1* line. The Pgb1-RNAi and *pgb1-1* lines were not directly compared in this study, but previous works revealed that Pgb1 is absent in the T-DNA insertion line (*pgb1-1*; Hartman *et al.*, 2019) while it is only reduced by half in the Pgb-RNAi line (Hebelstrup et al., 2006; Mira et al., 2023b).

4.1.3. Histone acetylation in response to nitric oxide in animal models

Nitric oxide can enhance global histone acetylation rates in animal models by inhibiting HDACs and activating specific KAT complexes. In mouse neuronal cell cultures, elevated NO synthesis led to inactivation of HDAC2 through S-nitrosylation of Cys 262 and Cys 274 (Nott *et al.*, 2008). S-nitrosylation of another HDAC, sirtuin-1 (SIRT1), was found to inactivate it as well (Kalous *et al.*, 2016). Nitric oxide-mediated HDAC inactivation is not ubiquitous in all cell types; in human umbilical endothelial cells, NO maintains deacetylase activity of two class II histone deacetylases, HDAC4 and HDAC5 (Illi *et al.*, 2008). Stress-induced NO decreased global H3K14ac levels (Illi *et al.*, 2008). This was found to be caused by nuclear shuttling of HDAC4 and HDAC5, mediated by NO-induced activation of protein phosphatase 2A (PP2A; Illi *et al.*, 2008).

Although no evidence exists for NO-regulated changes in KAT activity in plants, a connection has been established in animal models. Oral cancer cells with increased expression of NO synthase displayed elevated acetylation of H3K9, H3K14, H3K56, and H4K8 (Arif *et al.*, 2010). GAPDH, a necessary enzyme in glycolysis, can be S-nitrosylated and, in animal systems,

has been shown to translocate to the nucleus, where it enhances the KAT activity of CBP/p300 (Arif *et al.*, 2010). S-nitrosylation of GAPDH primes it for acetylation by CBP/p300 at Lys160, which further stimulates autoacetylation activity of CBP/p300 (Sen *et al.*, 2008). Autoacetylation of CBP/p300 increases its acetyltransferase activity and causes it to acetylate proteins in its proximity, including all four core histones and other regulatory proteins. However, CBP/p300 predominantly acetylates H3K18, H3K27, and H3K36 (Weinert *et al*., 2018). Additionally, H3K9 and H3K14 were found to be unaffected by differential CBP/p300 transcript expression (Weinert *et al*., 2018). This indicates that the relationship observed between Pgb1 and H3K9 and H3K14 acetylation is not modulated by CBP/p300. GAPDH was also found to interact with and trans-nitrosylate HDACs such as HDAC2 and sirtuin-1 (Kornberg *et al.*, 2010). GAPDH can be S-nitrosylated in plants (Lindermayr *et al.*, 2005; Zaffagnini *et al.*, 2013). Interestingly, in Arabidopsis, GAPC2, a plant GAPDH, expression is strongly upregulated in hypoxic QC cells in *Arabidopsis thaliana* roots (Hill *et al*., 2026). This could indicate a relationship between GAPDH and epigenetic regulation in QC cells, although a direct connection has not yet been made.

4.2. Histone deacetylase S-nitrosylation

Both HDA6 and HDA19 were found to be S-nitrosylated in response to elevated NO levels, and S-nitrosylation was found to reduce HDA6 activity and subsequently enhance H3K9 and H3K14 acetylation (Ageeva-Kieferle *et al.*, 2021). Alternatively, S-nitrosylated HDA19 exhibited increased HDAC activity (Zheng *et al.*, 2023). HDA19 was found to be S-nitrosylated primarily at the active site, Cys137 (Zheng *et al.*, 2023). S-nitrosylated HDA19 was found to remove H3K14ac residues from genes involved in oxidative stress, but large-scale global changes in H3K9 and H3K14 acetylation remained largely unchanged (Zheng *et al.*, 2023).

Therefore, S-nitrosylation-mediated inactivation of HDA6 is the most likely explanation for the elevation in H3K9 and H3K14 acetylation levels observed in response to hypoxia.

The difference in HDA6 and HDA19 response to S-nitrosylation may be related to their involvement in different pathways and processes. HDA6 and HDA19 share a similar structure and similar evolutionary origin and are both localized to the nucleus (Ageeva-Kieferle *et al.*, 2019; Kurita *et al.*, 2019; Guo *et al.*, 2023). Subsequently, both HDA6 and HDA19 recognize and deacetylate similar residues on both H3 and H4 (Early *et al.*, 2006; Choi *et al.,* 2012; Kotnik *et al.*, 2025). However, the two HDACs are involved in distinct regulatory pathways. HDA19 is engaged in development, as *hda19* mutants exhibit severe developmental defects that are absent in *hda6* mutants (Tian *et al.*, 2003; Ning *et al.*, 2019). HDA19 is involved in several developmental processes, including hypocotyl elongation, light signaling, and root cell elongation (Chen *et al.*, 2015; Jing *et al.*, 2020; Velez-Bermudez & Schmidt, 2023). HDA19 is also involved in several stress responses, including heat, drought, and salicylic acid-mediated biotic stress response (Choi *et al.*, 2012; Ueda *et al.*, 2018). Alternatively, HDA6 is a necessary component in transposon silencing, as *hda6* mutants show increased expression of transgenes and rRNA (Probst *et al.*, 2004; Early *et al*., 2012). HDA6 is also able to modulate mRNA polyadenylation patterning which can affect translational efficiency (Lin *et al.*, 2020). HDA6 interacts with DNA methyltransferase MET1 and the histone methyltransferases SUVH4/5/6 to contribute to heterochromatin formation through H3K9 methylation and H3 deacetylation (To *et al*, 2011; Liu *et al*, 2012). As with siRNA-mediated gene silencing, transposon silencing is mediated by HDA6, MET1, and SUVH4/5/6. HDA6 has also been shown to interact with multiple chromatin remodelers. SWI3B, an essential component of the SWI/SNF chromatin remodeling complex, directly interacts with HDA6 to maintain transposon silencing (Yang *et al.*,

2020). HDA6 can also interact with the chromodomain helicase DNA-binding domain 3 chromatin remodeler PICKLE to suppress the expression of specific genes and transposable elements (Li *et al.*, 2024). HDA6 is involved in several developmental pathways as well, such as flowering time, senescence, silique growth, and leaf growth (Wu *et al.*, 2008; Yu *et al.*, 2016; Yuan *et al.*, 2019; Du *et al.*, 2024) and several stress response pathways, such as cold tolerance, ABA signaling, and salt stress (To *et al.*, 2011; Luo *et al.*, 2012). Both HDA6 and HDA19 are involved in repressing embryonic properties after germination, creating contingency for this important developmental process (Tanaka *et al.*, 2008). Although HDA6 and HDA19 deacetylate similar lysine residues, they possess mostly independent functions.

4.3. Consequences of histone deacetylase S-nitrosylation

HDA6 deacetylates H3K9ac and H3K14ac (Ageeva-Kieferle *et al.*, 2021). Hypoxia-induced HDA6 inactivation and subsequent elevation in H3K9ac and H3K14ac are reliant on KATs to continue to apply acetylation marks. Arabidopsis has 4 KAT families: GCN5-related N-acetyltransferase (GNAT), MO2-YBF2/SAS3-SAS2-TIP60 (MYST), CREB-binding proteins (CBP), and TBP-associated factor (TAF1; Kornet & Scheres, 2009). GCN5 (also called HAG1), a member of the GNAT family, is the best studied KAT in *Arabidopsis thaliana* and is known to preferentially acetylate both H3K9 and H3K14. H3K14 is only known to be acetylated by GCN5, while H3K9 can be acetylated by both GCN5 and TAF1 (Gan *et al.*, 2021). CBP/p300, a member of the CBP family, was indicated in animal models to increase acetylation activity in response to NO: however, as mentioned above, this KAT tends to preferentially acetylate other lysines on H3 and H4 instead of H3K9 and H3K14 (Weinert *et al*., 2018).

HDA6 inactivation via S-nitrosylation could result in several regulatory outcomes. First, it could potentially enhance transposable element expression. Transposable elements can be

organized into two major categories, DNA transposons and retrotransposons. DNA transposons, when transcribed, utilize a transposase gene within the transposon to remove themselves from one location and insert themselves elsewhere in the genome (Muñoz-López & García-Pérez, 2010). Retrotransposons use an RNA intermediary and a reverse transcriptase encoded within the transposon to replicate and insert the copy into the genome (Muñoz-López & García-Pérez, 2010). Transposable elements, DNA transposons or retrotransposons, can be inserted into enhancer regions, promoters, and within the gene body (Dubin *et al.*, 2018). This can be harmful to stress responses because transposable elements have the potential to both activate genes that negatively affect stress responses and/or inactivate genes that positively affect stress responses.

Although increased transposable element expression could be harmful, it may provide an advantage under stress conditions. Hormones and several stress conditions have been shown to influence transcription of transposable elements in Arabidopsis. These include heat stress, osmotic stress, cold stress, nutrient starvation, and ABA (Duan *et al.*, 2008; Zeller *et al.*, 2009). Novel gene functions introduced by transposon insertion can confer an advantage against environmental stressors (Ramakrishnan *et al.*, 2021). This has been proposed as an evolutionary mechanism that enhanced genomic plasticity under environmental stress, because although random, the inactivation or activation of specific genes may confer an advantage under hypoxic stress (Dubin *et al.*, 2018). Additionally, some transposons contain stress-responsive elements that become upregulated in response to biotic or abiotic stresses (Casacuberta & González, 2013). The retrotransposon ONSEN contains a heat-responsive element, leading to increased expression of both the transposon and the surrounding genomic region in response to heat stress (Cavark *et al.*, 2014).

HDA6 inactivation could also lead to a significant global elevation in H3K9 and H3K14 acetylation levels. H3K9ac and H3K14ac tend to loosen chromatin conformation through their interactions with epigenetic and transcriptional modifiers. The proteins that recognize H3K9ac and H3K14ac contain bromodomains. Bromodomain containing proteins can be separated into three main categories: chromatin remodelers, transcriptional regulators, and epigenetic regulators (Bardani *et al.*, 2023). Chromatin remodelers, such as the SWI/SNF complex, recognize H3K9ac and H3K14ac and use their ATPase activity to mobilize nucleosomes, potentially allowing greater access of the transcriptional machinery to DNA (Fu *et al.*, 2023). Acetylation of H3, in conjunction with transcriptional regulators, is recognized by the SWI/SNF complex bromodomain, which can cause nucleosome mobility and H2A/H2B dimer displacement (Chatterjee *et al.*, 2011). Additionally, the bromodomain of the SWI/SNF complex binds preferentially to H3K14ac (Chatterjee *et al.*, 2011). Transcriptional regulators, such as the GENERAL TRANSCRIPTION FACTOR GROUP E (GTE) 1-12 in *A. thaliana*, can interact with the epigenome through the bromodomain. H3K9 and H3K14 acetylation can also recruit KATs, such as GCN5, which can continue to add acetyl groups to adjacent histone residues, positively enforcing an open chromatin conformation (Bardani *et al.*, 2023).

H3K9ac and H3K14ac both promote a more open chromatin conformation; however, not every modification is recognized or affects the epigenome in the same way. H3K9ac and H3K14ac tend to co-occur and are distributed together across active enhancers, CpG islands, and the transcription start sites (TSSs) of active genes (Lim *et al.*, 2010; Karmodiya *et al.*, 2012). H3K14ac, however, is distributed more over a subset of inactive promoters than H3K9ac (Karmodiya *et al.*, 2012). One potential explanation for the distribution of H3K14ac is that the modification is placed on specific promoters at low levels to prime them for future activation in

response to environmental stimuli. Additionally, once acetylation is placed onto H3K9 or H3K14, other modifications such as methylation or ubiquitination are blocked from those lysines (Koumbadinga *et al.*, 2015). The inhibition of ubiquitination in favor of acetylation, could lead to differential mRNA splicing patterns (Koumbadinga *et al.*, 2015).

H3K9ac and H3K14ac were the focus of this study; however, HDA6 can deacetylate other lysine residues on histones and non-histone proteins. HDA6 has been shown to affect global acetylation levels of both H3 and H4 (Zhou *et al.,* 2021; Vincent *et al.,* 2022). The confirmed acetylation sites of H3 and H4 are H3K9, H3K14, H3K27, H4K5, and H4K12, although there are likely more (Early et al., 2006; Lin *et al.,* 2020; Vincent *et al*., 2022). HDA6, in conjunction with GCN5, can also manage non-histone proteins such as the transcription factors WRKY63 and TOPLESS. HDA6 can deacetylate WRKY63 at lysine 31, reducing nuclear localization and WRKY63-mediated transcriptional activity (Shih *et al*., 2025). WRKY63 has been implicated in ABA response, drought tolerance, mitochondrial stress response, and vernalization (Ren *et al.,* 2010; Van Aken *et al.,* 2013; Hung *et al.*, 2022). HDA6-mediated deacetylation of TOPLESS inhibits its ability to interact with adaptor protein NINJA and recruitment to MYC2 promoters (An *et al*., 2022). TOPLESS deacetylation affects jasmonate signaling modifying the regulation of several jasmonate-responsive genes (An *et al*., 2022). Jasmonate is involved in various developmental processes and in biotic stress responses (An *et al*., 2022). TOPLESS is also involved in auxin signaling and it acts as a co-repressor of auxin response genes indicating potential involvement of auxin signaling following HDA6 inactivation (Szemenyei *et al.,* 2008). Deactivation of HDA6 through S-nitrosylation could affect acetylation rates of other histone residues and of transcription factors like WRKY63 and

TOPLESS. This can cause transcriptional changes in response to NO not strictly explained by H3K9ac and H3K14ac.

Enhancing H3K9 and H3K14 acetylation may be beneficial, as it could increase the expression of genes involved in the hypoxic response. However, the negative effects of large-scale histone acetylation are likely. HDA6 deactivation could have a greater impact than regulation of the hypoxic response, as HDA6 is a necessary component of many stress and developmental pathways. Additionally, global increases in H3K9 and H3K14 acetylation would be harmful if regulation was altered to inhibit the stress response or induce genes irrelevant to survival. Although the downstream regulatory effects of elevated global H3K9 and H3K14 acetylation in response to hypoxia are not known, it is plausible that Pgb1 provides an advantage under low oxygen stress. *PGB1* overexpression confers an advantage in hypoxic conditions, improving survival rates, growth rates, and QC functionality (Hunt *et al.*, 2002; Mira *et al.*, 2023b). Pgb1 has the potential to provide an advantage in hypoxic conditions by stabilizing the epigenome and potentially aberrant gene expression through NO scavenging.

4.4. Other epigenetic changes in response to hypoxia

Although histone acetylation was the focus of this study, DNA methylation, histone methylation, and nucleosome positioning may have affected the epigenome in low-oxygen conditions.

4.4.1. DNA methylation in response to hypoxia

In plant systems, a link has been established between hypoxia and the RNA-directed DNA methylation (RdDM) pathway. DNA methylation, the process of adding a methyl group to cytosine residues, tends to confer a closed, repressed chromatin state and is essential for gene

silencing. However, CG methylation is enriched over the transcription start and termination sites of actively transcribed genes in both plants and animals (Bewick & Schmitz, 2017). The RdDM pathway, a process unique to plants, directs DNA methylation through the recognition and matching of double-stranded RNAs to a genomic DNA sequence. Once the double-stranded RNA is matched to a DNA sequence, the matching DNA is methylated, preventing transcription of the gene. The RdDM pathway is involved in several processes, including silencing transposable elements, stress response, and developmental processes such as flowering (Erdmann & Picard, 2020). Small stranded RNAs can be organized into two groups: small interfering RNAs (siRNAs) and microRNAs (miRNAs). siRNAs tend to mediate persistent or long-term gene silencing, while miRNAs tend to mediate temporary gene downregulation (Tang, 2005). Hypoxia was found to change miRNA transcription in both *A. thaliana* and maize (Licausi *et al.*, 2010; Moldovan *et al.*, 2010). ARGONAUTE1 (AGO1) and ARGONAUTE4 (AGO4), components of the RdDM pathway that regulate miRNA production, were indicated in oxygen sensing in Arabidopsis. Loreti *et al.* (2019) found that the *ago1* mutant line was hypersensitive to submergence, while the *ago4* mutant line was tolerant to submergence. AGO4 in particular was found to increase DNA methylation in response to submergence (Loreti *et al.*, 2019). This indicates a potential connection between hypoxia and DNA methylation. However, this is insufficient to indicate how DNA methylation may be affected in plants.

Work on animal models provides in-depth insight into DNA methylation dynamics in response to hypoxia. DNA methylation is modulated by two kinds of enzymes, DNA methyltransferases (DNMTs), which add methyl groups to cytosine residues, and DNA demethylases, which remove methyl groups from cytosine residues. Hypoxia inhibits the activity of DNMTs and a family of DNA demethylases (TET enzymes). DNMTs require S-adenosyl

methionine (SAM) to catalyze the transfer of methyl groups to cytosines (Lyko, 2018). SAM, the main methyl donor in one-carbon metabolism, requires ATP to be cycled. Under hypoxic conditions with reduced energy availability, SAM levels are decline, thereby inhibiting DNA methylation. TET enzymes rely directly on oxygen availability to function, as they remove DNA methylation through a series of oxidation reactions (Kohli & Zhang., 2013). In animal systems, hypoxia is generally associated with global hypomethylation and is caused by reduced DNMT activity (Verdikt & Thienpont, 2024). Passive reductions in DNA methylation could cause this as DNA replicates without functional DNMT to replace preexisting DNA methylation. It could also be caused by other regulatory mechanisms that adjust DNMT or TET enzyme expression or activity. If the activity of DNMTs and TET enzymes remains the same across plants and animals, DNA hypomethylation may have impacted the epigenetic landscape by increasing the amount of open chromatin and potentially histone acetylation levels.

4.4.2. Histone methylation in response to hypoxia

Histone methylation can also be affected by hypoxia. In animal models, hypoxia inhibits Jumonji-C domain-containing lysine demethylase (JmjC-type KDM) enzymatic activity in a manner similar to that of the TET enzymes mentioned above, as both are non-heme iron dioxygenases (Kooistra & Helin, 2012; Islam *et al.*, 2018). Hypoxia induces increased expression of JmjC-type KDMs to compensate for decreased enzymatic activity (Beyer *et al.*, 2008; Xia *et al.*, 2009). However, despite increased expression of these JmjC-type KDMs, H3K27me3 still accumulated under hypoxic conditions (Batie *et al.*, 2019; Chakraborty *et al.*, 2019). A direct interaction between hypoxia and JmjC-type KDM activity has not been established in plants. Hypoxia can also inhibit lysine methyltransferase activity because SAM is required, as with DNMTs.

4.4.3. Nucleosome positioning in response to hypoxia

Nucleosome positioning can also be modulated by hypoxia. Chromatin remodeling enzymes rely on ATP to move nucleosomes (Chereji & Clark, 2018). Organisms under hypoxic stress may lack the ATP required to reposition nucleosomes. The SWI/SNF-type chromatin remodeler BRAHMA not only needs ATP to catalyze nucleosome movement, but is also stabilized through physical association with ERFVIIs in Arabidopsis (Vicente *et al.*, 2017). BRAHMA has also been found to co-target genes with KDMs, promoting active chromatin (Li *et al.*, 2016). Additionally, the ERFVIIs RAP2.2/RAP2.12, which are targets of the N-degron pathway, interact with the mediator complex subunit MED25 to promote transactivation of a subset of hypoxia responsive genes (HRGs) during hypoxic stress (Schippers *et al.*, 2024). The reduction in BRAHMA activity, combined with inefficient binding of the mediator complex to HRGs observed in hypoxia, could lead to diminished HRG upregulation under hypoxic stress.

4.5. Other epigenetic changes in response to nitric oxide

As with hypoxia, NO can influence other epigenetic modification such as DNA and histone methylation, potentially impacting the hypoxic response.

4.5.1. DNA methylation in response to nitric oxide

Nitric oxide, as one of the many signals of hypoxic stress, can also regulate DNA methylation. In rice, NO has also been implicated in the RdDM pathway and in modifying DNA methylation (Ou *et al.*, 2015; Zeng *et al.*, 2023). Nitric oxide regulated the expression of genes involved in meristematic regulation by inhibiting the interaction between AGO4 and WUSCHEL, a transcription factor involved in shoot stem cell fate (Zeng *et al.*, 2023). Hypomethylation of specific CHG sites was observed in response to NO application in rice (Ou

et al., 2015). However, these hypomethylations did not increase gene or transposon expression (Ou *et al.*, 2015).

DNA methylation was reported to be directly and indirectly regulated by NO in animal models. Unlike hypoxia, applications of either exogenous or endogenous NO caused an elevation in DNMT activity (Hmadcha *et al.*, 1999). The elevated in DNMT activity led to increased DNA methylation and, subsequently, induced gene silencing (Hmadcha *et al.*, 1999; Huang *et al.*, 2012). Nitric oxide inhibited the TET enzymes' dioxygenase activity by inhibiting oxygen binding to the enzymes' non-heme iron (Bovee *et al.*, 2018). Hypoxia and NO have both been implicated in regulating components of the RdDM pathway in plants and regulating DNMT and TET enzyme activity in animals. The inconsistency of global DNA methylation changes in response to both hypoxia and NO indicate that this response is likely dependent on species, tissue type, and internal and external signaling.

4.5.2. Histone methylation in response to nitric oxide

Histone methylation can also be affected by NO in plants through the modification of epigenetic enzymes and complexes. S-nitrosylation of Cys-125 on the arginine methyltransferase PRMT5 can enhance its enzymatic activity (Hu *et al.*, 2017). A *prmt5* mutant showed developmental defects and reduced abiotic stress tolerance; however, a PRMT5 transgenic line with a non-nitrosylable mutation at Cys-125 showed no developmental defects but remained stress sensitive (Hu *et al.*, 2017). The enhanced activity of PRMT5 enhanced the levels of Arg symmetric demethylation in Arabidopsis. S-nitrosylation of Cys125 of PRMT5 was reported to enhance stress tolerance by enabling specific pre-mRNA splicing patterns of stress-related genes (Hu *et al.*, 2017).

Nitric oxide can directly modify the polycomb repressive complex 2 (PRC2). PRC2 is a histone methyltransferase complex that primarily methylates H3K27 (Godwin & Farrona, 2022). VERNALIZATION2 (VRN2), a subunit of PRC2 in plants, is a target of the N-degron pathway (Gibbs *et al.*, 2018). During hypoxic stress, VRN2 has a repressive effect on growth, which is a common strategy employed during waterlogging or submergence responses (Voesenek & Bailey-Serres, 2015; Labandera *et al.*, 2021). This repressive effect could be caused by the deposition of H3K27me3 on genes involved in growth and aerobic metabolism, in association with PRC2. However, when NO accumulates under hypoxic conditions and targets VRN2 for degradation via the N-degron pathway, the growth repression observed during hypoxia could be reversed.

In animal systems, histone methylation is affected by NO through the formation of iron-nitrosyl complexes with the non-heme iron within the catalytic pocket of JMJC domain-containing KDM3A (Hickock *et al.*, 2013). This results in decreased KDM3A catalytic activity and a significant increase in global H3K9me2 levels (Hickock *et al.*, 2013). Although KDM3A activity and H3K9me2 activity decreased, KDM3A transcript levels were found to increase (Hickock *et al.*, 2013). Macrophages treated with NO and hypoxia showed increases in H3K9me2/3 and H3K36me3 in both treatment groups (Tausendschön *et al.*, 2011). Mouse embryonic stem cells treated with NO similarly showed increased levels of H3K9me3 and H3K4me1/2/3 (Mora-Castilla *et al.*, 2010). This indicates the possibility of large-scale changes in histone methylation in response to NO in both plants and animals.

Similar to the TET enzymes, if JmjC-type KDM activity declines in response to hypoxia and NO in plants, histone methylation can accumulate. This could increase heterochromatin formation and physically block acetylation placement on H3K9 and H3K14. JmjC-type KDMs could have been inactivated in Arabidopsis WT root tips during hypoxia increasing histone

methylation. Additionally, if NO inhibits JmjC-type KDMs then *PGB1* overexpression should be able to rescue some hypermethylation. However, histone methylation was not measured and global levels of H3K9ac and H3K14ac increased despite potential inhibition.

The main action of NO on histone methylation is through regulation of KDMs; however, histone methyltransferases (KMTs) may also be affected. Cells cultured in methionine-free media, which inhibited cellular SAM production during NO treatment, showed the same increase in global histone methylation (Hickock *et al.*, 2013). This provides evidence that KMTs are not the main focus of NO-mediated histone methylation changes. Additionally, when treated with NO, the H3K9 methyltransferases SETDB2 and SUV39H2 were transcriptionally upregulated while another H3K9 methyltransferase, G9a, was downregulated at the protein level (Hickock *et al.*, 2013).

4.5. The importance of antibody quality control

Antibody quality control measures were taken to ensure that antibodies were specific for the histone PTM for which they were raised. Multiple antibodies detecting H3K9ac were tested; however, only one detected oligo-H3K9ac without cross-reacting with oligo-H3, oligo-H3K14ac, or oligo-H3K27ac. Often, monoclonal antibodies that detect H3K9ac also detect H3K27ac, as the peptide sequences are very similar. The H3K9ac and H3K27ac sites share an identical four-amino acid sequence surrounding the PTM. H3K9ac and H3K27ac are associated with each other, and both confer an open chromatin conformation (Igolkina *et al.*, 2019). However, each modification can interact with distinct epigenetic readers and confer distinct functional outcomes. A few H3K14ac antibodies were tested for binding specificity. Both tested antibodies bound to the other oligopeptides (oligo-H3, oligo-H3K9ac, and oligo-H3K27ac); however, one antibody detected proteins other than H3 by Western blotting. The antibodies that detect

H3K14ac also tended to have much weaker binding efficiency. This consequently led to less successful immunoblots when H3K14ac levels were assessed, because more of each sample was required per replicate.

Linear curves were essential for data analysis and for ensuring the reproducibility and accuracy of quantitative immunoblotting. Identifying the linear range for each antibody was important to ensure that inaccurate data was excluded. These extensive measures are rarely implemented and can yield misleading results if not identified and accounted for (Pillai-Kastoori *et al.*, 2020). Understanding the binding accuracy of the antibodies used was important for assessing the accuracy of the results and the scope of the study.

4.6. Limitations

Although thorough antibody quality control is necessary, it does not always guarantee accurate results. Post-translational modifications on amino acids close to the modification of interest can potentially block antibody binding (Bock *et al.*, 2011). Results would become confounded with false negatives if adjacent modified amino acid residues blocked antibody binding. Oligopeptides with multiple modifications would need to be used in dot blot analysis to determine whether the antibodies can detect the PTM when adjacent amino acid residues are modified.

Another issue present was that loading controls were immunodetected on separate blots. Loading controls were essential for obtaining accurate, reproducible results. An antibody detecting H3 was used as the loading control, providing a direct comparison of H3 levels with PTM levels on H3. However, immunoblotting is a technique that involves many individual complex steps. Error can be introduced at any of these steps; therefore, loading controls on the same immunoblot would help mitigate errors. This was not done in this study. The linear

detection ranges for each antibody (anti-H3, anti-H3K9ac, and anti-H3K14ac) required different cell lysate loading amounts. Probing for the loading control and the histone PTM within the same blot became impossible. Different antibodies could have been procured and tested to ensure they all fit within the same linear range; however, this process was time-consuming and expensive.

The next limitation was that Western blotting was the main technique utilized. This technique can indicate global changes in acetylation; however, it does not elucidate how gene or transposon expression may have changed, how HDAC activity may have changed, or how this change in acetylation may affect the hypoxic stress response.

The last limitation is that NO was not measured in the sample root tip tissue. As explained in the literature review section, Pgb1, in its oxygenated form, can oxidize NO to nitrate (Igamberdiev *et al.*, 2004). This should allow Pgb1 to be used to investigate how NO levels can influence H3K9 and H3K14 acetylation. However, without measuring NO levels in the *A. thaliana* root tip samples in each line used (WT, 35S:PGB1, Pgb1-RNAi, and *pgb1-1*) following treatment (4% oxygen or ambient air for 12 hours), the correlation is indirect. The assumption that expected changes in NO occurred in the lines utilized is supported by previous studies. Nitric oxide levels were measured in the root tips of the WT, 35S:PGB1, and Pgb1-RNAi lines in response to 12-hour waterlogging treatment (Mira et al., 2023b). Nitric oxide levels increased by over 2 times in the WT (Col-0) line, showed no significant change in the 35S:PGB1 line, and increased 4 times in the Pgb1-RNAi line following treatment (Mira et al., 2023b). Nitric oxide levels were also measured in the Pgb1-RNAi line, and NO emissions in untreated samples were higher in the inflorescence than in WT (Hebelstrup et al., 2006). In Hartman *et al.* (2019), NO levels were measured in the *pgb1-1* line in response to 100% N2 for 4 hours; only a comparison between an ethylene pretreatment and an ambient air pretreatment was made. They found an

elevation in NO emission between anoxia-treated WT and *pgb1-1* root tips (Hartman *et al.*, 2019). Although these lines are well studied and there is a well-documented relationship between Pgb1 and NO, NO levels were not measured following the specific treatment conditions used in this study.

4.7. Future Work

Past work and the work completed in this thesis provide little insight into how gene expression may be modified by global increases in H3K9ac and H3K14ac. To solve this, RNA-seq could be done. Additionally, ChIP-seq would also be helpful to understand where H3K9ac and H3K14ac are distributed within the genome. Which genes increase/decrease H3K9ac and H3K14ac distribution on and which genomic regions (enhancer, promoter, or gene body) H3K9ac/H3K14ac are distributed on could provide insight into the epigenetic changes caused by hypoxia. Finally, HDA6, and potentially other HDACs, should have S-nitrosylation and activity levels in hypoxic conditions measured to understand whether HDA6 is responsible for the global increase in H3K9ac and H3K14ac observed in hypoxic conditions.

4.8. Conclusion

Hypoxia induced an enhancement in H3K9 and H3K14 acetylation levels in *Arabidopsis thaliana* root tip tissue. Pgb1 inhibited the enhancement in H3K9 and H3K14 acetylation observed under hypoxic conditions. This implied NO involvement in this epigenetic change. If NO is responsible for the increase in H3K9ac and H3K14ac, then the most likely mechanism of action is S-nitrosylation and inactivation of HDA6. Increased H3K9 and H3K14 acetylation may improve transcription of stress-response genes by opening chromatin. However, enhanced histone acetylation at genes not involved in stress response may hinder plant survival. Further work is needed to elucidate how elevated levels of H3K9 and H3K14 acetylation affect the

hypoxic response and how Pgb1 influences this regulatory change. Overall, understanding the relationship between hypoxia and epigenetic regulation is important for elucidating how stress responses can be modified or accommodated to improve survivability under waterlogging.

REFERENCES

Ackerman-Lavert, M., Fridman, Y., Matosevich, R., Khandal, H., Friedlander-Shani, L., Vragović, K., Ben El, R., Horev, G., Tarkowská, D., Efroni, I., & Savaldi-Goldstein, S. (2021). Auxin requirements for a meristematic state in roots depend on a dual brassinosteroid function. *Current Biology*, *31*(20), 4462-4472. https://doi.org/10.1016/j.cub.2021.07.075

Ageeva-Kieferle, A., Rudolf, E. E., & Lindermayr, C. (2019). Redox-dependent chromatin remodeling: A new function of nitric oxide as architect of chromatin structure in plants. *Frontiers in Plant Science 10*.. https://doi.org/10.3389/fpls.2019.00625

Ageeva-Kieferle, A., Georgii, E., Winkler, B., Ghirardo, A., Albert, A., Hüther, P., Mengel, A., Becker, C., Schnitzler, J.-P., Durner, J., & Lindermayr, C. (2021). Nitric oxide coordinates growth, development, and stress response via histone modification and gene expression. *Plant Physiology*, *187*(1), 336–360. https://doi.org/10.1093/plphys/kiab222

Alinsug, M. V., Chen, F. F., Luo, M., Tai, R., Jiang, L., & Wu, K. (2012). Subcellular localization of class II HDAs in Arabidopsis thaliana: Nucleocytoplasmic shuttling of HDA15 is driven by light. *PLoS ONE*, *7*(2). https://doi.org/10.1371/journal.pone.0030846

Alonso, J. M., Stepanova, A. N., Leisse, T. J., Kim, C. J., Chen, H., Shinn, P., Stevenson, D. K., Zimmerman, J., Barajas, P., Cheuk, R., Gadrinab, C., Heller, C., Jeske, A., Koesema, E., Meyers, C. C., Parker, H., Prednis, L., Ansari, Y., Choy, N., … Ecker, J. R. (2003). Genome-wide insertional mutagenesis of Arabidopsis *thaliana*. *Science*, *301*(5633), 653–657. https://doi.org/10.1126/science.1086391

An, C., Deng, L., Zhai, H., You, Y., Wu, F., Zhai, Q., Goossens, A., & Li, C. (2022). Regulation of jasmonate signaling by reversible acetylation of TOPLESS in Arabidopsis. *Molecular Plant*, *15*(8), 1329–1346. https://doi.org/10.1016/j.molp.2022.06.014

Andrzejczak, O. A., Havelund, J. F., Wang, W.-Q., Kovalchuk, S., Hagensen, C. E., Hasler-Sheetal, H., Jensen, O. N., Rogowska-Wrzesinska, A., Møller, I. M., & Hebelstrup, K. H. (2020). The hypoxic proteome and metabolome of barley (*Hordeum vulgare L.*) with and without phytoglobin priming. *International Journal of Molecular Sciences*, *21*(4), 1546. https://doi.org/10.3390/ijms21041546

Anee, T. I., Nahar, K., Rahman, A., Mahmud, J. A., Bhuiyan, T. F., Alam, M. U., Fujita, M., & Hasanuzzaman, M. (2019). Oxidative damage and antioxidant defense in *Sesamum indicum* after different waterlogging durations. *Plants*, *8*(7), 196. https://doi.org/10.3390/plants8070196

Arif, M., Vedamurthy, B. M., Choudhari, R., Ostwal, Y. B., Mantelingu, K., Kodaganur, G. S., & Kundu, T. K. (2010). Nitric oxide-mediated histone hyperacetylation in oral cancer: Target for a water-soluble hat inhibitor, CTK7A. *Chemistry & Biology*, *17*(8), 903–913. https://doi.org/10.1016/j.chembiol.2010.06.014

Armstrong, J., & Armstrong, W. (2005). Rice: Sulfide-induced barriers to root radial oxygen loss, Fe^{2+} and water uptake, and lateral root emergence. *Annals of Botany*, *96*(4), 625–638. https://doi.org/10.1093/aob/mci215

Babcock, G. T. (1999). How oxygen is activated and reduced in respiration. *Proceedings of the National Academy of Sciences*, *96*(23), 12971–12973. https://doi.org/10.1073/pnas.96.23.12971

Bagautdinova, Z. Z., Omelyanchuk, N., Tyapkin, A. V., Kovrizhnykh, V. V., Lavrekha, V. V., & Zemlyanskaya, E. V. (2022). Salicylic acid in root growth and development. *International Journal of Molecular Sciences*, *23*(4), 2228. https://doi.org/10.3390/ijms23042228

Bailey-Serres, J., & Voesenek, L. A. C. J. (2008). Flooding stress: acclimations and genetic diversity. *Annu. Rev. Plant Biol.*, *59*, 313-339. https://doi.org/10.1146/annurev.arplant.59.032607.092752

Bailey-Serres, J., Fukao, T., Gibbs, D. J., Holdsworth, M. J., Lee, S. C., Licausi, F., Perata, P., Voesenek, L. A. C. J., & van Dongen, J. T. (2012). Making sense of low oxygen sensing. *Trends in Plant Science*, *17*(3), 129–138. https://doi.org/10.1016/j.tplants.2011.12.004

Bannister, A. J., & Kouzarides, T. (2011). Regulation of chromatin by histone modifications. *Cell Research*, *21*(3), 381–395. https://doi.org/10.1038/cr.2011.22

Bannister, A. J., Schneider, R., & Kouzarides, T. (2002). Histone Methylation. *Cell*, *109*(7), 801–806. https://doi.org/10.1016/S0092-8674(02)00798-5

Bardani, E., Kallemi, P., Tselika, M., Katsarou, K., & Kalantidis, K. (2023). Spotlight on plant bromodomain proteins. *Biology*, *12*(8), 1076. https://doi.org/10.3390/biology12081076

Batie, M., Frost, J., Frost, M., Wilson, J. W., Schofield, P., & Rocha, S. (2019). Hypoxia induces rapid changes to histone methylation and reprograms chromatin. *Science*, *363*(6432), 1222–1226. https://doi.org/10.1126/science.aau5870

Beacon, T. H., Delcuve, G. P., López, C., Nardocci, G., Kovalchuk, I., van Wijnen, A. J., & Davie, J. R. (2021). The dynamic broad epigenetic (H3K4me3, H3K27ac) domain as a mark of essential genes. *Clinical Epigenetics*, *13*(1). https://doi.org/10.1186/s13148-021-01126-1

Begara-Morales, J. C., Sánchez-Calvo, B., Luque, F., Leyva-Pérez, M. O., Leterrier, M., Corpas, F. J., & Barroso, J. B. (2014). Differential transcriptomic analysis by RNA-Seq of GSNO-responsive genes between Arabidopsis roots and leaves. *Plant and Cell Physiology*, *55*(6), 1080–1095. https://doi.org/10.1093/pcp/pcu044

Berr, A., Shafiq, S., & Shen, W.-H. (2011). Histone modifications in transcriptional activation during plant development. *Biochimica et Biophysica Acta (BBA) - Gene Regulatory Mechanisms*, *1809*(10), 567–576. https://doi.org/10.1016/j.bbagrm.2011.07.001

Bethke, P. C., Badger, M. R., & Jones, R. L. (2004). Apoplastic synthesis of nitric oxide by plant tissues. *The Plant Cell*, *16*(2), 332–341. https://doi.org/10.1105/tpc.017822

Bewick, A. J., & Schmitz, R. J. (2017). Gene body DNA methylation in plants. *Current Opinion in Plant Biology*, *36*, 103–110. https://doi.org/10.1016/j.pbi.2016.12.007

Beyer, S., Kristensen, M. M., Jensen, K. S., Johansen, J. V., & Staller, P. (2008). The histone demethylases JMJD1A and JMJD2B are transcriptional targets of hypoxia-inducible factor HIF. *Journal of Biological Chemistry*, *283*(52), 36542–36552. https://doi.org/10.1074/jbc.m804578200

Blilou, I., Xu, J., Wildwater, M., Willemsen, V., Paponov, I., Frimi, J., Heldstra, R., Aida, M., Palme, K., & Scheres, B. (2005). The PIN auxin efflux facilitator network controls growth and patterning in *Arabidopsis* roots. *Nature*, *433*(7021), 39–44. https://doi.org/10.1038/nature03184

Bock, I., Dhayalan, A., Kudithipudi, S., Brandt, O., Rathert, P., & Jeltsch, A. (2011). Detailed specificity analysis of antibodies binding to modified histone tails with peptide arrays. *Epigenetics*, *6*(2), 256–263. https://doi.org/10.4161/epi.6.2.13837

Bonhoure, N., Bounova, G., Bernasconi, D., Praz, V., Lammers, F., Canella, D., Willis, I. M., Herr, W., Hernandez, N., & Delorenzi, M. (2014). Quantifying chip-seq data: A spiking method providing an internal reference for sample-to-sample normalization. *Genome Research*, *24*(7), 1157–1168. https://doi.org/10.1101/gr.168260.113

Borg, M., Jiang, D., & Berger, F. (2021). Histone variants take center stage in shaping the epigenome. *Current Opinion in Plant Biology*, *61*, 101991. https://doi.org/10.1016/j.pbi.2020.101991

Bovee, R., Pham, V., Fernandez, J., Tretyakova, N., & Thomas, D. D. (2018). Nitric oxide is an epigenetic regulator of gene expression by directly controlling DNA methylation patterns. *Free Radical Biology and Medicine*, *120*. https://doi.org/10.1016/j.freeradbiomed.2018.04.375

Butler, T. A., Paul, J. W., Chan, E.-C., Smith, R., & Tolosa, J. M. (2019). Misleading westerns: Common quantification mistakes in western blot densitometry and proposed corrective measures. *BioMed Research International*, *2019*, 1–15. https://doi.org/10.1155/2019/5214821

Capuano, F., Mülleder, M., Kok, R., Blom, H. J., & Ralser, M. (2014). Cytosine DNA methylation is found in *Drosophila melanogaster* but absent in *Saccharomyces*

cerevisiae, Schizosaccharomyces pombe, and other yeast species. *Analytical Chemistry*, *86*(8), 3697–3702. https://doi.org/10.1021/ac500447w

Cavrak, V. V., Lettner, N., Jamge, S., Kosarewicz, A., Bayer, L. M., & Mittelsten Scheid, O. (2014). How a retrotransposon exploits the plant's heat stress response for its activation. *PLoS Genetics*, *10*(1). https://doi.org/10.1371/journal.pgen.1004115

Casacuberta, E., & González, J. (2013). The impact of transposable elements in environmental adaptation. *Molecular Ecology*, *22*(6), 1503–1517. https://doi.org/10.1111/mec.12170

Castello, P. R., Woo, D. K., Ball, K., Wojcik, J., Liu, L., & Poyton, R. O. (2008). Oxygen-regulated isoforms of cytochrome *c* oxidase have differential effects on its nitric oxide production and on hypoxic signaling. *Proceedings of the National Academy of Sciences*, *105*(24), 8203–8208. https://doi.org/10.1073/pnas.0709461105

Chabouté, M. E., Chaubet, N., Gigot, C., & Philipps, G. (1993). Histones and histone genes in higher plants: Structure and genomic organization. *Biochimie*, *75*(7), 523–531. https://doi.org/10.1016/0300-9084(93)90057-y

Chakraborty, A. A., Laukka, T., Myllykoski, M., Ringel, A. E., Booker, M. A., Tolstorukov, M. Y., Meng, Y. J., Meier, S. R., Jennings, R. B., Creech, A. L., Herbert, Z. T., McBrayer, S. K., Olenchock, B. A., Jaffe, J. D., Haigis, M. C., Beroukhim, R., Signoretti, S., Koivunen, P., & Kaelin, W. G. (2019). Histone demethylase KDM6A directly senses oxygen to control chromatin and cell fate. *Science*, *363*(6432), 1217–1222. https://doi.org/10.1126/science.aaw1026

Chamizo-Ampudia, A., Sanz-Luque, E., Llamas, A., Galvan, A., & Fernandez, E. (2017). Nitrate reductase regulates plant nitric oxide homeostasis. *Trends in Plant Science*, *22*(2), 163–174. https://doi.org/10.1016/j.tplants.2016.12.001

Chatterjee, N., Sinha, D., Lemma-Dechassa, M., Tan, S., Shogren-Knaak, M. A., & Bartholomew, B. (2011). Histone H3 tail acetylation modulates ATP-dependent remodeling through multiple mechanisms. *Nucleic Acids Research*, *39*(19), 8378–8391. https://doi.org/10.1093/nar/gkr535

Chaubet, N., Clement, B., & Gigot, C. (1992). Genes encoding a histone H3.3-like variant in Arabidopsis contain intervening sequences. *Journal of Molecular Biology*, *225*(2), 569–574. https://doi.org/10.1016/0022-2836(92)90943-e

Chen, C.-Y., Wu, K., & Schmidt, W. (2015). The histone deacetylase HDA19 controls root cell elongation and modulates a subset of phosphate starvation responses in Arabidopsis. *Scientific Reports*, *5*(1). https://doi.org/10.1038/srep15708

Chereji, R. V., & Clark, D. J. (2018). Major determinants of nucleosome positioning. *Biophysical Journal*, *114*(10), 2279–2289. https://doi.org/10.1016/j.bpj.2018.03.015

Cheung, P., Allis, C. D., & Sassone-Corsi, P. (2000). Signaling to chromatin through histone modifications. *Cell*, *103*(2), 263–271. https://doi.org/10.1016/s0092-8674(00)00118-5

Chirinos, X., & Licausi, F. (2024). Suffocated shoots: Hypoxia-induced synthesis of salicylic acid inhibits plant regeneration. *Molecular Plant*, *17*(4), 528–530. https://doi.org/10.1016/j.molp.2024.03.008

Choi, S., Song, H., Han, S., Han, M., Kim, C., Park, J., Lee, Y., Jeon, J., Noh, Y., & Noh, B. (2012). HDA19 is required for the repression of salicylic acid biosynthesis and salicylic acid-mediated defense responses in Arabidopsis. *The Plant Journal*, *71*(1), 135–146. https://doi.org/10.1111/j.1365-313x.2012.04977.x

Cochrane, D. W., Shah, J. K., Hebelstrup, K. H., & Igamberdiev, A. U. (2017). Expression of phytoglobin affects nitric oxide metabolism and energy state of barley plants exposed to anoxia. *Plant Science*, *265*, 124–130. https://doi.org/10.1016/j.plantsci.2017.10.001

Colmer, T. D. (2003). Long-distance transport of gases in plants: A perspective on internal aeration and radial oxygen loss from roots. *Plant, Cell & Environment*, *26*(1), 17–36. https://doi.org/10.1046/j.1365-3040.2003.00846.x

Daniel, K., & Hartman, S. (2024). How plant roots respond to waterlogging. *Journal of Experimental Botany*, *75*(2), 511–525. https://doi.org/10.1093/jxb/erad332

De Col, V., Fuchs, P., Nietzel, T., Elsässer, M., Voon, C. P., Candeo, A., Seeliger, I., Fricker, M. D., Grefen, C., Møller, I. M., Bassi, A., Lim, B. L., Zancani, M., Meyer, A. J., Costa, A., Wagner, S., & Schwarzländer, M. (2017). ATP sensing in living plant cells reveals tissue gradients and stress dynamics of Energy Physiology. *eLife*, *6*. https://doi.org/10.7554/elife.26770

Dordas, C., Rivoal, J., & Hill, R. D. (2003). Plant haemoglobins, nitric oxide and hypoxic stress. *Annals of Botany*, *91*(2), 173-178. https://doi.org/10.1093/aob/mcf115

Du, X., Gao, Y., Zhang, H., Xu, X., Li, Y., Zhao, L., Luo, M., & Wang, H. (2024). HDA6 modulates Arabidopsis pavement cell morphogenesis through epigenetic suppression of *ROP6 GTPase* expression and signaling. *New Phytologist*, *241*(6), 2523–2539. https://doi.org/10.1111/nph.19532

Duan, K., Ding, X., Zhang, Q., Zhu, H., Pan, A., & Huang, J. (2008). AtCOPEG1, the unique gene originated from AtCOPIA95 Retrotransposon family, is sensitive to external hormones and abiotic stresses. *Plant Cell Reports*, *27*(6), 1065–1073. https://doi.org/10.1007/s00299-008-0520-2

Dubin, M. J., Mittelsten Scheid, O., & Becker, C. (2018). Transposons: A blessing curse. *Current Opinion in Plant Biology*, *42*, 23–29. https://doi.org/10.1016/j.pbi.2018.01.003

Earley, K., Lawrence, R. J., Pontes, O., Reuther, R., Enciso, A. J., Silva, M., Neves, N., Gross, M., Viegas, W., & Pikaard, C. S. (2006). Erasure of histone acetylation by *Arabidopsis HDA6* mediates large-scale gene silencing in nucleolar dominance. *Genes & Development*, *20*(10), 1283–1293. https://doi.org/10.1101/gad.1417706

Earley, K. W., Pontvianne, F., Wierzbicki, A. T., Blevins, T., Tucker, S., Costa-Nunes, P., Pontes, O., & Pikaard, C. S. (2010). Mechanisms of HDA6-mediated rRNA gene silencing: Suppression of intergenic Pol II transcription and differential effects on maintenance versus siRNA-directed cytosine methylation. *Genes & Development*, *24*(11), 1119–1132. https://doi.org/10.1101/gad.1914110

Egelhofer, T. A., Minoda, A., Klugman, S., Lee, K., Kolasinska-Zwierz, P., Alekseyenko, A. A., Cheung, M.-S., Day, D. S., Gadel, S., Gorchakov, A. A., Gu, T., Kharchenko, P. V., Kuan, S., Latorre, I., Linder-Basso, D., Luu, Y., Ngo, Q., Perry, M., Rechtsteiner, A., … Lieb, J. D. (2010). An assessment of histone-modification antibody quality. *Nature Structural & Molecular Biology*, *18*(1), 91–93. https://doi.org/10.1038/nsmb.1972

Ejiri, M., Fukao, T., Miyashita, T., & Shiono, K. (2021). A barrier to radial oxygen loss helps the root system cope with waterlogging-induced hypoxia. *Breeding Science*, *71*(1), 40–50. https://doi.org/10.1270/jsbbs.20110

El-Khateeb, E. A., Youssef, M. S., Mira, M. M., Igamberdiev, A. U., Hill, R. D., & Stasolla, C. (2023). Interplay between the *Brassica napus* phytoglobin (BnPGB1), folic acid, and antioxidant responses enhances plant tolerance to waterlogging. *Plant Science*, *334*, 111775. https://doi.org/10.1016/j.plantsci.2023.111775

Erdmann, R. M., & Picard, C. L. (2020). RNA-directed DNA methylation. *PLOS Genetics*, *16*(10). https://doi.org/10.1371/journal.pgen.1009034

Evans, D. E. (2003). Aerenchyma Formation. *New Phytologist*, *161*(1), 35–49. https://doi.org/10.1046/j.1469-8137.2003.00907.x

Feng, S., & Jacobsen, S. E. (2011). Epigenetic modifications in plants: An evolutionary perspective. *Current Opinion in Plant Biology*, *14*(2), 179–186. https://doi.org/10.1016/j.pbi.2010.12.002

Fernández-Marcos, M., Sanz, L., Lewis, D. R., Muday, G. K., & Lorenzo, O. (2011). Nitric oxide causes root apical meristem defects and growth inhibition while reducing PIN-FORMED 1 (PIN1)-dependent acropetal auxin transport. *Proceedings of the National Academy of Sciences*, *108*(45), 18506-18511. https://doi.org/10.1073/pnas.1108644108

Fong, P. M., Tian, L., & Chen, Z. J. (2006). *Arabidopsis thaliana* histone deacetylase 1 (AtHD1) is localized in euchromatic regions and demonstrates histone deacetylase activity in vitro. *Cell Research*, *16*(5), 479–488. https://doi.org/10.1038/sj.cr.7310059

Forzani, C., Aichinger, E., Sornay, E., Willemsen, V., Laux, T., Dewitte, W., & Murray, J. A. H. (2014). WOX5 suppresses CYCLIN D activity to establish quiescence at the center of the root stem cell niche. *Current Biology*, *24*(16), 1939–1944. https://doi.org/10.1016/j.cub.2014.07.019

Friml, J., Vieten, A., Sauer, M., Weijers, D., Schwarz, H., Hamann, T., Offringa, R., & Jürgens, G. (2003). Efflux-dependent auxin gradients establish the apical–basal axis of Arabidopsis. *Nature*, *426*(6963), 147–153. https://doi.org/10.1038/nature02085

Fu, W., Yu, Y., Shu, J., Yu, Z., Zhong, Y., Zhu, T., Zhang, Z., Liang, Z., Cui, Y., Chen, C., & Li, C. (2023). Organization, genomic targeting, and assembly of three distinct SWI/SNF chromatin remodeling complexes in Arabidopsis. *The Plant Cell*, *35*(7), 2464–2483. https://doi.org/10.1093/plcell/koad111

Fukao, T., & Bailey-Serres, J. (2004). Plant responses to hypoxia – is survival a balancing act? *Trends in Plant Science*, *9*(9), 449–456. https://doi.org/10.1016/j.tplants.2004.07.005

Gallego-Bartolomé, J. (2020). DNA methylation in plants: Mechanisms and tools for targeted manipulation. *New Phytologist*, *227*(1), 38–44. https://doi.org/10.1111/nph.16529

Gan, L., Wei, Z., Yang, Z., Li, F., & Wang, Z. (2021). Updated mechanisms of GCN5—the monkey king of the plant kingdom in plant development and resistance to abiotic stresses. *Cells*, *10*(5), 979. https://doi.org/10.3390/cells10050979

Gibbs, D. J., Lee, S. C., Md Isa, N., Gramuglia, S., Fukao, T., Bassel, G. W., Correia, C. S., Corbineau, F., Theodoulou, F. L., Bailey-Serres, J., & Holdsworth, M. J. (2011). Homeostatic response to hypoxia is regulated by the N-end rule pathway in plants. *Nature*, *479*(7373), 415–418. https://doi.org/10.1038/nature10534

Gibbs, D. J., Md Isa, N., Movahedi, M., Lozano-Juste, J., Mendiondo, G. M., Berckhan, S., Marín-de la Rosa, N., Vicente Conde, J., Sousa Correia, C., Pearce, S. P., Bassel, G. W., Hamali, B., Talloji, P., Tomé, D. F. A., Coego, A., Beynon, J., Alabadí, D., Bachmair, A., León, J., … Holdsworth, M. J. (2014). Nitric oxide sensing in plants is mediated by proteolytic control of Group VII ERF transcription factors. *Molecular Cell*, *53*(3), 369–379. https://doi.org/10.1016/j.molcel.2013.12.020

Gibbs, D. J., Conde, J. V., Berckhan, S., Prasad, G., Mendiondo, G. M., & Holdsworth, M. J. (2015). Group VII ethylene response factors coordinate oxygen and nitric oxide signal transduction and stress responses in plants. *Plant Physiology*, *169*(1), 23–31. https://doi.org/10.1104/pp.15.00338

Gibbs, D. J., Tedds, H. M., Labandera, A.-M., Bailey, M., White, M. D., Hartman, S., Sprigg, C., Mogg, S. L., Osborne, R., Dambire, C., Boeckx, T., Paling, Z., Voesenek, L. A., Flashman, E., & Holdsworth, M. J. (2018). Oxygen-dependent proteolysis regulates the stability of angiosperm Polycomb Repressive Complex 2 subunit VERNALIZATION 2. *Nature Communications*, *9*(1). https://doi.org/10.1038/s41467-018-07875-7

Giuntoli, B., & Perata, P. (2018). Group VII Ethylene Response Factors in Arabidopsis: Regulation and Physiological Roles. *Plant Physiology*, *176*(2), 1143–1155. https://doi.org/10.1104/pp.17.01225

Godee, C., Mira, M. M., Wally, O., Hill, R. D., & Stasolla, C. (2017). Cellular localization of the Arabidopsis class 2 phytoglobin influences somatic embryogenesis. *Journal of Experimental Botany*, *68*(5), 1013–1023. https://doi.org/10.1093/jxb/erx003

Godwin, J., & Farrona, S. (2022). The importance of networking: Plant Polycomb Repressive Complex 2 and its Interactors. *Epigenomes*, *6*(1), 8. https://doi.org/10.3390/epigenomes6010008

Greve, T. M., Borum, J., & Pedersen, O. (2003). Meristematic oxygen variability in eelgrass (*Zostera marina*). *Limnology and Oceanography*, *48*(1), 210–216. https://doi.org/10.4319/lo.2003.48.1.0210

Guillotin, B., & Birnbaum, K. D. (2020). Just passing through: The auxin gradient of the root meristem. *Current Topics in Developmental Biology*, 433–454. https://doi.org/10.1016/bs.ctdb.2019.12.001

Gunawardena, A. H., Pearce, D. M., Jackson, M. B., Hawes, C. R., & Evans, D. E. (2001). Characterization of programmed cell death during aerenchyma formation induced by ethylene or hypoxia in roots of maize (*Zea mays L.*). *Planta*, *212*(2), 205–214. https://doi.org/10.1007/s004250000381

Guo, M., Wang, S., Liu, H., Yao, S., Yan, J., Wang, C., Miao, B., Guo, J., Ma, F., Guan, Q., & Xu, J. (2023). Histone deacetylase MdHDA6 is an antagonist in regulation of transcription factor MdTCP15 to promote cold tolerance in Apple. *Plant Biotechnology Journal*, *21*(11), 2254–2272. https://doi.org/10.1111/pbi.14128

Gupta, K. J., Hebelstrup, K. H., Mur, L. A. J., & Igamberdiev, A. U. (2011). Plant hemoglobins: Important players at the crossroads between oxygen and nitric oxide. *FEBS Letters*, *585*(24), 3843–3849. https://doi.org/10.1016/j.febslet.2011.10.036

Gupta, K. J., Kolbert, Z., Durner, J., Lindermayr, C., Corpas, F. J., Brouquisse, R., Barroso, J. B., Umbreen, S., Palma, J. M., Hancock, J. T., Petrivalsky, M., Wendehenne, D., & Loake, G. J. (2020). Regulating the regulator: Nitric oxide control of post-translational modifications. *New Phytologist*, *227*(5), 1319–1325. https://doi.org/10.1111/nph.16622

Gupta, K. J., Kaladhar, V. C., Fitzpatrick, T. B., Fernie, A. R., Møller, I. M., & Loake, G. J. (2022). Nitric oxide regulation of plant metabolism. *Molecular Plant*, *15*(2), 228–242. https://doi.org/10.1016/j.molp.2021.12.012

Hacham, Y., Holland, N., Butterfield, C., Ubeda-Tomas, S., Bennett, M. J., Chory, J., & Savaldi-Goldstein, S. (2011). Brassinosteroid perception in the epidermis controls root meristem size. *Development*, *138*(5), 839–848. https://doi.org/10.1242/dev.061804

Harris, K. D., & Zemach, A. (2020). Contiguous and stochastic CHH methylation patterns of plant DRM2 and CMT2 revealed by single-read methylome analysis. *Genome Biology*, *21*(1). https://doi.org/10.1186/s13059-020-02099-9

Hartman, S., Liu, Z., van Veen, H., Vicente, J., Reinen, E., Martopawiro, S., Zhang, H., van Dongen, N., Bosman, F., Bassel, G. W., Visser, E. J. W., Bailey-Serres, J., Theodoulou, F. L., Hebelstrup, K. H., Gibbs, D. J., Holdsworth, M. J., Sasidharan, R., & Voesenek, L. A. C. J. (2019). Ethylene-mediated nitric oxide depletion pre-adapts plants to hypoxia stress. *Nature Communications*, *10*(1), 4020. https://doi.org/10.1038/s41467-019-12045-4

He, Cj., Finlayson, S. A., Drew, M. C., Jordan, W. R., & Morgan, P. W. (1996). Ethylene biosynthesis during aerenchyma formation in roots of maize subjected to mechanical impedance and hypoxia. *Plant Physiology*, *112*(4), 1679–1685. https://doi.org/10.1104/pp.112.4.1679

Hebelstrup, K. H., Hunt, P., Dennis, E., Jensen, S. B., & Jensen, E. Ø. (2006). Hemoglobin is essential for normal growth of Arabidopsis organs. *Physiologia Plantarum*, *127*(1), 157–166. https://doi.org/10.1111/j.1399-3054.2006.00653.x

Hebelstrup, K. H., van Zanten, M., Mandon, J., Voesenek, L. A. C. J., Harren, F. J. M., Cristescu, S. M., Møller, I. M., & Mur, L. A. J. (2012). Haemoglobin modulates NO emission and hyponasty under hypoxia-related stress in Arabidopsis thaliana. *Journal of Experimental Botany*, *63*(15), 5581–5591. https://doi.org/10.1093/jxb/ers210

Heyman, J., Kumpf, R. P., & De Veylder, L. (2014). A quiescent path to plant longevity. *Trends in Cell Biology*, *24*(8), 443–448. https://doi.org/10.1016/j.tcb.2014.03.004

Hickok, J. R., Vasudevan, D., Antholine, W. E., & Thomas, D. D. (2013). Nitric oxide modifies global histone methylation by inhibiting Jumonji C domain-containing demethylases. *Journal of Biological Chemistry*, *288*(22), 16004–16015. https://doi.org/10.1074/jbc.m112.432294

Hill, R., Hargrove, M., & Arredondo-Peter, R. (2016). Phytoglobin: a novel nomenclature for plant globins accepted by the globin community at the 2014 XVIII conference on Oxygen-Binding and Sensing Proteins. *F1000Research*, *5*(212), 212. https://doi.org/10.12688/f1000research.8133.1

Hill, R. D., Robertson, S. M., Igamberdiev, A. U., Mira, M. M., Wilkins, O., & Stasolla, C. (2026). Discrete and cell-specific hypoxic responses in Arabidopsis roots resolved by single-nuclei transcriptomics. *New Phytologist*, *249*(6), 2652–2667. https://doi.org/10.1111/nph.70874

Hmadcha, A., Bedoya, F. J., Sobrino, F., & Pintado, E. (1999). Methylation-dependent gene silencing induced by interleukin 1β via nitric oxide production. *The Journal of Experimental Medicine*, *190*(11), 1595–1604. https://doi.org/10.1084/jem.190.11.1595

Hu, R.-G., Sheng, J., Qi, X., Xu, Z., Takahashi, T. T., & Varshavsky, A. (2005). The N-end rule pathway as a nitric oxide sensor controlling the levels of multiple regulators. *Nature*, *437*(7061), 981–986. https://doi.org/10.1038/nature04027

Hu, J., Yang, H., Mu, J., Lu, T., Peng, J., Deng, X., Kong, Z., Bao, S., Cao, X., & Zuo, J. (2017). Nitric oxide regulates protein methylation during stress responses in plants. *Molecular Cell*, *67*(4). https://doi.org/10.1016/j.molcel.2017.06.031

Huang, F., Chan, A. O., Rashid, A., Wong, D. K., Cho, C., & Yuen, M. (2012). *Helicobacter pylori* induces promoter methylation of E-cadherin via interleukin-1β activation of nitric oxide production in gastric cancer cells. *Cancer*, *118*(20), 4969–4980. https://doi.org/10.1002/cncr.27519

Hung, F.-Y., Shih, Y.-H., Lin, P.-Y., Feng, Y.-R., Li, C., & Wu, K. (2022). WRKY63 transcriptional activation of *COOLAIR* and *COLDAIR* regulates vernalization-induced flowering. *Plant Physiology*, *190*(1), 532–547. https://doi.org/10.1093/plphys/kiac295

Hunt, P. W., Klok, E. J., Trevaskis, B., Watts, R. A., Ellis, M. H., Peacock, W. J., & Dennis, E. S. (2002). Increased level of hemoglobin 1 enhances survival of hypoxic stress and promotes early growth in *Arabidopsis thaliana*. *Proceedings of the National Academy of Sciences*, *99*(26), 17197-17202. https://doi.org/10.1073/pnas.212648799

Igamberdiev, A. U., Baron, K., Manac'h-Little, N., Stoimenova, M., & Hill, R. D. (2005). The haemoglobin/nitric oxide cycle: involvement in flooding stress and effects on hormone signaling. *Annals of Botany*, *96*(4), 557–564. https://doi.org/10.1093/aob/mci210

Igolkina, A. A., Zinkevich, A., Karandasheva, K. O., Popov, A. A., Selifanova, M. V., Nikolaeva, D., Tkachev, V., Penzar, D., Nikitin, D. M., & Buzdin, A. (2019). H3K4me3, H3K9ac, H3K27ac, H3K27me3 and H3K9me3 histone tags suggest distinct regulatory evolution of open and condensed chromatin landmarks. *Cells*, *8*(9), 1034. https://doi.org/10.3390/cells8091034

Illi, B., Russo, C. D., Colussi, C., Rosati, J., Pallaoro, M., Spallotta, F., Rotili, D., Valente, S., Ragone, G., Martelli, F., Biglioli, P., Steinkuhler, C., Gallinari, P., Mai, A., Capogrossi, M. C., & Gaetano, C. (2008). Nitric oxide modulates chromatin folding in human endothelial cells via protein phosphatase 2A activation and class II histone deacetylases nuclear shuttling. *Circulation Research*, *102*(1), 51–58. https://doi.org/10.1161/circresaha.107.157305

Islam, Md. S., Leissing, T. M., Chowdhury, R., Hopkinson, R. J., & Schofield, C. J. (2018). 2-oxoglutarate-dependent oxygenases. *Annual Review of Biochemistry*, *87*(1), 585–620. https://doi.org/10.1146/annurev-biochem-061516-044724

Jardine, K. J., & McDowell, N. (2023). Fermentation-mediated growth, signaling, and defense in plants. *New Phytologist*, *239*(3), 839–851. https://doi.org/10.1111/nph.19015

Jiang, K., & Feldman, L. J. (2005). Regulation of root apical meristem development. *Annual Review of Cell and Developmental Biology*, *21*, 485–509. https://doi.org/10.1146/annurev.cellbio.21.122303.114753

Jiang, J., Ding, A. B., Liu, F., & Zhong, X. (2020). Linking signaling pathways to histone acetylation dynamics in plants. *Journal of Experimental Botany*, *71*(17), 5179–5190. https://doi.org/10.1093/jxb/eraa202

Kalous, K. S., Wynia-Smith, S. L., Olp, M. D., & Smith, B. C. (2016). Mechanism of SIRT1 NAD^+-dependent protein deacetylase inhibition by cysteine S-nitrosation. *Journal of Biological Chemistry*, *291*(49), 25398–25410. https://doi.org/10.1074/jbc.m116.754655

Karmodiya, K., Krebs, A. R., Oulad-Abdelghani, M., Kimura, H., & Tora, L. (2012). H3K9 and H3K14 acetylation co-occur at many gene regulatory elements, while H3K14ac marks a subset of inactive inducible promoters in mouse embryonic stem cells. *BMC Genomics*, *13*(1). https://doi.org/10.1186/1471-2164-13-424

Khan, M., Ali, S., Al Azzawi, T. N., & Yun, B.-W. (2023). Nitric oxide acts as a key signaling molecule in plant development under stressful conditions. *International Journal of Molecular Sciences*, *24*(5), 4782. https://doi.org/10.3390/ijms24054782

Kohli, R. M., & Zhang, Y. (2013). TET enzymes, TDG and the dynamics of DNA demethylation. *Nature*, *502*(7472), 472–479. https://doi.org/10.1038/nature12750

Kong, X., Tian, H., Yu, Q., Zhang, F., Wang, R., Gao, S., Xu, W., Liu, J., Shani, E., Fu, C., Zhou, G., Zhang, L., Zhang, X., & Ding, Z. (2018). PHB3 maintains root stem cell niche identity through ROS-responsive AP2/ERF transcription factors in Arabidopsis. *Cell Reports*, *22*(5), 1350–1363. https://doi.org/10.1016/j.celrep.2017.12.105

Kooistra, S. M., & Helin, K. (2012). Molecular mechanisms and potential functions of histone demethylases. *Nature Reviews Molecular Cell Biology*, *13*(5), 297–311. https://doi.org/10.1038/nrm3327

Kornberg, M. D., Sen, N., Hara, M. R., Juluri, K. R., Nguyen, J. V., Snowman, A. M., Law, L., Hester, L. D., & Snyder, S. H. (2010). GAPDH mediates nitrosylation of nuclear proteins. *Nature Cell Biology*, *12*(11), 1094–1100. https://doi.org/10.1038/ncb2114

Kornet, N., & Scheres, B. (2009). Members of the GCN5 histone acetyltransferase complex regulate Plethora-mediated root stem cell niche maintenance and transit amplifying cell proliferation in *Arabidopsis*. *The Plant Cell*, *21*(4), 1070–1079. https://doi.org/10.1105/tpc.108.065300

Kotnik, F., Ueda, M., Ito, A., Ishida, J., Sakai, K., Takagi, H., Seidel, J., Abe, T., Eirich, J., Takahashi, S., Schwarzer, D., Seki, M., & Finkemeier, I. (2025). HDA19-mediated deacetylation of histone H3.3 lysine 27 and 36 regulates plant sensitivity to salt stress. *bioRxiv*. https://doi.org/10.1101/2025.11.04.686508

Koumbadinga, G. A., Mahmood, N., Lei, L., Kan, Y., Cao, W., Lobo, V. G., Yao, X., Zhang, S., & Xie, J. (2015). Increased stability of heterogeneous ribonucleoproteins by a deacetylase inhibitor. *Biochimica et Biophysica Acta (BBA) - Gene Regulatory Mechanisms*, *1849*(8), 1095–1103. https://doi.org/10.1016/j.bbagrm.2015.05.001

Kuai, J., Liu, Z., Wang, Y., Meng, Y., Chen, B., Zhao, W., Zhou, Z., & Oosterhuis, D. M. (2014). Waterlogging during flowering and boll forming stages affects sucrose metabolism in the leaves subtending the Cotton Boll and its relationship with boll weight. *Plant Science*, *223*, 79–98. https://doi.org/10.1016/j.plantsci.2014.03.010

Kumar, V., Thakur, J. K., & Prasad, M. (2021). Histone acetylation dynamics regulating plant development and stress responses. *Cellular and Molecular Life Sciences*, *78*(10), 4467–4486. https://doi.org/10.1007/s00018-021-03794-x

Kurita, K., Sakamoto, Y., Naruse, S., Matsunaga, T. M., Arata, H., Higashiyama, T., Habu, Y., Utsumi, Y., Utsumi, C., Tanaka, M., Takahashi, S., Kim, J.-M., Seki, M., Sakamoto, T., & Matsunaga, S. (2019). Intracellular localization of histone deacetylase HDA6 in plants. *Journal of Plant Research*, *132*(5), 629–640. https://doi.org/10.1007/s10265-019-01124-8

Labandera, A., Tedds, H. M., Bailey, M., Sprigg, C., Etherington, R. D., Akintewe, O., Kalleechurn, G., Holdsworth, M. J., & Gibbs, D. J. (2020). The PRT6 N-degron pathway restricts VERNALIZATION2 to endogenous hypoxic niches to modulate plant development. *New Phytologist*, *229*(1), 126–139. https://doi.org/10.1111/nph.16477

Leeggangers, H. A. C. F., Rodriguez-Granados, N. Y., Macias-Honti, M. G., & Sasidharan, R. (2023). A helping hand when drowning: The versatile role of ethylene in root flooding resilience. *Environmental and Experimental Botany*, *213*, 105422. https://doi.org/10.1016/j.envexpbot.2023.105422

Lewis, J., & Bird, A. (1991). DNA methylation and chromatin structure. *FEBS Letters*, *285*(2), 155–159. https://doi.org/10.1016/0014-5793(91)80795-5

Li, C., Gu, L., Gao, L., Chen, C., Wei, C.-Q., Qiu, Q., Chien, C.-W., Wang, S., Jiang, L., Ai, L.-F., Chen, C.-Y., Yang, S., Nguyen, V., Qi, Y., Snyder, M. P., Burlingame, A. L., Kohalmi, S. E., Huang, S., Cao, X., … Cui, Y. (2016). Concerted genomic targeting of H3K27 demethylase REF6 and chromatin-remodeling ATPase BRM in Arabidopsis. *Nature Genetics*, *48*(6), 687–693. https://doi.org/10.1038/ng.3555

Li, W., Zhang, X., Zhang, Q., Li, Q., Li, Y., Lv, Y., Liu, Y., Cao, Y., Wang, H., Chen, X., & Yang, H. (2024). PICKLE and HISTONE DEACETYLASE6 coordinately regulate genes and transposable elements in *Arabidopsis*. *Plant Physiology*, *196*(2), 1080–1094. https://doi.org/10.1093/plphys/kiae369

Licausi, F., Weits, D. A., Pant, B. D., Scheible, W., Geigenberger, P., & van Dongen, J. T. (2010). Hypoxia responsive gene expression is mediated by various subsets of

transcription factors and miRNAs that are determined by the actual oxygen availability. *New Phytologist*, *190*(2), 442–456. https://doi.org/10.1111/j.1469-8137.2010.03451.x

Licausi, F., Kosmacz, M., Weits, D. A., Giuntoli, B., Giorgi, F. M., Voesenek, L. A., Perata, P., & van Dongen, J. T. (2011). Oxygen sensing in plants is mediated by an N-end rule pathway for protein destabilization. *Nature*, *479*(7373), 419–422. https://doi.org/10.1038/nature10536

Lim, P. S., Shannon, M. F., & Hardy, K. (2010). Epigenetic control of inducible gene expression in the immune system. *Epigenomics*, *2*(6), 775–795. https://doi.org/10.2217/epi.10.55

Lin, J., Hung, F.-Y., Ye, C., Hong, L., Shih, Y.-H., Wu, K., & Li, Q. Q. (2020). HDA6-dependent histone deacetylation regulates mRNA polyadenylation in *Arabidopsis*. *Genome Research*, *30*(10), 1407–1417. https://doi.org/10.1101/gr.255232.119

Lindermayr, C., Saalbach, G., & Durner, J. (2005). Proteomic identification of S-nitrosylated proteins in *Arabidopsis*; *Plant Physiology*, *137*(3), 921–930. https://doi.org/10.1104/pp.104.058719

Liu, X., Yu, C.-W., Duan, J., Luo, M., Wang, K., Tian, G., Cui, Y., & Wu, K. (2012). HDA6 directly interacts with DNA methyltransferase MET1 and maintains transposable element silencing in Arabidopsis. *Plant Physiology*, *158*(1), 119–129. https://doi.org/10.1104/pp.111.184275

Liu, X., Wei, W., Zhu, W., Su, L., Xiong, Z., Zhou, M., Zheng, Y., & Zhou, D.-X. (2017). Histone deacetylase AtSRT1 links metabolic flux and stress response in Arabidopsis. *Molecular Plant*, *10*(12), 1510–1522. https://doi.org/10.1016/j.molp.2017.10.010

Liu, Z., Hartman, S., van Veen, H., Zhang, H., Leeggangers, H. A. C. F., Martopawiro, S., Bosman, F., de Deugd, F., Su, P., Hummel, M., Rankenberg, T., Hassall, K. L., Bailey-Serres, J., Theodoulou, F. L., Voesenek, L. A. C. J., & Sasidharan, R. (2022). Ethylene augments root hypoxia tolerance via growth cessation and reactive oxygen species amelioration. *Plant Physiology*, *190*(2), 1365–1383. https://doi.org/10.1093/plphys/kiac245

Loreti, E., & Perata, P. (2020). The many facets of hypoxia in plants. *Plants*, *9*(6), 745. https://doi.org/10.3390/plants9060745

Loreti, E., Betti, F., Ladera-Carmona, M. J., Fontana, F., Novi, G., Valeri, M. C., & Perata, P. (2019). ARGONAUTE1 and ARGONAUTE4 regulate gene expression and hypoxia tolerance. *Plant Physiology*, *182*(1), 287–300. https://doi.org/10.1104/pp.19.00741

Luger, K., Mäder, A. W., Richmond, R. K., Sargent, D. F., & Richmond, T. J. (1997). Crystal structure of the nucleosome core particle at 2.8 Å resolution. *Nature*, *389*(6648), 251–260. https://doi.org/10.1038/38444

Luo, M., Wang, Y.-Y., Liu, X., Yang, S., Lu, Q., Cui, Y., & Wu, K. (2012). HD2C interacts with HDA6 and is involved in ABA and salt stress response in Arabidopsis. *Journal of Experimental Botany*, *63*(8), 3297–3306. https://doi.org/10.1093/jxb/ers059

Lyko, F. (2018). The DNA methyltransferase family: A versatile toolkit for epigenetic regulation. *Nature Reviews Genetics*, *19*(2), 81–92. https://doi.org/10.1038/nrg.2017.80

McDonald, M. P., Galwey, N. W., & Colmer, T. D. (2002). Similarity and diversity in adventitious root anatomy as related to root aeration among a range of wetland and dryland grass species. *Plant, Cell & Environment*, *25*(3), 441–451. https://doi.org/10.1046/j.0016-8025.2001.00817.x

Mengel, A., Ageeva, A., Georgii, E., Bernhardt, J., Wu, K., Durner, J., & Lindermayr, C. (2017). Nitric oxide modulates histone acetylation at stress genes by inhibition of histone deacetylases. *Plant Physiology*, *173*(2), 1434–1452. https://doi.org/10.1104/pp.16.01734

Mira, M. M., Hill, R. D., & Stasolla, C. (2016). Phytoglobins improve hypoxic root growth by alleviating apical meristem cell death. *Plant Physiology*, *172*(3), 2044–2056. https://doi.org/10.1104/pp.16.01150

Mira, M. M., Huang, S., Hill, R. D., & Stasolla, C. (2021). Tolerance to excess moisture in soybean is enhanced by over-expression of the *Glycine max* Phytoglobin (*GmPgb1*). *Plant Physiology and Biochemistry*, *159*, 322–334. https://doi.org/10.1016/j.plaphy.2020.12.033

Mira, M. M., Hill, R. D., Hilo, A., Langer, M., Robertson, S., Igamberdiev, A. U., Wilkins, O., Rolletschek, H., & Stasolla, C. (2023a). Plant stem cells under low oxygen: Metabolic rewiring by phytoglobin underlies stem cell functionality. *Plant Physiology*, *193*(2), 1416–1432. https://doi.org/10.1093/plphys/kiad344

Mira, M. M., El-Khateeb, E. A., Youssef, M. S., Ciacka, K., So, K., Duncan, R. W., Hill, R. D., & Stasolla, C. (2023b). Arabidopsis root apical meristem survival during waterlogging is determined by phytoglobin through nitric oxide and auxin. *Planta*, *258*(5). https://doi.org/10.1007/s00425-023-04239-4

Moldovan, D., Spriggs, A., Yang, J., Pogson, B. J., Dennis, E. S., & Wilson, I. W. (2009). Hypoxia-responsive microRNAs and trans-acting small interfering RNAs in Arabidopsis. *Journal of Experimental Botany*, *61*(1), 165–177. https://doi.org/10.1093/jxb/erp296

Mora-Castilla, S., Tejedo, J. R., Hmadcha, A., Cahuana, G. M., Martín, F., Soria, B., & Bedoya, F. J. (2010). Nitric oxide repression of NANOG promotes mouse embryonic stem cell differentiation. *Cell Death & Differentiation*, *17*(6), 1025–1033. https://doi.org/10.1038/cdd.2009.204

Mukhi, N., Dhindwal, S., Uppal, S., Kapoor, A., Arya, R., Kumar, P., Kaur, J., & Kundu, S. (2016). Structural and functional significance of the N- and C-terminal appendages in

Arabidopsis truncated hemoglobin. *Biochemistry*, *55*(12), 1724–1740. https://doi.org/10.1021/acs.biochem.5b01013

Munoz-Lopez, M., & Garcia-Perez, J. (2010). DNA transposons: nature and applications in genomics. *Current Genomics*, *11*(2), 115–128. https://doi.org/10.2174/138920210790886871

Mustroph, A., & Albrecht, G. (2003). Tolerance of crop plants to oxygen deficiency stress: fermentative activity and photosynthetic capacity of entire seedlings under hypoxia and anoxia. *Physiologia Plantarum*, *117*(4), 508–520. https://doi.org/10.1034/j.1399-3054.2003.00051.x

Mustroph, A. (2018). Improving flooding tolerance of crop plants. *Agronomy*, *8*(9), 160. https://doi.org/10.3390/agronomy8090160

Ngcamu, B. S. (2023). Application of the disaster management cycle and climate change: Studying flood disasters in South Africa. *Social Sciences & Humanities Open*, *8*(1), 100657. https://doi.org/10.1016/j.ssaho.2023.100657

Ning, Y., Chen, Q., Lin, R., Li, Y., Li, L., Chen, S., & He, X. (2019). The HDA19 histone deacetylase complex is involved in the regulation of flowering time in a photoperiod-dependent manner. *The Plant Journal*, *98*(3), 448–464. https://doi.org/10.1111/tpj.14229

Nóia Júnior, R. de, Asseng, S., García-Vila, M., Liu, K., Stocca, V., dos Santos Vianna, M., Weber, T. K. D., Zhao, J., Palosuo, T., & Harrison, M. T. (2023). A call to action for global research on the implications of waterlogging for wheat growth and yield. *Agricultural Water Management*, *284*, 108334. https://doi.org/10.1016/j.agwat.2023.108334

North, B. J., & Verdin, E. (2004). Sirtuins: Sir2-related NAD-dependent protein deacetylases. *Genome Biology*, *5*(224). https://doi.org/10.1186/gb-2004-5-5-224

Nott, A., Watson, P. M., Robinson, J. D., Crepaldi, L., & Riccio, A. (2008). S-nitrosylation of histone deacetylase 2 induces chromatin remodeling in neurons. *Nature*, *455*(7211), 411–415. https://doi.org/10.1038/nature07238

Ornes, S. (2018). How does climate change influence extreme weather? Impact attribution research seeks answers. *Proceedings of the National Academy of Sciences*, *115*(33), 8232–8235. https://doi.org/10.1073/pnas.1811393115

Ou, X., Zhuang, T., Yin, W., Miao, Y., Wang, B., Zhang, Y., Lin, X., Xu, C., von Wettstein, D., Rustgi, S., & Liu, B. (2015). DNA methylation changes induced in rice by exposure to high concentrations of the nitric oxide modulator, Sodium Nitroprusside. *Plant Molecular Biology Reporter*, *33*(5), 1428–1440. https://doi.org/10.1007/s11105-014-0843-9

Pan, J., Sharif, R., Xu, X., & Chen, X. (2021). Mechanisms of waterlogging tolerance in plants: Research progress and prospects. *Frontiers in Plant Science*, *11*. https://doi.org/10.3389/fpls.2020.627331

Parani, M., Rudrabhatla, S., Myers, R., Weirich, H., Smith, B., Leaman, D. W., & Goldman, S. L. (2004). Microarray analysis of nitric oxide responsive transcripts in *Arabidopsis*. *Plant Biotechnology Journal*, *2*(4), 359–366. https://doi.org/10.1111/j.1467-7652.2004.00085.x

Pandey, R. (2002). Analysis of histone acetyltransferase and histone deacetylase families of *Arabidopsis thaliana* suggests functional diversification of chromatin modification among multicellular eukaryotes. *Nucleic Acids Research*, *30*(23), 5036–5055. https://doi.org/10.1093/nar/gkf660

Parent, C., Capelli, N., & Dat, J. (2008). Reactive oxygen species, stress and cell death in plants. *Comptes Rendus. Biologies*, *331*(4), 255–261. https://doi.org/10.1016/j.crvi.2008.02.001

Perata, P., & Alpi, A. (1993). Plant responses to anaerobiosis. *Plant science*, *93*(1-2), 1-17. https://doi.org/10.1016/0168-9452(93)90029-Y

Perazzolli, M., Romero-Puertas, M. C., & Delledonne, M. (2006). Modulation of nitric oxide bioactivity by plant haemoglobins. *Journal of Experimental Botany*, *57*(3), 479–488. https://doi.org/10.1093/jxb/erj051

Petricka, J. J., Winter, C. M., & Benfey, P. N. (2012). Control of *Arabidopsis* root development. *Annual Review of Plant Biology*, *63*(1), 563–590. https://doi.org/10.1146/annurev-arplant-042811-105501

Pillai-Kastoori, L., Schutz-Geschwender, A. R., & Harford, J. A. (2020). A systematic approach to quantitative Western blot analysis. *Analytical Biochemistry*, *593*, 113608. https://doi.org/10.1016/j.ab.2020.113608

Polverari, A., Molesini, B., Pezzotti, M., Buonaurio, R., Marte, M., & Delledonne, M. (2003). Nitric oxide-mediated transcriptional changes in *Arabidopsis thaliana*. *Molecular Plant-Microbe Interactions®*, *16*(12), 1094–1105. https://doi.org/10.1094/mpmi.2003.16.12.1094

Probst, A. V., Fagard, M., Proux, F., Mourrain, P., Boutet, S., Earley, K., Lawrence, R. J., Pikaard, C. S., Murfett, J., Furner, I., Vaucheret, H., & Scheid, O. M. (2004). Arabidopsis histone deacetylase *HDA6* is required for maintenance of transcriptional gene silencing and determines nuclear organization of rDNA repeats. *The Plant Cell*, *16*(4), 1021–1034. https://doi.org/10.1105/tpc.018754

Rahim, W., Khan, M., Al Azzawi, T. N. I., Pande, A., Methela, N. J., Ali, S., Imran, M., Lee, D.-S., Lee, G.-M., Mun, B.-G., Moon, Y.-S., Lee, I.-J., & Yun, B.-W. (2022). Exogenously Applied Sodium Nitroprusside Mitigates Lead Toxicity in Rice by Regulating

Antioxidants and Metal Stress-Related Transcripts. *International Journal of Molecular Sciences*, *23*(17), 9729. https://doi.org/10.3390/ijms23179729

Rahman, M. S., & Di, L. (2020). A systematic review on case studies of remote-sensing-based flood crop loss assessment. *Agriculture*, *10*(4), 131. https://doi.org/10.3390/agriculture10040131

Ramakrishnan, M., Satish, L., Kalendar, R., Narayanan, M., Kandasamy, S., Sharma, A., Emamverdian, A., Wei, Q., & Zhou, M. (2021). The dynamism of transposon methylation for plant development and stress adaptation. *International Journal of Molecular Sciences*, *22*(21), 11387. https://doi.org/10.3390/ijms222111387

Reeder, B. J., & Hough, M. A. (2014). The structure of a class 3 nonsymbiotic plant haemoglobin from *Arabidopsis thaliana* reveals a novel N-terminal helical extension. *Acta Crystallographica Section D Biological Crystallography*, *70*(5), 1411–1418. https://doi.org/10.1107/s1399004714004878

Ren, X., Chen, Z., Liu, Y., Zhang, H., Zhang, M., Liu, Q., Hong, X., Zhu, J.-K., & Gong, Z. (2010). ABO3, a WRKY transcription factor, mediates plant responses to abscisic acid and drought tolerance in Arabidopsis. *The Plant Journal*, *63*(3), 417–429. https://doi.org/10.1111/j.1365-313x.2010.04248.x

Samoilov, M., Churilova, A., Gluschenko, T., Vetrovoy, O., Dyuzhikova, N., & Rybnikova, E. (2016). Acetylation of histones in neocortex and hippocampus of rats exposed to different modes of hypobaric hypoxia: Implications for brain hypoxic injury and tolerance. *Acta Histochemica*, *118*(2), 80–89. https://doi.org/10.1016/j.acthis.2015.11.008

Sasidharan, R., Bailey-Serres, J., Ashikari, M., Atwell, B. J., Colmer, T. D., Fagerstedt, K., Fukao, T., Geigenberger, P., Hebelstrup, K. H., Hill, R. D., Holdsworth, M. J., Ismail, A. M., Licausi, F., Mustroph, A., Nakazono, M., Pedersen, O., Perata, P., Sauter, M., Shih, M., … Voesenek, L. A. C. J. (2017). Community recommendations on terminology and procedures used in flooding and low oxygen stress research. *New Phytologist*, *214*(4), 1403–1407. https://doi.org/10.1111/nph.14519

Sasidharan, R., & Mustroph, A. (2011). Plant oxygen sensing is mediated by the N-end rule pathway: A milestone in plant anaerobiosis. *The Plant Cell*, *23*(12), 4173–4183. https://doi.org/10.1105/tpc.111.093880

Sauter, M. (2013). Root responses to flooding. *Current Opinion in Plant Biology*, *16*(3), 282–286. https://doi.org/10.1016/j.pbi.2013.03.013

Schippers, J. H., von Bongartz, K., Laritzki, L., Frohn, S., Frings, S., Renziehausen, T., Augstein, F., Winkels, K., Sprangers, K., Sasidharan, R., Vertommen, D., Van Breusegem, F., Hartman, S., Beemster, G. T., Mhamdi, A., van Dongen, J. T., & Schmidt-Schippers, R. R. (2024). ERFVII-controlled hypoxia responses are in part

facilitated by Mediator subunit 25 in *Arabidopsis thaliana*. *The Plant Journal*, *120*(2), 748–768. https://doi.org/10.1111/tpj.17018

Sen, N., Hara, M. R., Kornberg, M. D., Cascio, M. B., Bae, B.-I., Shahani, N., Thomas, B., Dawson, T. M., Dawson, V. L., Snyder, S. H., & Sawa, A. (2008). Nitric oxide-induced nuclear GAPDH activates p300/CBP and mediates apoptosis. *Nature Cell Biology*, *10*(7), 866–873. https://doi.org/10.1038/ncb1747

Shih, Y., Lin, P., Hung, F., & Wu, K. (2025). Dynamic acetylation of WRKY63 is antagonistically regulated by HAG1 and HDA6 in *Arabidopsis thaliana*. *The Plant Journal*, *123*(6). https://doi.org/10.1111/tpj.70495

Simontacchi, M., Galatro, A., Ramos-Artuso, F., & Santa-María, G. E. (2015). Plant Survival in a Changing Environment: The Role of Nitric Oxide in Plant Responses to Abiotic Stress. *Frontiers in Plant Science*, *6*. https://doi.org/10.3389/fpls.2015.00977

Steffens, B., & Rasmussen, A. (2015). The Physiology of Adventitious Roots. *Plant Physiology*, *170*(2), 603–617. https://doi.org/10.1104/pp.15.01360

Stoimenova, M., Igamberdiev, A. U., Gupta, K. J., & Hill, R. D. (2007). Nitrite-driven anaerobic ATP synthesis in barley and rice root mitochondria. *Planta*, *226*(2), 465–474. https://doi.org/10.1007/s00425-007-0496-0

Strahl, B. D., & Allis, C. D. (2000). The language of covalent histone modifications. *Nature*, *403*(6765), 41–45. https://doi.org/10.1038/47412

Strotmann, V. I., & Stahl, Y. (2021). At the root of quiescence: function and regulation of the quiescent center. *Journal of Experimental Botany*, *72*(19), 6716-6726. https://doi.org/10.1093/jxb/erab275

Stroud, H., Otero, S., Desvoyes, B., Ramírez-Parra, E., Jacobsen, S. E., & Gutierrez, C. (2012). Genome-wide analysis of histone H3.1 and H3.3 variants in *arabidopsis thaliana*. *Proceedings of the National Academy of Sciences*, *109*(14), 5370–5375. https://doi.org/10.1073/pnas.1203145109

Sun, H., Feng, F., Liu, J., & Zhao, Q. (2018). Nitric oxide affects rice root growth by regulating auxin transport under nitrate supply. *Frontiers in Plant Science*, *9*. https://doi.org/10.3389/fpls.2018.00659

Swain, D. L., Wing, O. E. J., Bates, P. D., Done, J. M., Johnson, K. A., & Cameron, D. R. (2020). Increased Flood Exposure Due to Climate Change and Population Growth in the United States. *Earth's Future*, *8*(11). https://doi.org/10.1029/2020EF001778

Szemenyei, H., Hannon, M., & Long, J. A. (2008). Topless mediates auxin-dependent transcriptional repression during *Arabidopsis* embryogenesis. *Science*, *319*(5868), 1384–1386. https://doi.org/10.1126/science.1151461

Tadege, M., Kuhlemeier, C., & Dupuis, I. (1999). Ethanolic fermentation: New functions for an old pathway. *Trends in Plant Science*, *4*(8), 320–325. https://doi.org/10.1016/s1360-1385(99)01450-8

Tanaka, M., Kikuchi, A., & Kamada, H. (2008). The Arabidopsis Histone Deacetylases HDA6 and HDA19 Contribute to the Repression of Embryonic Properties after Germination. *Plant Physiology*, *146*(1), 149–161. https://doi.org/10.1104/pp.107.111674

Tang, G. (2005). siRNA and miRNA: An insight into RISCs. *Trends in Biochemical Sciences*, *30*(2), 106–114. https://doi.org/10.1016/j.tibs.2004.12.007

Tausendschön, M., Dehne, N., & Brüne, B. (2011). Hypoxia causes epigenetic gene regulation in macrophages by attenuating Jumonji histone demethylase activity. *Cytokine*, *53*(2), 256–262. https://doi.org/10.1016/j.cyto.2010.11.002

Tian, L., Wang, J., Fong, M. P., Chen, M., Cao, H., Gelvin, S. B., & Chen, Z. J. (2003). Genetic control of developmental changes induced by disruption of Arabidopsis histone deacetylase 1 (*AtHD1*) expression. *Genetics*, *165*(1), 399–409. https://doi.org/10.1093/genetics/165.1.399

To, T. K., Kim, J.-M., Matsui, A., Kurihara, Y., Morosawa, T., Ishida, J., Tanaka, M., Endo, T., Kakutani, T., Toyoda, T., Kimura, H., Yokoyama, S., Shinozaki, K., & Seki, M. (2011). Arabidopsis HDA6 regulates locus-directed heterochromatin silencing in cooperation with MET1. *PLoS Genetics*, *7*(4). https://doi.org/10.1371/journal.pgen.1002055

Trevaskis, B., Watts, R.A., Andersson, C.R., Llewellyn, D.J., Hargrove, M.S., Olson, J.S., Dennis, E.S. and Peacock, W.J. (1997). Two hemoglobin genes in *Arabidopsis thaliana*: the evolutionary origins of leghemoglobins. *Proceedings of the National Academy of Sciences*, *94*(22), 12230-12234. https://doi.org/10.1073/pnas.94.22.12230

Ueda, M., Matsui, A., Nakamura, T., Abe, T., Sunaoshi, Y., Shimada, H., & Seki, M. (2018). Versatility of HDA19-deficiency in increasing the tolerance of Arabidopsis to different environmental stresses. *Plant Signaling & Behavior*, 1–4. https://doi.org/10.1080/15592324.2018.1475808

Van Aken, O., Zhang, B., Law, S., Narsai, R., & Whelan, J. (2013). AtWRKY40 and AtWRKY63 modulate the expression of stress-responsive nuclear genes encoding mitochondrial and chloroplast proteins. *Plant Physiology*, *162*(1), 254–271. https://doi.org/10.1104/pp.113.215996

van den Berg, C., Willemsen, V., Hendriks, G., Weisbeek, P., & Scheres, B. (1997). Short-range control of cell differentiation in the Arabidopsis root meristem. *Nature*, *390*(6657), 287–289. https://doi.org/10.1038/36856

van Dongen, J. T., & Licausi, F. (2015). Oxygen sensing and signaling. *Annual Review of Plant Biology*, *66*(1), 345–367. https://doi.org/10.1146/annurev-arplant-043014-114813

Vélez-Bermúdez, I. C., & Schmidt, W. (2023). Iron sensing in plants. *Frontiers in Plant Science*, *14*. https://doi.org/10.3389/fpls.2023.1145510

Verdikt, R., & Thienpont, B. (2024). Epigenetic remodeling under hypoxia. *Seminars in Cancer Biology*, *98*, 1–10. https://doi.org/10.1016/j.semcancer.2023.10.005

Vicente, J., Mendiondo, G. M., Movahedi, M., Peirats-Llobet, M., Juan, Y., Shen, Y., Dambire, C., Smart, K., Rodriguez, P. L., Charng, Y., Gray, J. E., & Holdsworth, M. J. (2017). The Cys-Arg/N-end rule pathway is a general sensor of abiotic stress in flowering plants. *Current Biology*, *27*(20), 3183–3190. https://doi.org/10.1016/j.cub.2017.09.006

Vieten, A., Vanneste, S., Wiśniewska, J., Benková, E., Benjamins, R., Beeckman, T., Luschnig, C., & Friml, J. (2005). Functional redundancy of PIN proteins is accompanied by auxin-dependent cross-regulation of pin expression. *Development*, *132*(20), 4521–4531. https://doi.org/10.1242/dev.02027

Vincent, S. A., Kim, J.-M., Pérez-Salamó, I., To, T. K., Torii, C., Ishida, J., Tanaka, M., Endo, T. A., Bhat, P., Devlin, P. F., Seki, M., & Devoto, A. (2022). Jasmonates and Histone deacetylase 6 activate Arabidopsis genome-wide histone acetylation and methylation during the early acute stress response. *BMC Biology*, *20*(1). https://doi.org/10.1186/s12915-022-01273-8

Visser, E. J., Colmer, T. D., Blom, C. W., & Voesenek, L. A. (2000). Changes in growth, porosity, and radial oxygen loss from adventitious roots of selected mono- and dicotyledonous wetland species with contrasting types of Aerenchyma. *Plant, Cell & Environment*, *23*(11), 1237–1245. https://doi.org/10.1046/j.1365-3040.2000.00628.x

Visser, E. J. W. , Voesenek, L. A. C. J., Vartapetian, B. B., & Jackson, M. B. (2003). Flooding and plant growth. *Annals of Botany*, *91*(2), 107–109. https://doi.org/10.1093/aob/mcg014

Voesenek, L. A., & Bailey-Serres, J. (2015). Flood adaptive traits and processes: an overview. *New Phytologist*, *206*(1), 57-73. https://doi.org/10.1111/nph.13209

Wang, C., Gao, F., Wu, J., Dai, J., Wei, C., & Li, Y. (2010). Arabidopsis putative deacetylase AtSRT2 regulates basal defense by suppressing PAD4, EDS5 and SID2 expression. *Plant and Cell Physiology*, *51*(8), 1291–1299. https://doi.org/10.1093/pcp/pcq087

Weinert, B. T., Narita, T., Satpathy, S., Srinivasan, B., Hansen, B. K., Schölz, C., Hamilton, W. B., Zucconi, B. E., Wang, W. W., Liu, W. R., Brickman, J. M., Kesicki, E. A., Lai, A., Bromberg, K. D., Cole, P. A., & Choudhary, C. (2018). Time-resolved analysis reveals rapid dynamics and broad scope of the CBP/p300 acetylome. *Cell*, *174*(1). https://doi.org/10.1016/j.cell.2018.04.033

Weits, D. A., Giuntoli, B., Kosmacz, M., Parlanti, S., Hubberten, H.-M., Riegler, H., Hoefgen, R., Perata, P., van Dongen, J. T., & Licausi, F. (2014). Plant cysteine oxidases control the

oxygen-dependent branch of the N-end-rule pathway. *Nature Communications*, *5*(1). https://doi.org/10.1038/ncomms4425

Wu, K., Zhang, L., Zhou, C., Yu, C.-W., & Chaikam, V. (2008). HDA6 is required for jasmonate response, senescence and flowering in Arabidopsis. *Journal of Experimental Botany*, *59*(2), 225–234. https://doi.org/10.1093/jxb/erm300

Xia, X., Lemieux, M. E., Li, W., Carroll, J. S., Brown, M., Liu, X. S., & Kung, A. L. (2009). Integrative analysis of HIF binding and transactivation reveals its role in maintaining histone methylation homeostasis. *Proceedings of the National Academy of Sciences*, *106*(11), 4260–4265. https://doi.org/10.1073/pnas.0810067106

Xu, Z.-S., Chen, M., Li, L.-C., & Ma, Y.-Z. (2008). Functions of the ERF transcription factor family in plants. *Botany*, *86*(9), 969–977. https://doi.org/10.1139/b08-041

Yamasaki, H., Sakihama, Y., & Takahashi, S. (1999). An alternative pathway for nitric oxide production in plants: New features of an old enzyme. *Trends in Plant Science*, *4*(4), 128–129. https://doi.org/10.1016/s1360-1385(99)01393-x

Yamoune, A., Cuyacot, A. R., Zdarska, M., & Hejatko, J. (2021). Hormonal orchestration of root apical meristem formation and maintenance in Arabidopsis. *Journal of Experimental Botany*, *72*(19), 6768–6788. https://doi.org/10.1093/jxb/erab360

Yan, X., Qu, X., Tian, R., Xu, L., Jin, X., Yu, S., Zhao, Y., Ma, J., Liu, Y., Sun, L., & Su, J. (2020). Hypoxia-induced NAD^+ interventions promote tumor survival and metastasis by regulating mitochondrial dynamics. *Life Sciences*, *259*, 118171. https://doi.org/10.1016/j.lfs.2020.118171

Yang, J., Yuan, L., Yen, M., Zheng, F., Ji, R., Peng, T., Gu, D., Yang, S., Cui, Y., Chen, P., Wu, K., & Liu, X. (2020). SWI3B and HDA6 interact and are required for transposon silencing in *Arabidopsis*. *The Plant Journal*, *102*(4), 809–822. https://doi.org/10.1111/tpj.14666

Yu, C.-W., Chang, K.-Y., & Wu, K. (2016). Genome-wide analysis of gene regulatory networks of the FVE-HDA6-FLD complex in Arabidopsis. *Frontiers in Plant Science*, *7*. https://doi.org/10.3389/fpls.2016.00555

Yuan, L., Chen, X., Chen, H., Wu, K., & Huang, S. (2019). Histone deacetylases HDA6 and HDA9 coordinately regulate valve cell elongation through affecting auxin signaling in Arabidopsis. *Biochemical and Biophysical Research Communications*, *508*(3), 695–700. https://doi.org/10.1016/j.bbrc.2018.11.082

Zaffagnini, M., Fermani, S., Costa, A., Lemaire, S. D., & Trost, P. (2013). Plant cytoplasmic GAPDH: Redox post-translational modifications and moonlighting properties. *Frontiers in Plant Science*, *4*. https://doi.org/10.3389/fpls.2013.00450

Zahra, N., Hafeez, M. B., Shaukat, K., Wahid, A., Hussain, S., Naseer, R., Raza, A., Iqbal, S., & Farooq, M. (2021). Hypoxia and anoxia stress: Plant responses and Tolerance Mechanisms. *Journal of Agronomy and Crop Science*, *207*(2), 249–284. https://doi.org/10.1111/jac.12471

Zeller, G., Henz, S. R., Widmer, C. K., Sachsenberg, T., Rätsch, G., Weigel, D., & Laubinger, S. (2009). Stress-induced changes in the *Arabidopsis thaliana* transcriptome analyzed using whole-genome tiling arrays. *The Plant Journal*, *58*(6), 1068–1082. https://doi.org/10.1111/j.1365-313x.2009.03835.x

Zeng, J., Zhao, X., Liang, Z., Hidalgo, I., Gebert, M., Fan, P., Wenzl, C., Gornik, S. G., & Lohmann, J. U. (2023). Nitric oxide controls shoot meristem activity via regulation of DNA methylation. *Nature Communications*, *14*(1). https://doi.org/10.1038/s41467-023-43705-1

Zhang, W., Swarup, R., Bennett, M., Schaller, G. E., & Kieber, J. J. (2013). Cytokinin induces cell division in the quiescent center of the Arabidopsis root apical meristem. *Current Biology*, *23*(20), 1979–1989. https://doi.org/10.1016/j.cub.2013.08.008

Zheng, Y., Li, Z., Cui, X., Yang, Z., Bao, C., Pan, L., Liu, X., Chatel-Innocenti, G., Vanacker, H., Noctor, G., Dard, A., Reichheld, J., Issakidis-Bourguet, E., & Zhou, D. (2023). S-Nitrosylation of the histone deacetylase HDA19 stimulates its activity to enhance plant stress tolerance in Arabidopsis. *The Plant Journal*, *114*(4), 836–854. https://doi.org/10.1111/tpj.16174

Zhou, X., He, J., Velanis, C. N., Zhu, Y., He, Y., Tang, K., Zhu, M., Graser, L., de Leau, E., Wang, X., Zhang, L., Andy Tao, W., Goodrich, J., Zhu, J., & Zhang, C. (2021). A domesticated *Harbinger* transposase forms a complex with HDA6 and promotes histone H3 deacetylation at genes but not TEs in *Arabidopsis*. *Journal of Integrative Plant Biology*, *63*(8), 1462–1474. https://doi.org/10.1111/jipb.13108

SUPPLEMENTAL FIGURES

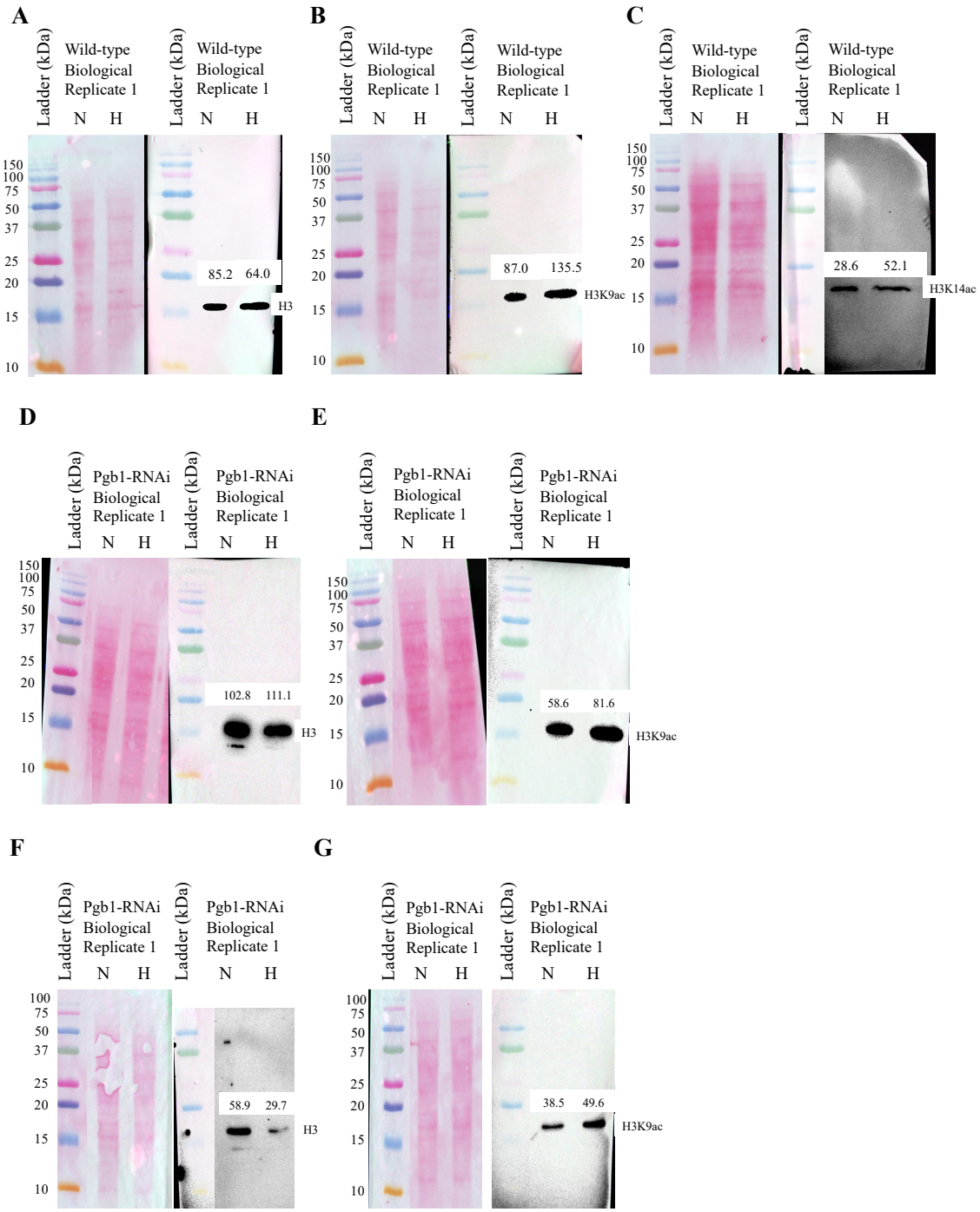

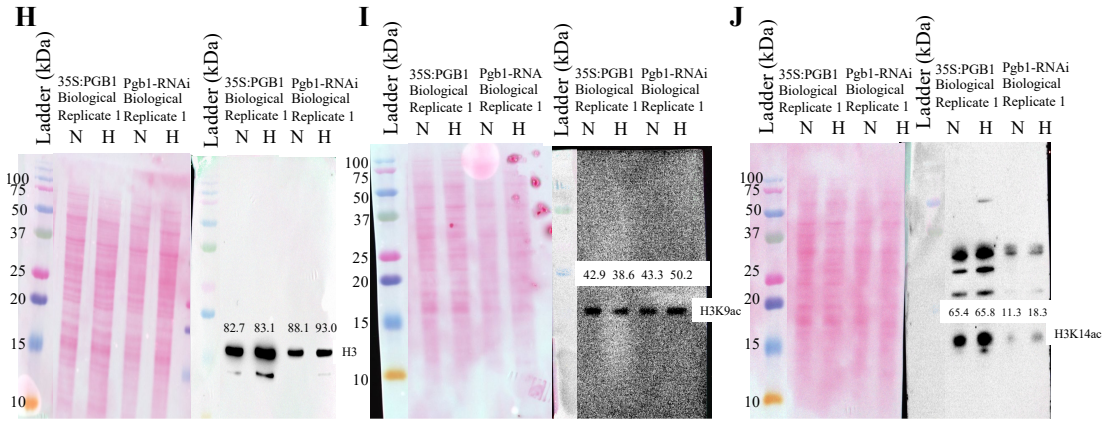
H
Ladder (kDa)
35S:PGB1 Biological Replicate 1
Pgb1-RNAi Biological Replicate 1
N H N H
100
75
50
37
25
20
15
10
82.7 83.1 88.1 93.0
H3
I
Pgb1-RNA Biological Replicate 1
42.9 38.6 43.3 50.2
H3K9ac
J
65.4 65.8 11.3 18.3
H3K14ac

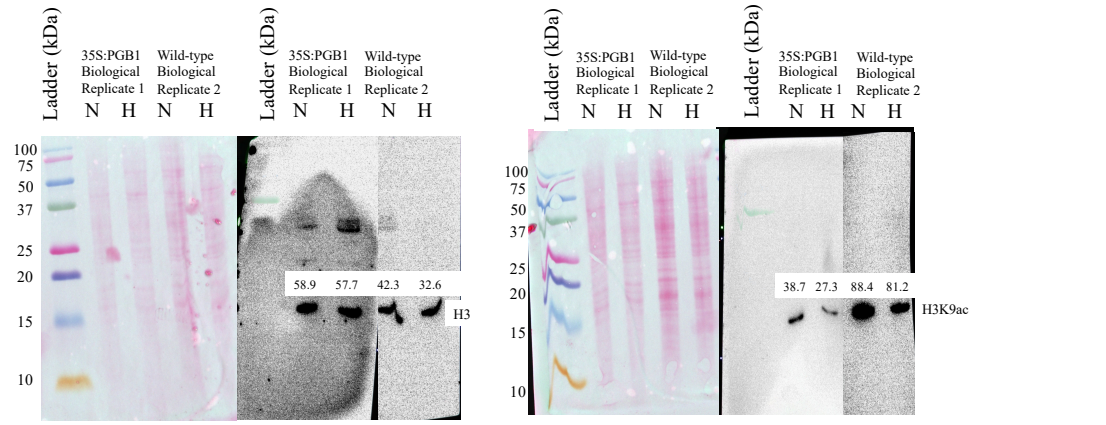
K
Wild-type Biological Replicate 2
58.9 57.7 42.3 32.6
H3
L
38.7 27.3 88.4 81.2
H3K9ac

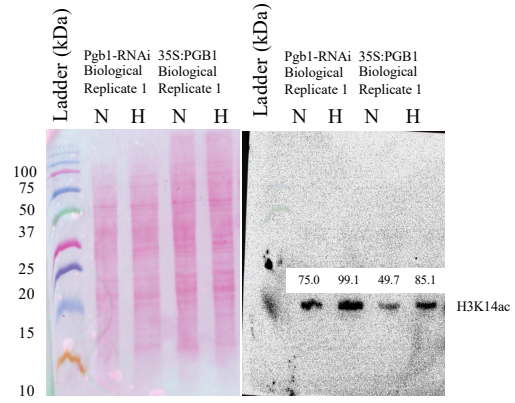
M
75.0 99.1 49.7 85.1
H3K14ac

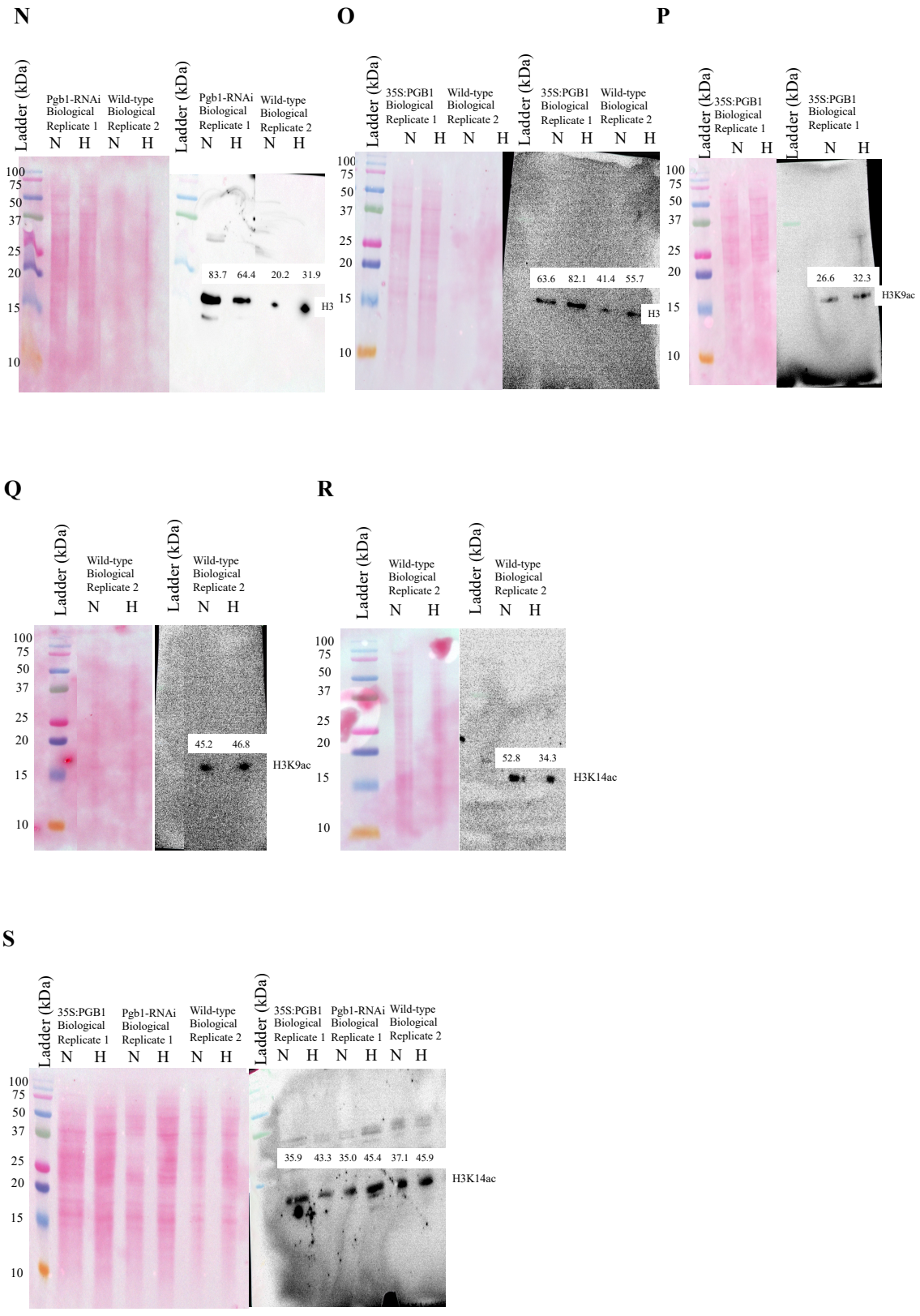
N
O
P
Q
R
S
Ladder (kDa)
Pgb1-RNAi Biological Replicate 1
Wild-type Biological Replicate 2
35S:PGB1 Biological Replicate 1
N H
100
75
50
37
25
20
15
10
83.7 64.4 20.2 31.9
H3
63.6 82.1 41.4 55.7
26.6 32.3
H3K9ac
45.2 46.8
52.8 34.3
H3K14ac
35.9 43.3 35.0 45.4 37.1 45.9

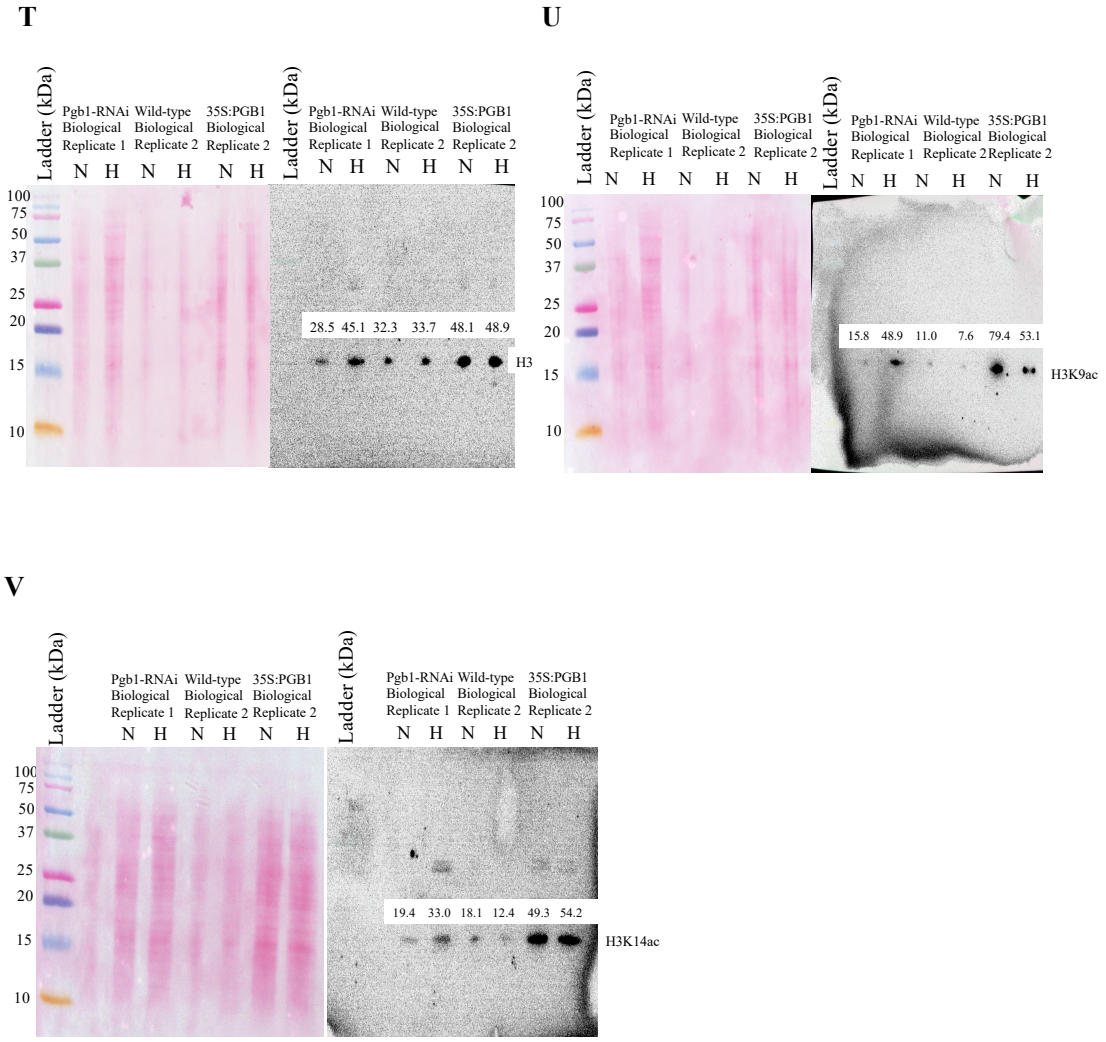

Supplemental Figure S1: Biological replicate 1 and biological replicate 2 (WT technical replicate 1-3, 35S:PGB1 technical replicates 1) of WT, 35S:PGB1, and Pgb-RNAi. The Ponceau S-stained blot of normoxic and hypoxic cell lysates (left panels), and the accompanying blot immunostained with antibodies against the H3 loading control **(A, D, H, K, N, O, T)**, H3K9ac **(B E, I, L, P, Q, U)**, and H3K14ac **(C, J, M, S, R, V)** are shown (right panels). WT biolgical replicate 1 includes technical replicates tech. rep. 1 in Figure 8, tech. rep. 2 (**A-C)** and biological replicate 2 includes technical replicates H3K9ac tech. rep. 1 (**T, U**), H3K9ac tech. rep. 2 (**O, Q**), H3K14ac tech. rep. 1 (**N, R**), H3K14ac tech. rep. 2 (**O, S**), H3K14ac tech. rep. 3 (**T, V**) in the figure. 35S:PGB1 biological replicate 1 includes technical replicates: tech. rep. 1 (**H, I, J**), tech. rep. 2 (**O, L, M**), tech. rep. 3 (**O, P, S**) and biological replicate 2 includes technical replicates: tech. rep. 1 (**T, U, V**) in this figure. Pgb1-RNAi biological replicate 1 includes technical replicates: H3K9ac tech. rep. 1 **(D, E)**, H3K9ac tech. rep. 2 (**F, G**), H3K9ac tech. rep. 3 (**H, I**), H3K14ac tech. rep. 1 (**H, M**), H3K14ac tech. rep. 2 (**N, M**), H3K14ac tech. rep. 3 (**K, S**), tech. rep. 4 (**T, U, V**). Abcam mouse anti-H3 (cat# 10799) primary antibody and Invitrogen goat anti-

mouse (cat# 31430) were used for the H3 blots **(A, D, H, K, N, O, T)**. Abcam rabbit anti-H3K9ac (cat# ab32129) primary antibody and Invitrogen goat anti-rabbit secondary (cat# 32460) were used for the H3K9ac blots **(B, E, I, L, P, Q, U)**. Invitrogen rabbit anti-H3K14ac (cat# MA5-32814) primary antibody for blots **C** and **J.** Abcam rabbit anti-H3K14ac (cat# ab52946) was used for blots **M, S, R,** and **V**. An Invitrogen goat anti-rabbit (cat# 32460) secondary antibody were used for the H3K14ac blots. The values above each band represent the band intensity value (band volume/band area) provided by the Azure SpotPro software.

A

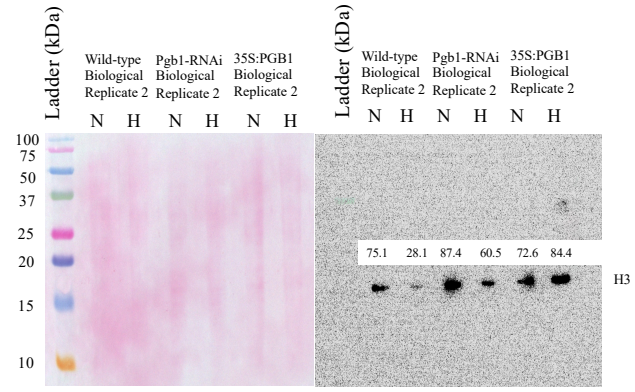
Ladder (kDa)
Wild-type Biological Replicate 2
Pgb1-RNAi Biological Replicate 2
35S:PGB1 Biological Replicate 2
N H N H N H
100
75
50
37
25
20
15
10
75.1 28.1 87.4 60.5 72.6 84.4
H3

B

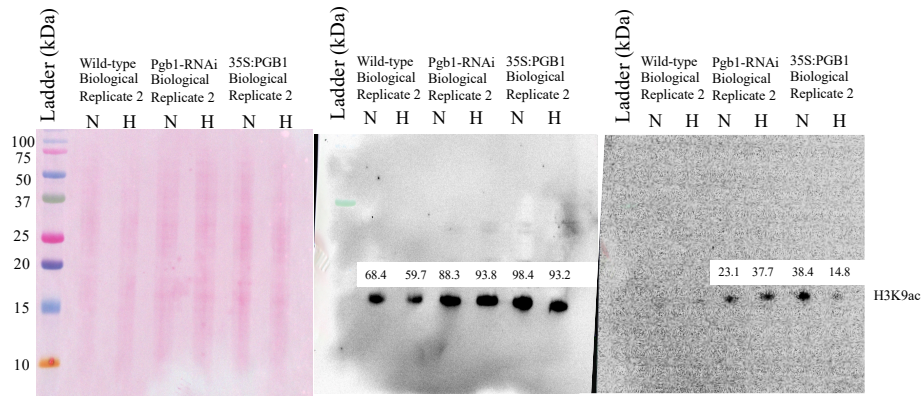
Ladder (kDa)
Wild-type Biological Replicate 2
Pgb1-RNAi Biological Replicate 2
35S:PGB1 Biological Replicate 2
N H N H N H
100
75
50
37
25
20
15
10
68.4 59.7 88.3 93.8 98.4 93.2
23.1 37.7 38.4 14.8
H3K9ac

C

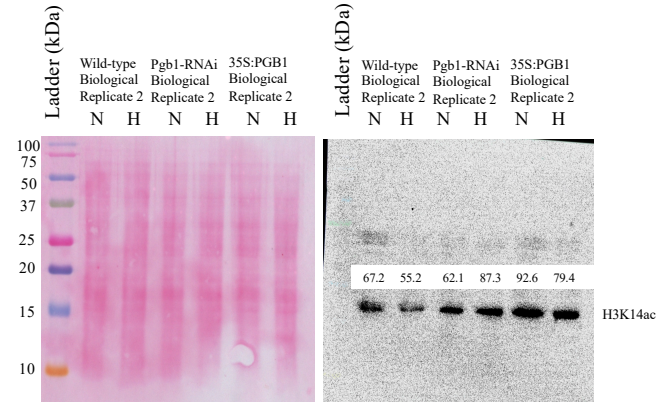
Ladder (kDa)
Wild-type Biological Replicate 2
Pgb1-RNAi Biological Replicate 2
35S:PGB1 Biological Replicate 2
N H N H N H
100
75
50
37
25
20
15
10
67.2 55.2 62.1 87.3 92.6 79.4
H3K14ac

D

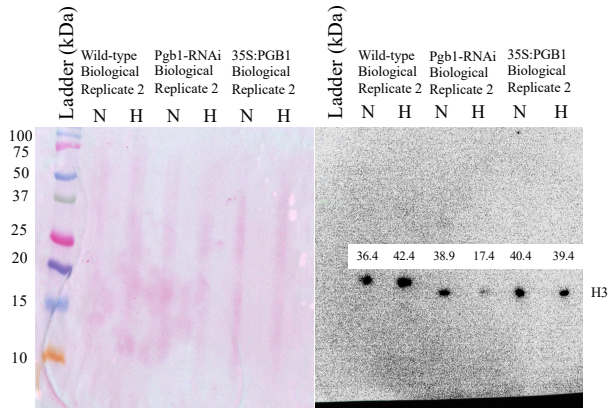
Ladder (kDa)
Wild-type Biological Replicate 2
Pgb1-RNAi Biological Replicate 2
35S:PGB1 Biological Replicate 2
N H N H N H
100
75
50
37
25
20
15
10
Ladder (kDa)
Wild-type Biological Replicate 2
Pgb1-RNAi Biological Replicate 2
35S:PGB1 Biological Replicate 2
N H N H N H
36.4 42.4 38.9 17.4 40.4 39.4
H3

E

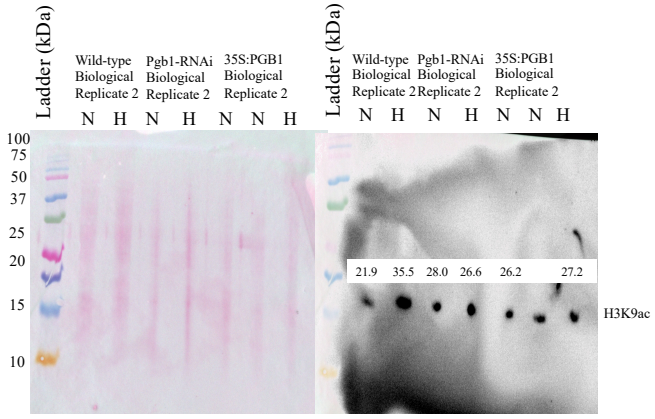
Ladder (kDa)
Wild-type Biological Replicate 2
Pgb1-RNAi Biological Replicate 2
35S:PGB1 Biological Replicate 2
N H N H N N H
100
75
50
37
25
20
15
10
Ladder (kDa)
Wild-type Biological Replicate 2
Pgb1-RNAi Biological Replicate 2
35S:PGB1 Biological Replicate 2
N H N H N N H
21.9 35.5 28.0 26.6 26.2 27.2
H3K9ac

F

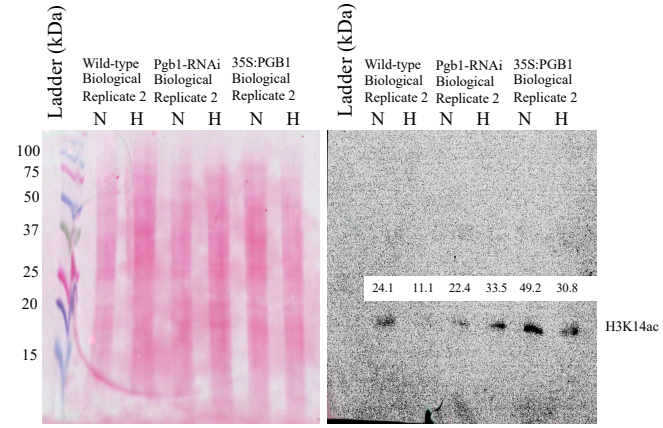
Ladder (kDa)
Wild-type Biological Replicate 2
Pgb1-RNAi Biological Replicate 2
35S:PGB1 Biological Replicate 2
N H N H N H
100
75
50
37
25
20
15
Ladder (kDa)
Wild-type Biological Replicate 2
Pgb1-RNAi Biological Replicate 2
35S:PGB1 Biological Replicate 2
N H N H N H
24.1 11.1 22.4 33.5 49.2 30.8
H3K14ac

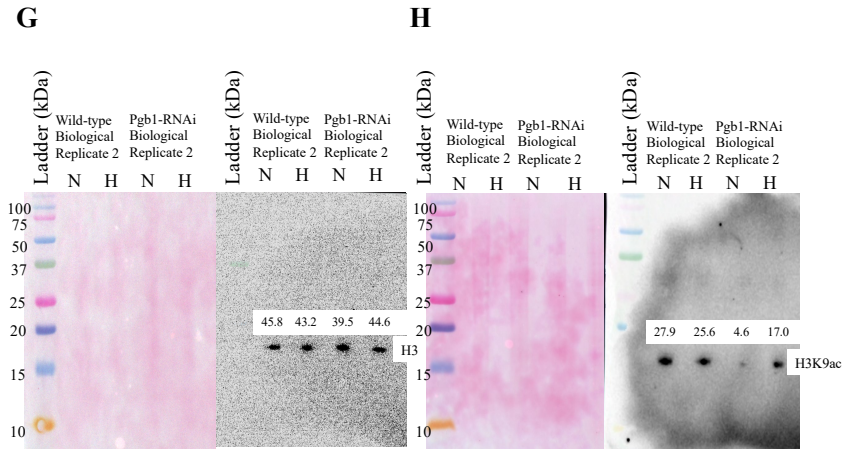
G
H
Ladder (kDa)
Wild-type Biological Replicate 2
Pgb1-RNAi Biological Replicate 2
N H N H
100
75
50
37
25
20
15
10
45.8 43.2 39.5 44.6
H3
27.9 25.6 4.6 17.0
H3K9ac

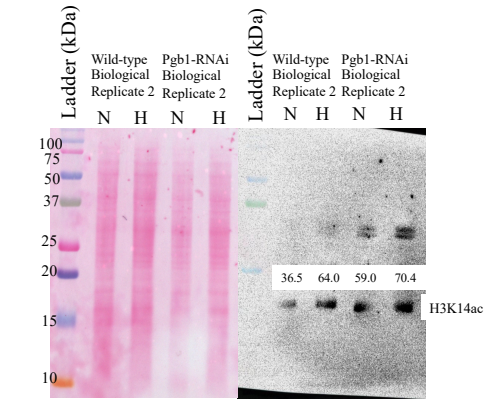
I
Ladder (kDa)
Wild-type Biological Replicate 2
Pgb1-RNAi Biological Replicate 2
N H N H
100
75
50
37
25
20
15
10
36.5 64.0 59.0 70.4
H3K14ac

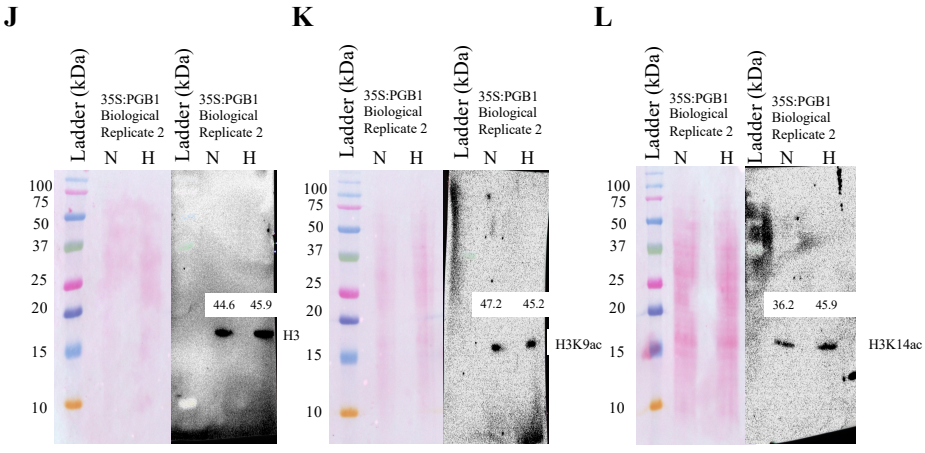
J
K
L
Ladder (kDa)
35S:PGB1 Biological Replicate 2
N H
100
75
50
37
25
20
15
10
44.6 45.9
H3
47.2 45.2
H3K9ac
36.2 45.9
H3K14ac

Supplemental Figure S2: Biological replicate 2 of the WT (tech. rep. 3-6), 35S:PGB1 (tech. rep. 2-4), and Pgb-RNAi lines (all tech. reps.). The Ponceau S-stained blot of normoxic and hypoxic cell lysates (left panels), and the accompanying blot immunostained with antibodies against the H3 loading control **(A, D, G, J)**, H3K9ac **(B, E, H, K)**, and H3K14ac **(C, F, I, L)** are shown (right panels). WT biolgical replicate 2 includes technical replicates: H3K9ac tech. rep. 3 **(A, B),** H3K9ac tech. rep. 4 **(D, E),** H3K9ac tech. rep. **(G, H),** H3K14ac tech. rep. 4 **(A, C),** H3K14ac tech. rep. 5 **(D, E),** H3K14ac tech. rep. 6 **(G, I).** 35S:PGB1 biological replicate 2 includes technical replicates: tech. rep. 2 **(A, B, C),** tech. rep. 3 **(D, E, F),** tech. rep. 4 **(J, K, L).** Pgb1-RNAi biological replicate 1 includes technical replicates: tech. rep. 1 **(D, E, F),** tech. rep. 2 **(A, B, C)**, tech. rep. 3 **(G, H, I).** Abcam mouse anti-H3 (cat# 10799) primary antibody and Invitrogen goat anti-mouse (cat# 31430) were used for the H3 blots **(A, D, G, J)**. Abcam rabbit anti-H3K9ac (cat# ab32129) primary antibody and Invitrogen goat anti-rabbit secondary (cat# 32460) were used for the H3K9ac blots **(B, E, H, K)**. Abcam rabbit anti-H3K14ac (cat# ab52946) was used for all H3K14ac blots **(C, F, I, L)**. An Invitrogen goat anti-rabbit (cat# 32460) secondary antibody were used for the H3K14ac blots. The values above each band represent the band intensity value (band volume/band area) provided by the Azure SpotPro software.

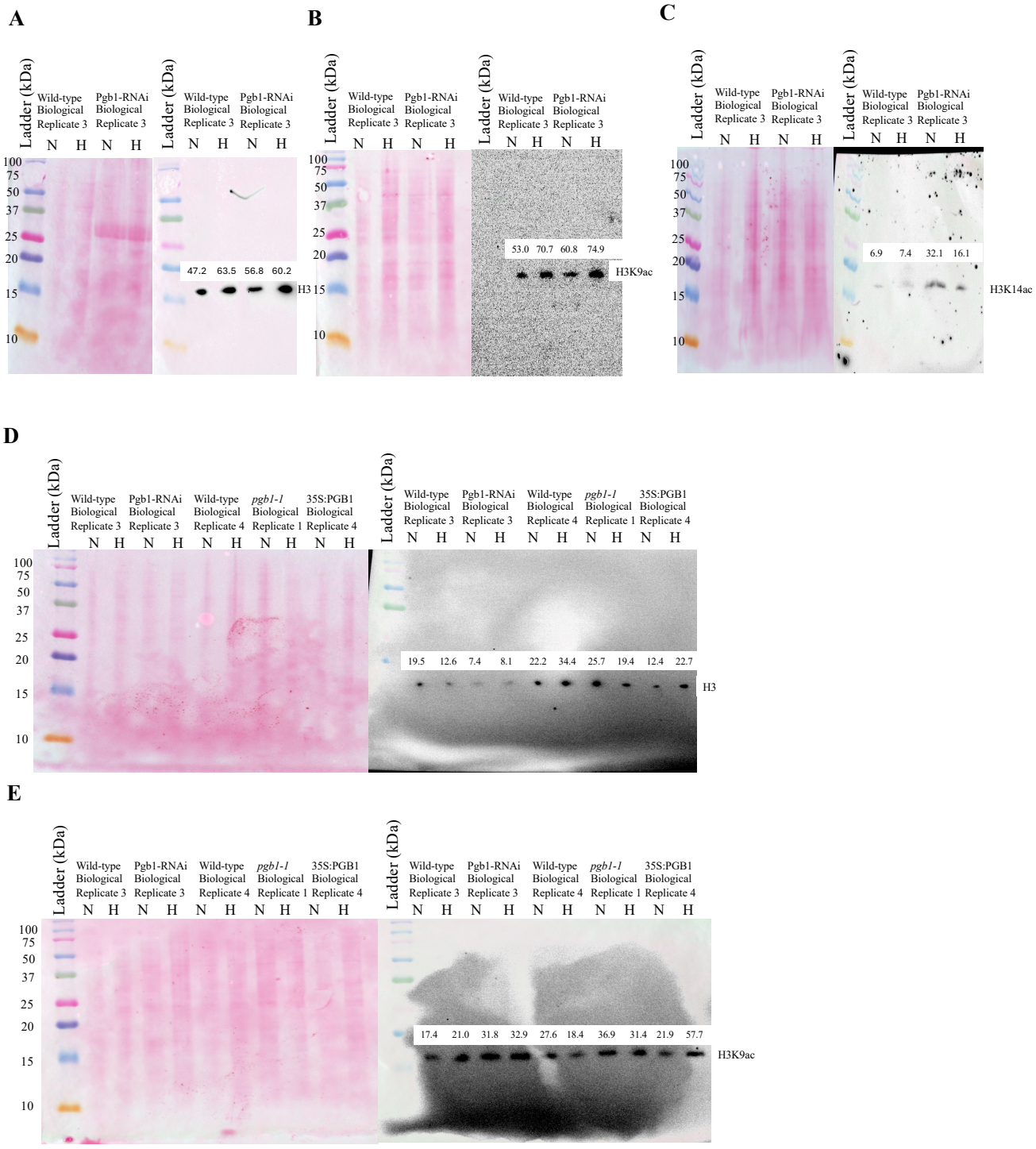
A
B
C
D
E
Ladder (kDa)
Wild-type Biological Replicate 3
Pgb1-RNAi Biological Replicate 3
Wild-type Biological Replicate 4
pgb1-1 Biological Replicate 1
35S:PGB1 Biological Replicate 4
N H
100
75
50
37
25
20
15
10
47.2 63.5 56.8 60.2
H3
53.0 70.7 60.8 74.9
H3K9ac
6.9 7.4 32.1 16.1
H3K14ac
19.5 12.6 7.4 8.1 22.2 34.4 25.7 19.4 12.4 22.7
H3
17.4 21.0 31.8 32.9 27.6 18.4 36.9 31.4 21.9 57.7
H3K9ac

F

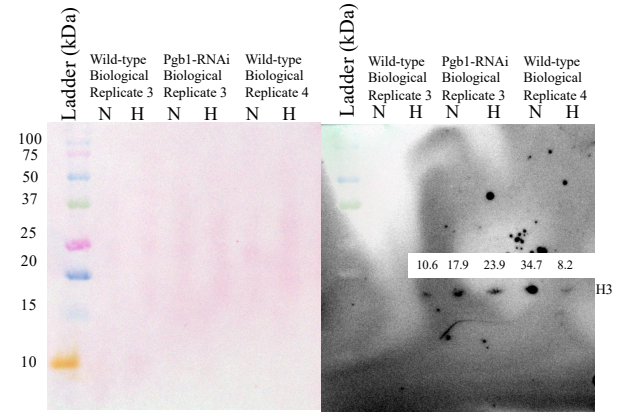
Ladder (kDa)
Wild-type Biological Replicate 3
Pgb1-RNAi Biological Replicate 3
Wild-type Biological Replicate 4
N H N H N H
100
75
50
37
25
20
15
10
Ladder (kDa)
Wild-type Biological Replicate 3
Pgb1-RNAi Biological Replicate 3
Wild-type Biological Replicate 4
N H N H N H
10.6 17.9 23.9 34.7 8.2
H3

G

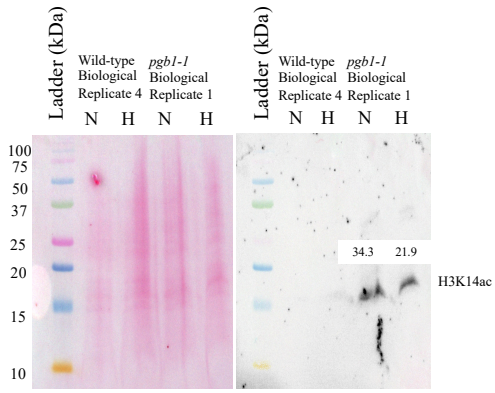
Ladder (kDa)
Wild-type Biological Replicate 4
pgb1-1 Biological Replicate 1
N H N H
100
75
50
37
25
20
15
10
Ladder (kDa)
Wild-type Biological Replicate 4
pgb1-1 Biological Replicate 1
N H N H
34.3 21.9
H3K14ac

H

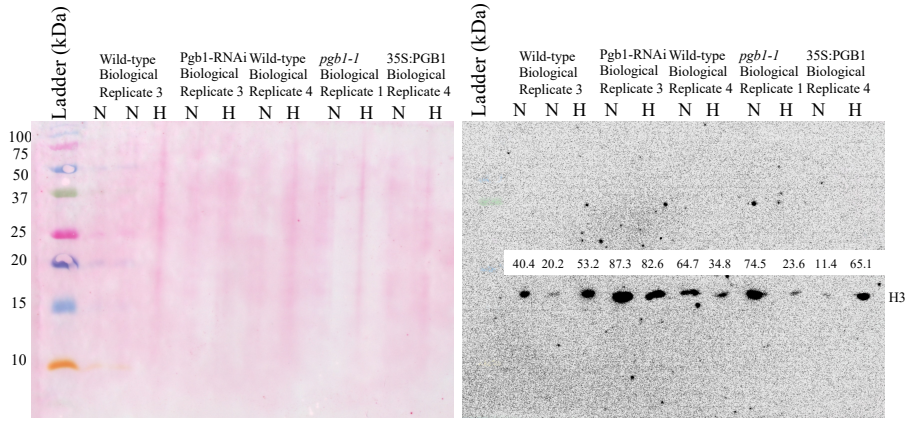
Ladder (kDa)
Wild-type Biological Replicate 3
Pgb1-RNAi Biological Replicate 3
Wild-type Biological Replicate 4
pgb1-1 Biological Replicate 1
35S:PGB1 Biological Replicate 4
N N H N H N H N H N H
100
75
50
37
25
20
15
10
Ladder (kDa)
Wild-type Biological Replicate 3
Pgb1-RNAi Biological Replicate 3
Wild-type Biological Replicate 4
pgb1-1 Biological Replicate 1
35S:PGB1 Biological Replicate 4
N N H N H N H N H N H
40.4 20.2 53.2 87.3 82.6 64.7 34.8 74.5 23.6 11.4 65.1
H3

I

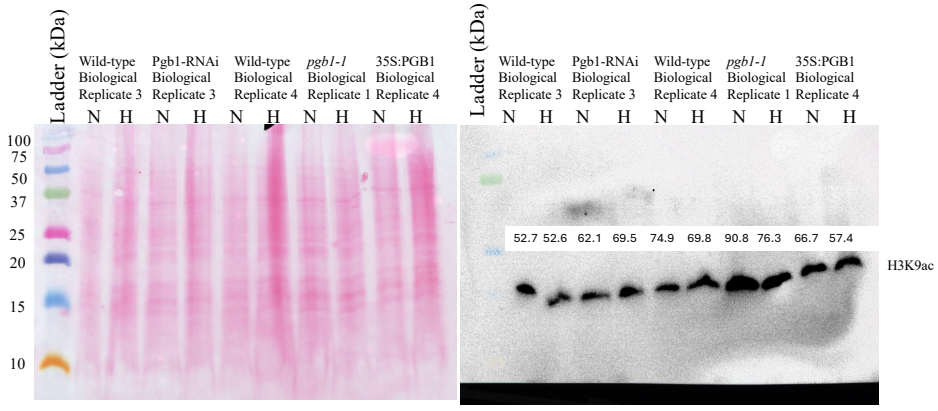
Ladder (kDa)
Wild-type Biological Replicate 3
Pgb1-RNAi Biological Replicate 3
Wild-type Biological Replicate 4
pgb1-1 Biological Replicate 1
35S:PGB1 Biological Replicate 4
N H N H N H N H N H
100
75
50
37
25
20
15
10
Ladder (kDa)
Wild-type Biological Replicate 3
Pgb1-RNAi Biological Replicate 3
Wild-type Biological Replicate 4
pgb1-1 Biological Replicate 1
35S:PGB1 Biological Replicate 4
N H N H N H N H N H
52.7 52.6 62.1 69.5 74.9 69.8 90.8 76.3 66.7 57.4
H3K9ac

J

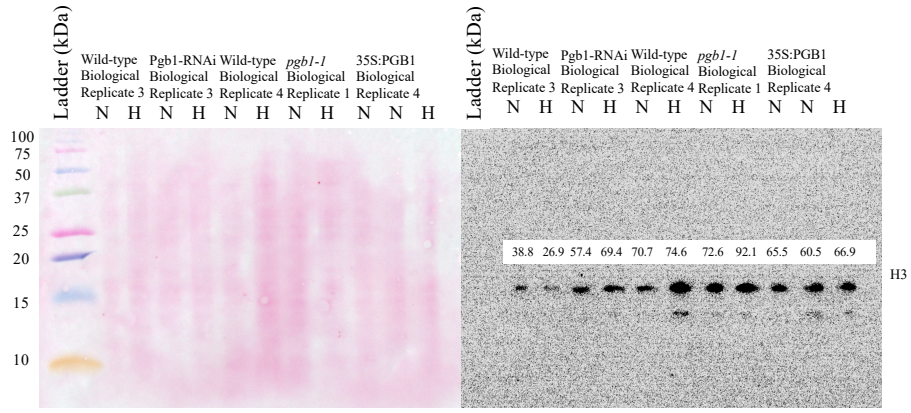
Ladder (kDa)
Wild-type Biological Replicate 3
Pgb1-RNAi Biological Replicate 3
Wild-type Biological Replicate 4
pgb1-1 Biological Replicate 1
35S:PGB1 Biological Replicate 4
N H N H N H N H N N H
100
75
50
37
25
20
15
10
38.8 26.9 57.4 69.4 70.7 74.6 72.6 92.1 65.5 60.5 66.9
H3

K

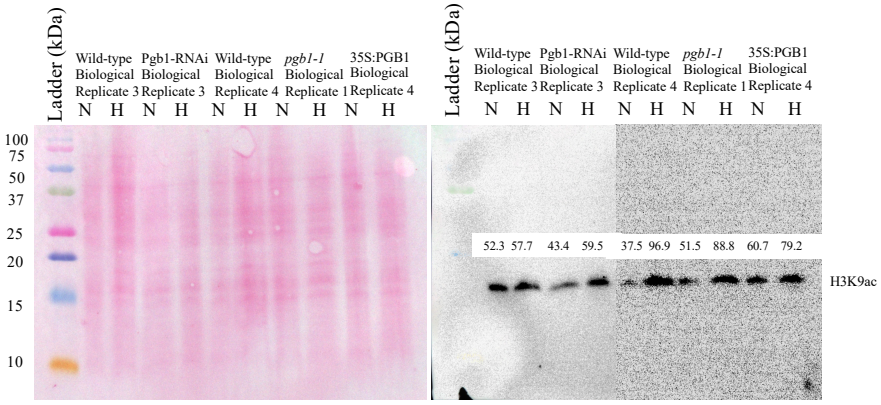
Ladder (kDa)
Wild-type Biological Replicate 3
Pgb1-RNAi Biological Replicate 3
Wild-type Biological Replicate 4
pgb1-1 Biological Replicate 1
35S:PGB1 Biological Replicate 4
N H N H N H N H N H
100
75
50
37
25
20
15
10
52.3 57.7 43.4 59.5 37.5 96.9 51.5 88.8 60.7 79.2
H3K9ac

L

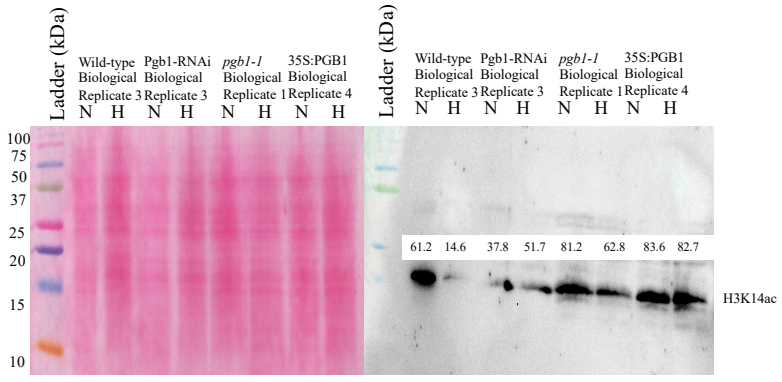
Ladder (kDa)
Wild-type Biological Replicate 3
Pgb1-RNAi Biological Replicate 3
pgb1-1 Biological Replicate 1
35S:PGB1 Biological Replicate 4
N H N H N H N H
100
75
50
37
25
20
15
10
61.2 14.6 37.8 51.7 81.2 62.8 83.6 82.7
H3K14ac

M

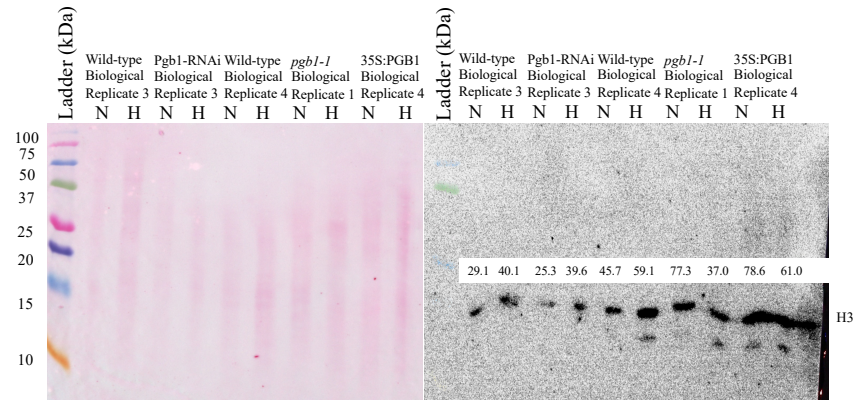
Ladder (kDa)
Wild-type Biological Replicate 3
Pgb1-RNAi Biological Replicate 3
Wild-type Biological Replicate 4
pgb1-1 Biological Replicate 1
35S:PGB1 Biological Replicate 4
N H N H N H N H N H
100
75
50
37
25
20
15
10
29.1 40.1 25.3 39.6 45.7 59.1 77.3 37.0 78.6 61.0
H3

N

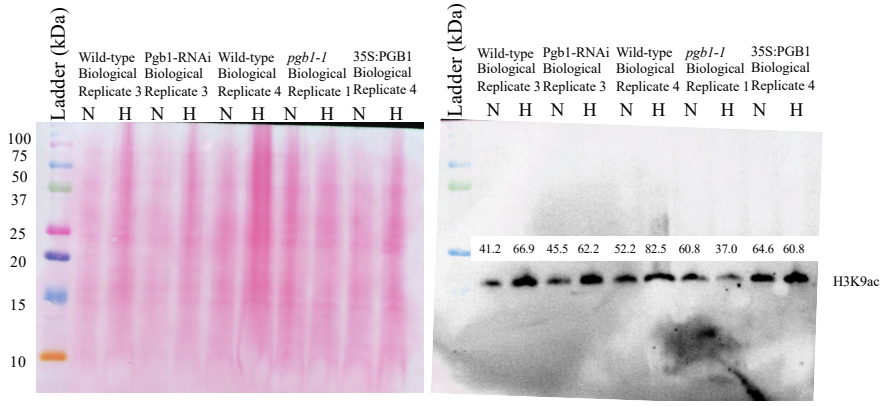
Ladder (kDa)
Wild-type Biological Replicate 3
Pgb1-RNAi Biological Replicate 3
Wild-type Biological Replicate 4
pgb1-1 Biological Replicate 1
35S:PGB1 Biological Replicate 4
N H N H N H N H N H
100
75
50
37
25
20
15
10
41.2 66.9 45.5 62.2 52.2 82.5 60.8 37.0 64.6 60.8
H3K9ac

O

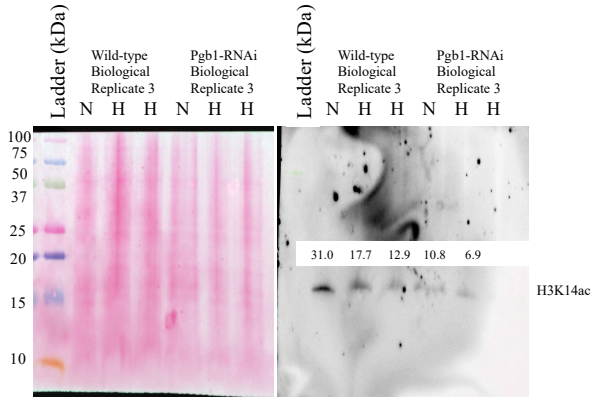
Ladder (kDa)
Wild-type Biological Replicate 3
Pgb1-RNAi Biological Replicate 3
N H H N H H
100
75
50
37
25
20
15
10
31.0 17.7 12.9 10.8 6.9
H3K14ac

P

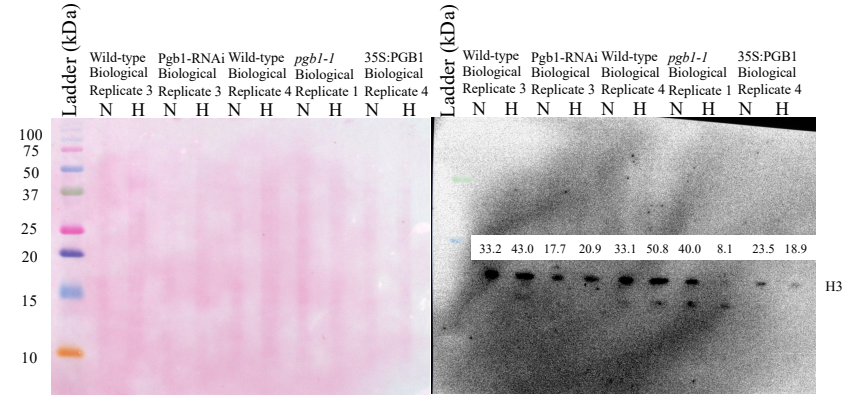
Ladder (kDa)
Wild-type Biological Replicate 3
Pgb1-RNAi Biological Replicate 3
Wild-type Biological Replicate 4
pgb1-1 Biological Replicate 1
35S:PGB1 Biological Replicate 4
N H N H N H N H N H
100
75
50
37
25
20
15
10
33.2 43.0 17.7 20.9 33.1 50.8 40.0 8.1 23.5 18.9
H3

Q

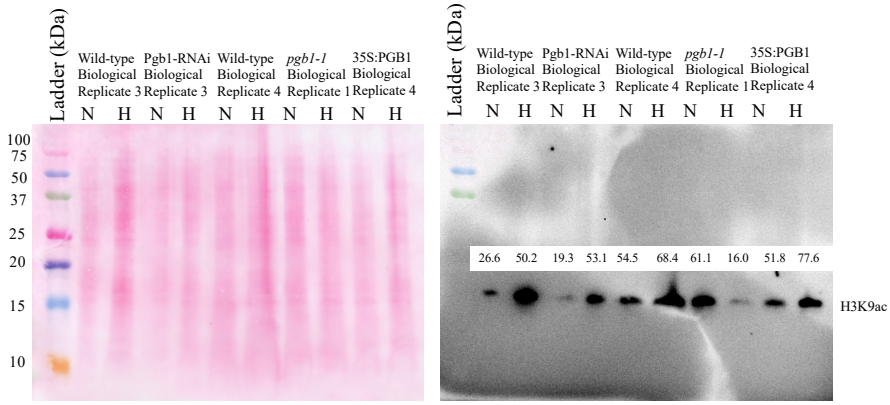
Ladder (kDa)
Wild-type Biological Replicate 3
Pgb1-RNAi Biological Replicate 3
Wild-type Biological Replicate 4
pgb1-1 Biological Replicate 1
35S:PGB1 Biological Replicate 4
N H N H N H N H N H
100
75
50
37
25
20
15
10
26.6 50.2 19.3 53.1 54.5 68.4 61.1 16.0 51.8 77.6
H3K9ac

U

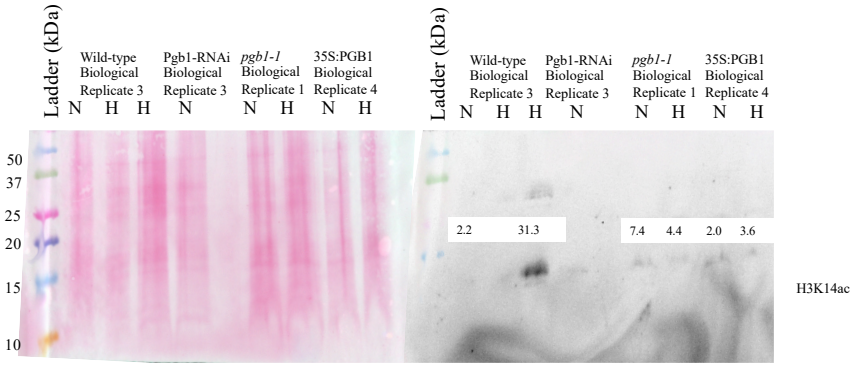
Ladder (kDa)
Wild-type Biological Replicate 3
Pgb1-RNAi Biological Replicate 3
pgb1-1 Biological Replicate 1
35S:PGB1 Biological Replicate 4
N H H N N H N H
50
37
25
20
15
10
2.2 31.3 7.4 4.4 2.0 3.6
H3K14ac

S

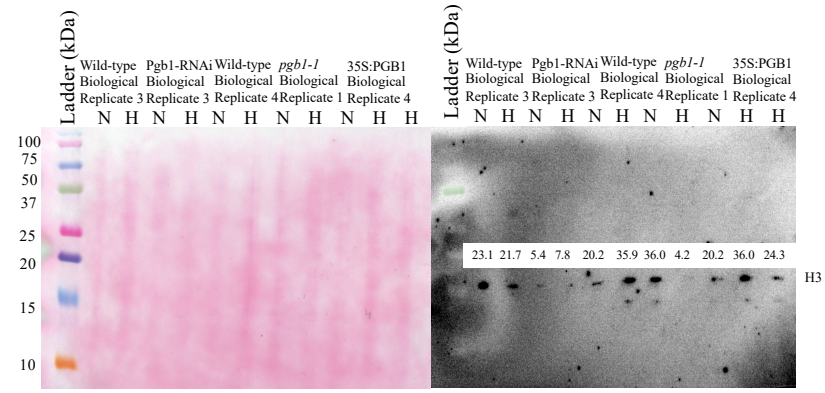
Ladder (kDa)
Wild-type Biological Replicate 3
Pgb1-RNAi Biological Replicate 3
Wild-type Biological Replicate 4
pgb1-1 Biological Replicate 1
35S:PGB1 Biological Replicate 4
N H N H N H N H N H
100
75
50
37
25
20
15
10
23.1 21.7 5.4 7.8 20.2 35.9 36.0 4.2 20.2 36.0 24.3
H3

T

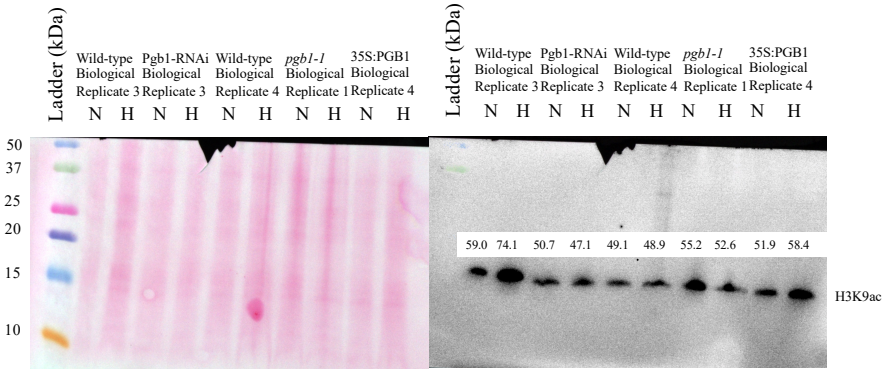
Ladder (kDa)
Wild-type Biological Replicate 3
Pgb1-RNAi Biological Replicate 3
Wild-type Biological Replicate 4
pgb1-1 Biological Replicate 1
35S:PGB1 Biological Replicate 4
N H N H N H N H N H
50
37
25
20
15
10
59.0 74.1 50.7 47.1 49.1 48.9 55.2 52.6 51.9 58.4
H3K9ac

U

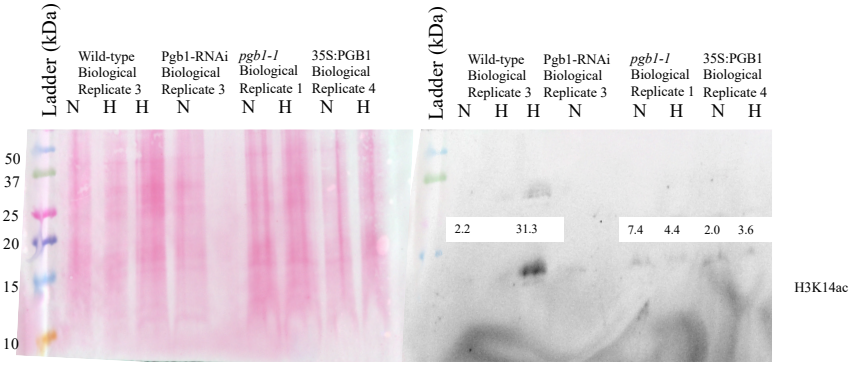
Ladder (kDa)
Wild-type Biological Replicate 3
Pgb1-RNAi Biological Replicate 3
pgb1-1 Biological Replicate 1
35S:PGB1 Biological Replicate 4
N H H N N H N H
50
37
25
20
15
10
2.2 31.3 7.4 4.4 2.0 3.6
H3K14ac

Supplemental Figure S3: Biological replicate 3 of the WT and Pgb1-RNAi lines, biological replicate 4 of the WT and 35S:PGB1 lines, and biological replicate 1 of the *pgb1-1* line. The Ponceau S-stained blot of normoxic and hypoxic cell lysates (left panels), and the accompanying blot immunostained with antibodies against the H3 loading control **(A, D, E, H, J, M, P, S)**, H3K9ac **(B, E, I, K, N, Q, T)**, and H3K14ac **(C, G, L, O, R, U)** are shown (right panels). WT biolgical replicate 3 includes technical replicates: H3K9ac tech. rep. 1 **(A, B),** H3K9ac tech. rep. 2 **(D, E),** H3K9ac tech. rep. 3 **(H, I),** H3K9ac tech. rep. 4 **(J, K),** H3K9ac tech. rep. 5 **(M, N)**, H3K9ac tech. rep. 6 **(P, Q),** H3K9ac tech. rep. 7 **(S, T),** H3K14ac tech rep 1 **(H, C),** H3K14ac tech. rep. 2 **(J, L),** H3K14ac tech. rep. 3 **(M, O),** H3K14ac tech. rep. 4 **(S, U)** and biological replicate 4 includes technical replicates: H3K9ac tech. rep. 1 **(D, E),** H3K9ac tech. rep. 2 **(H, I),** H3K9ac tech. rep. 3 **(J, K),** H3K9ac tech. rep 4 **(M, N)**, H3K9ac tech. rep. 5 **(P, Q),** H3K9ac tech. rep. 6 **(S, T)**. Pgb1-RNAi biological replicate 3 includes technical replicates: H3K9ac tech. rep. 1 **(A, B),** H3K9ac tech. rep. 2 **(D, E),** H3K9ac tech. rep. 3 **(F, I),** H3K9ac tech. rep. 4 **(J,K),** H3K9ac tech. rep. 5 **(M, N),** H3K9ac tech. rep. 6 **(P, Q),** H3K9ac tech. rep. 7 **(S, T),** H3K14ac tech rep 1 **(H, C),** H3K14ac tech. rep. 2 **(J, L),** H3K14ac tech. rep. 3 **(M, O).** 35S:PGB1 biological replicate 4 includes technical replicates: H3K9ac tech. rep. 1 **(D, E),** H3K9ac tech. rep. 2 **(H, I),** H3K9ac tech. rep. 3 **(J, K),** H3K9ac tech. rep 4 **(M, N),** H3K9ac tech. rep. 5 **(P, Q),** H3K9ac tech. rep. 6 **(S, T),** H3K14ac tech. rep. 1 **(J, K),** H3K14ac tech. rep. 1 **(J, L)**, H3K14ac tech. rep. 2 **(P, R),** H3K14ac tech. rep. 3 **(S, U).** *pgb1-1* biological replicate 1 includes technical replicates: H3K9ac tech. rep. 1 **(D, E),** H3K9ac tech. rep. 2 **(H, I),** H3K9ac tech. rep. 3 **(J, K),** H3K9ac tech. rep 4 **(M, N),** H3K9ac tech. rep. 5 **(P, Q),** H3K9ac tech. rep. 6 **(S, T),** H3K14ac tech. rep. 1 **(H, G),** H3K14ac tech. rep. 2 **(J, L),** H3K14ac tech. rep. 3 **(P, R),** H3K14ac tech. rep. 4 **(S, U).** Abcam mouse anti-H3 (cat# 10799) primary antibody and Invitrogen goat anti-mouse (cat# 31430) were used for the H3 blots **(A, D, E, H, J, M, P, S)**. Abcam rabbit anti-H3K9ac (cat# ab32129) primary antibody and Invitrogen goat anti-rabbit secondary (cat# 32460) were used for the H3K9ac blots **(B, E, I, K, N, Q, T)**. Abcam rabbit anti-H3K14ac (cat# ab52946) was used for all H3K14ac blots **(C, G, L, O, R, U)**. An Invitrogen goat anti-rabbit (cat# 32460) secondary antibody were used for the H3K14ac blots. The values above each band represent the band intensity value (band volume/band area) provided by the Azure SpotPro software.

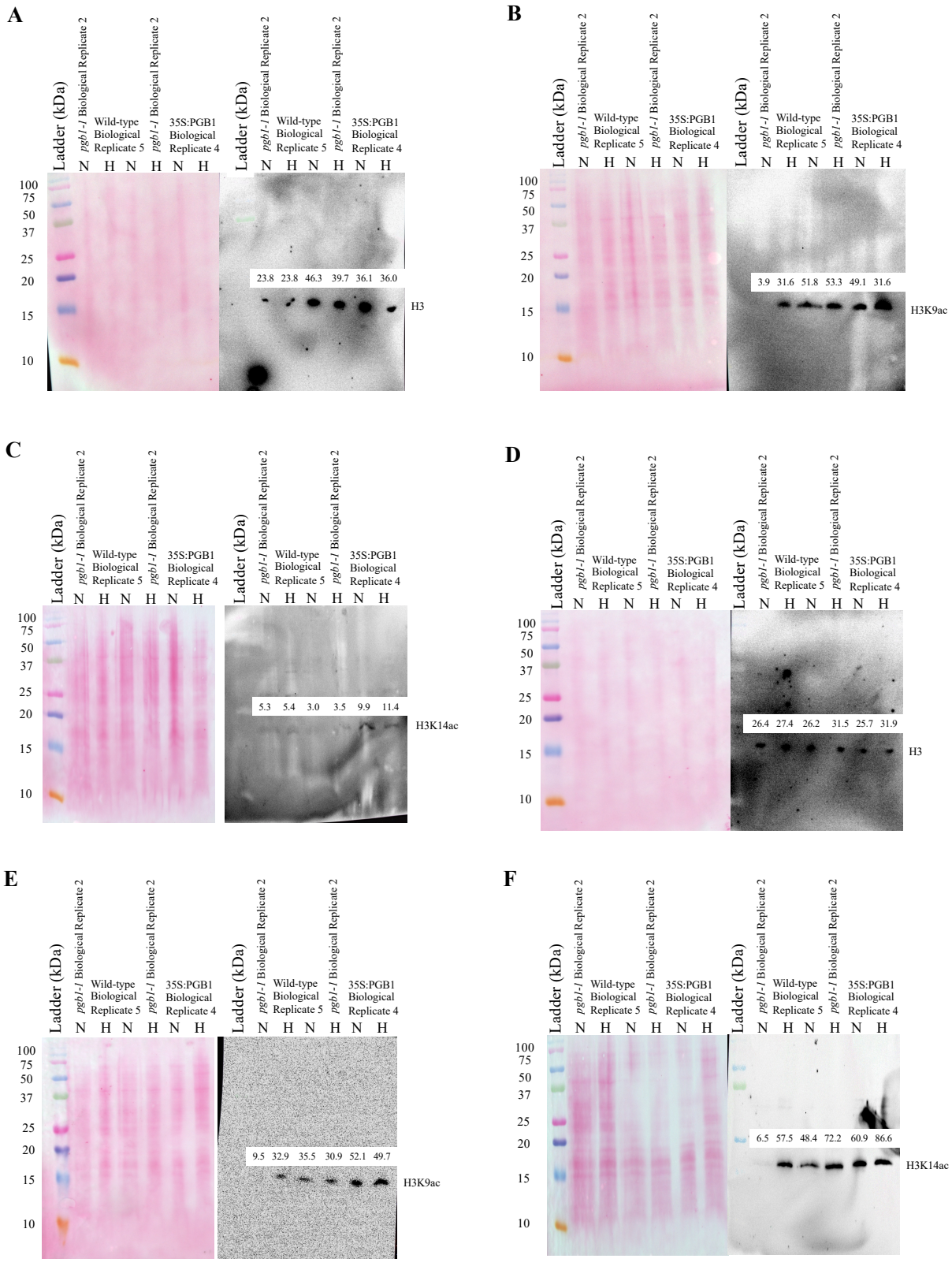
A
B
C
D
E
F
Ladder (kDa)
pgb1-1 Biological Replicate 2
Wild-type Biological Replicate 5
pgb1-1 Biological Replicate 2
35S:PGB1 Biological Replicate 4
N H N H N H
100
75
50
37
25
20
15
10
23.8 23.8 46.3 39.7 36.1 36.0
H3
3.9 31.6 51.8 53.3 49.1 31.6
H3K9ac
5.3 5.4 3.0 3.5 9.9 11.4
H3K14ac
26.4 27.4 26.2 31.5 25.7 31.9
H3
9.5 32.9 35.5 30.9 52.1 49.7
H3K9ac
6.5 57.5 48.4 72.2 60.9 86.6
H3K14ac

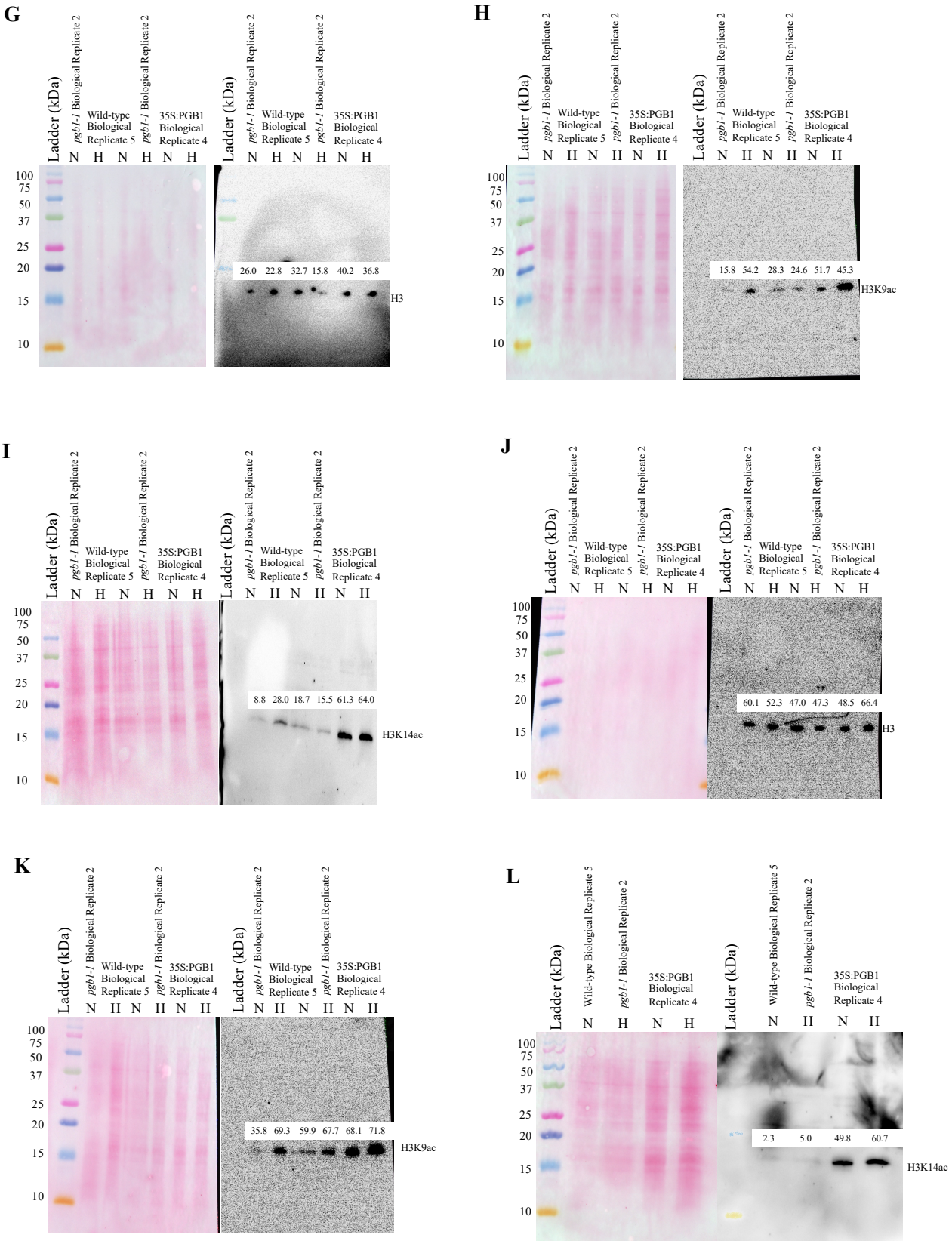
G
H
I
J
K
L
Ladder (kDa)
pgb1-1 Biological Replicate 2
Wild-type Biological Replicate 5
35S:PGB1 Biological Replicate 4
N H N H N H
100
75
50
37
25
20
15
10
26.0 22.8 32.7 15.8 40.2 36.8
H3
15.8 54.2 28.3 24.6 51.7 45.3
H3K9ac
8.8 28.0 18.7 15.5 61.3 64.0
H3K14ac
60.1 52.3 47.0 47.3 48.5 66.4
H3
35.8 69.3 59.9 67.7 68.1 71.8
H3K9ac
Wild-type Biological Replicate 5
2.3 5.0 49.8 60.7
H3K14ac

Supplemental Figure S4: Biological replicate 5 of the WT and 35S:PGB1 lines, and biological replicate 2 of the *pgb1-1* line. The Ponceau S-stained blot of normoxic and hypoxic cell lysates (left panels), and the accompanying blot immunostained with antibodies against the H3 loading control **(A, D, G, J)**, H3K9ac **(B, E, H, K)**, and H3K14ac **(C, F, I, L)** are shown (right panels). WT biolgical replicate 5 includes technical replicates: tech. rep. 1 **(A, B, C),** tech. rep. 2 **(D, E, F)**, tech. rep 3 **(G, H, I),** H3K9ac tech. rep 4 **(J, K).** 35S:PGB1 biological replicate 5 includes technical replicates: tech. rep. 1 **(A, B, C)**, tech. rep. 2 **(D, E, F)**, tech. rep 3 **(G, H, I)**, tech. rep 4 **(J, K, L).** *pgb1-1* biological replicate 2 includes technical replicates: tech. rep. 1 **(A, B, C),** tech. rep. 2 **(D, E, F)**, tech. rep 3 **(G, H, I)**, H3K9ac tech. rep 4 **(J, K).** Abcam mouse anti-H3 (cat# 10799) primary antibody and Invitrogen goat anti-mouse (cat# 31430) were used for the H3 blots **(A, D, G, J)**. Abcam rabbit anti-H3K9ac (cat# ab32129) primary antibody and Invitrogen goat anti-rabbit secondary (cat# 32460) were used for the H3K9ac blots **(B, E, H, K)**. Abcam rabbit anti-H3K14ac (cat# ab52946) was used for all H3K14ac blots **(C, F, I, L)**. An Invitrogen goat anti-rabbit (cat# 32460) secondary antibody were used for the H3K14ac blots. The values above each band represent the band intensity value (band volume/band area) provided by the Azure SpotPro software.